Czech Technical University in Prague
Faculty of Electrical Engineering
Department of Electromagnetic Field

Hybrid Free–Space Optical and Visible Light Communication Link

Doctoral thesis by Petr Pešek

Ph.D. Programme: Electrical Engineering and Information Technology [P2612]
Branch of study: Radioelectronics [2601V010]

Supervisor: prof. Ing. Stanislav Zvánovec, Ph.D.
Co-Supervisor: Ing. Matěj Komanec, Ph.D.

2020

Declaration of Originality

I, the undersigned, hereby declare that this doctoral thesis is the result of my research in our research team and my contribution corresponds to that specified at the beginning of each research chapter. The thesis was written under the professional supervision of Prof. Stanislav Zvánovec and Dr. Matěj Komanec, using the literature and resources listed in the Bibliography and References.

In Prague, 2020

....
Ing. Petr Pešek

Acknowledgement

Firstly, I would like to express my thanks to my supervisor Stanislav Zvanovec, who supported and guided me during my studies and gave me the opportunity to be a part of a great team of people. Many thanks also belong to our optical team, it was my pleasure to collaborate with them on optic topics.

I would like to acknowledge Paul Anthony Haigh, for opportunity to spend one month at University of Bristol, and Fary Ghassemlooy for theirs opinions and advice, which have significant impact on the results presented in this thesis.

Finally, special thank goes to my family and Jana for their never ending support and patience.

Abstract

The field of optical wireless communications (OWC) has recently attracted significant attention as a complementary technology to radio frequency (RF). OWC systems offer several advantages including higher bandwidth, an unregulated spectrum, resistance to electromagnetic interference and a high order of reusability. The thesis focuses on the deployment and analyses of end-user interconnections using the OWC systems. Interconnection can be established by many wireless technologies, for instance, by a single OWC technology, a combination of OWC technologies, or by hybrid OWC/RF links.

In order to establish last mile outdoor interconnection, a free-space optical (FSO) has to be investigated. In this thesis, the performance of all-optical multi-hop scenarios is analyzed under atmospheric conditions. However, nowadays, many end users spend much time in indoor environments where visible light communication (VLC) technology can provide better transmission parameters and, significantly, better coverage. An analytical description of bit error rate for relaying VLC schemes is derived and experimentally verified. Nonetheless, for the last mile, interconnection of a provider and end users (joint outdoor and indoor connection) can be advantageous when combining multiple technologies. Therefore, a hybrid FSO/VLC system is proposed and analyzed for the interconnection of the last mile and last meter bottleneck.

Key Words

Optical wireless communication, free space optics, visible light communication

Abstrakt

V součastnosti bezdrátové optické komunikace (optical wireless communication, OWC) získávají širokou pozornost jako vhodný doplněk ke komunikačním přenosům v rádiovém pásmu. OWC nabízejí několik výhod včetně větší šířky přenosového pásma, neregulovaného frekvenčního pásma či odolnosti vůči elektromagnetickému rušení. Tato práce se zabývá návrhem OWC systémů pro připojení koncových uživatelů. Samotná realizace spojení může být provedena za pomoci různých variant bezdrátových technologií, například pomocí OWC, kombinací různých OWC technologií nebo hybridním rádio-optickým spojem.

Za účelem propojení tzv. poslední míle je analyzován optický bezvláknový spoj (free space optics, FSO). Tato práce se dále zabývá analýzou přenosových vlastností celo-optického více skokového spoje s důrazem na vliv atmosférických podmínek. V dnešní době mnoho uživatelů tráví čas ve vnitřních prostorech kanceláří či doma, kde komunikace ve viditelném spektru (visible light communication, VLC) poskytuje lepší přenosové parametry pokrytí než úzce směrové FSO. V rámci této práce byla odvozena a experimentálně ověřena závislost pro bitovou chybovost přesměrovaného (relaying) spoje ve VLC. Pro propojení poskytovatele datavých služeb s koncovým uživatelem může být výhodné zkombinovat více přenosových technologií. Proto je navržen a analyzovám systém pro překonání tzv. problému poslední míle a posledního metru kombinující hybridní FSO a VLC technologie.

Klíčová Slova

Optické bezvláknové komunikace, optika volným prostorem, komunikace ve viditelném světle

Contents

Page

Abbreviations

4G	Fourth Generation
5G	Fifth Generation
Am-CAP	Allocated Multi Carrierless Amplitude Phase Modulation
ACO-OFDM	Asymmetrically Clipped Optical Orthogonal Frequency Division Multiplexing
AF	Amplify and Forward
ASE	Amplified Spontaneous Emission
AV	Augmented Reality
BER	Bit Error Rate
C2C	Car to Car
CAP	Carrierless Amplitude Phase Modulation
CSI	Channel State Information
CSMA/CA	Carrier Sense Multiple Access with Collision Avoidance
D2D	Device to Device
DCO-OFDM	DC Biased Orthogonal Frequency Division Multiplexing
DF	Decode and Forward
DMT	Discrete Multitone Modulation
DP	Dual Polarization
DWDM	Dense Wavelength Division Multiplexing
DoF	Degree of Freedom
EDFA	Erbium Doped Fibre Amplifier
EO	Electrical to Optical
FIR	Finite Impulse Response
FOV	Field Of View
FSO	Free Space Optics
ICI	InterChannel Interference
IFFT	Inverse Fast Fourier Transform
IM/DD	Intensity Modulation and Direct Detection
IR	InfraRed
ISI	Inter Symbol Interference
IoT	Internet of Things
LD	Laser Diode

LED	Light Emitted Diode
LOS	Line of Sight
LTE	Long Term Evolution
M2M	Machine to Machine
MAC	Medium Access Control
MIMO	Multiple Input Multiple Output
NLOS	Non Line of Sight
NOMA	Non Orthogonal Multiplexing Access
NRZ	Non-Return-to-Zero
OE	Optical to Electrical
OFDM	Orthogonal Frequency Division Multiplexing
OFDMA	Orthogonal Frequency Division Multiplexing Access
OLED	Organic Light Emitted Diode
OOK	On Off Keying
OWC	Optical Wireless Communication
PAM	Pulse Amplitude Modulation
PAPR	Peak-to-Average power Ratio
PC	Personal Computer
PD	PhotoDetector
PLC	Power Line Communication
PPM	Pulse Position Modulation
PWM	Pulse Width Modulation
QAM	Quadrature Amplitude Modulation
QoS	Quality of Service
RF	Radio Frequency
RGB	Red-Green-Blue
RoF	Radio over Fiber
RoFSO	Radio over Free Space Optics
SINR	Signal to Interference plus Noise Ratio
SNR	Signal to Noise Ratio
SSL	Solid State Lighting
TDMA	Time Division Multiplexing Access
TV	Television
UV	UltraViolet
VL	Visible Light
VLC	Visible Light Communication
VR	Virtual Reality
WDM	Wavelength Division Multiplexing
WIFI	Wireless Fidelity

WiMAX	Worldwide Interoperability for Microwave Access
m-CAP	Multi Carrierless Amplitude Phase Modulation
m-ESCAP	Expanded Non-orthogonal Multi-band Super-Nyquist CAP
μ-LED	Micro Light Emitted Diode

CHAPTER 1 Introduction

In recent years, we have been living in a period of massive implementation of networking technologies. Concepts such as the Internet of things (IoT), clouds, video streaming, virtual reality (VR) or augmented reality (AV) have become an everyday part of our lives. However, the tremendous expansion of applications, together with data traffic relying on wireless communication, results in a massive increase of overall data rates. According to a Cisco networking forecast, smartphone data traffic exceeded personal computer (PC) traffic in 2018 and will grow sevenfold from 2018 to 2022, reaching 77.5 EB per month in 2022 [1]. Moreover, the massive development and popularity of smart devices are changing internet connections from "human → human" to "human → things" or "things → things" called machine to machine (M2M) [2]. In 2022, M2M will be more than half of all global connected devices reaching 1.8 times M2M connections for each member of the global population [1]. These demands, along with many others, will require a tremendous deployment of high-speed wireless communication. Due to the limited radio frequency (RF) spectrum (physically, fees or licensed for non-communication technology), research and private sectors need to focus on improving current technology or on developing a new one capable of avoiding so-called "spectrum congestion" [3].

The fifth generation (5G) mobile network aims to address the limitations of the previous generation of cellular standards: increase channel capacity and scalability, decrease latency and power consumption, reduce costs and ensure massive device connectivity. To meet these performance criteria, 5G will have to cover numerous technical challenges arising from end-user requirements. Several improved technologies including massive multiple input multiple output (MIMO) [4], spectrum sharing [5], device to device (D2D) communication technology [6] and shift to higher frequencies [7] meet the criteria for implementation in 5G.

Nonetheless, the massive deployment of mobile networks contradicts previous legislative proposals presented by the European Commission, representing a reduction of carbon dioxide ($C0_2$) by 40% by 2030 compared with 1990 [8]. For instance, the number of public wireless fidelity (WIFI) hotspots exceeded 362 million devices in 2019, resulting in estimated energy consumption of more than 18 billion kWh per year costing more than 2 billion dollars [9]. As one possible solution to the reduction of CO_2 values, the European Commission has recommended banning the use of incandescent and fluorescent light. This recommendation and improvements in technology have brought a massive deployment of solid state lighting (SSL) such as a light emitted diode (LED). It is expected that LED power efficiency will have achieved 300 lumens per Watt around 2025 [10]. By comparison, an incandescent light has a luminous efficiency determined in the manner above 18 lumens per Watt, with 6% of the light in the 400-–700 nm band [11].

The deployment of LED has created an additional important capability, LED can also be used for wireless communication by the direct and rapid modulation of a light source that the human eye cannot perceive. This technology is known as visible light communication (VLC) [3] and can provide high-speed-data rate communication, especially for indoor applications [12, 13]. However, it is extremely challenging to reach satisfactory results for an outdoor application due to ambient light causing increased shot noise and limited transmission distances. Due to its relatively low complexity, the ever-decreasing cost of LED sources and the availability of a vast bandwidth ~10 000 wider than in the case of RF, VLC technology is an ideal candidate for future indoor applications providing both illumination and data communication at a global level [14]. VLC, together with infrared (IR) and ultraviolet (UV), create a base of optical wireless communication (OWC) [3, 15]. OWC, in most cases, operates in the 350–2000 nm wavelength band addressing a solution for "last mile" and "last meter" issues in access networks.

In recent years, last mile access networks have undergone massive development and mature technologies, such as microwave and optical fibers, are not always cost effective, especially in dense urban areas. To overcome these challenges, free space optics (FSO) communication links are becoming an attractive high-rate, cost-effective technology for access networks [16, 17]. FSO communication mainly uses a laser diode (LD) as the source of light in the near IR band for a wide-range communication span from inter-chip to inter-satellite communication [18, 19]. A terrestrial point-to-point FSO communication system, however, can operate at a wide frequency range including the UV, visible light (VL) bands and IR, which offers the best transmission properties [14]. Despite the many advantages of FSO, long-range systems, in particular, are susceptible to atmospheric conditions which can render a system inoperable. FSO link impairments are caused predominantly by scattering on fog droplets, absorption on water vapor, as well as by atmospheric turbulence (causing a fluctuation in air density, leading to a change in the refractive index of air), beam spreading, and by physical obstacles which can temporally block the signal [20].

OWC and next wireless communication technologies follow different standards, have distinct properties, can use many modulation techniques and transmission media, and can have different requirements for transmitters and receivers. Last but not least, the level of security, attenuation characteristics and different operational principles play a key role in the deployment of wireless communication technologies. However, OWC provides several interesting advantages: (*i*) a highly achievable signal to noise ratio (SNR); (*ii*) no interference with electronic instruments; (*iii*) a high level of security; (*iv*) vast unregulated bandwidth; (*v*) a relatively low-cost solution and (*vi*) easy implementation into existing lighting systems [21, 22]. On the other hand, high-data rate OWC systems have several limitations: (*i*) OWC is widely used for line of sight (LOS) links where obstacles can interrupt the signal; (*ii*) in the case of a near-IR source, high optical power represents a danger to the human eye; (*iv*) ambient light interference negatively affects system performance and (*iii*) alignment leads to operational constraints [23].

	VLC	**FSO**	**RF**
Transmitter	LED LD	LD	Antenna
Receiver	photodetector (PD) Camera	PD	Antenna
Distance	Indoor	Satellite Terrestrial	Indoor, Satellite Terrestrial
Interference level	Low [24]	Low [25]	Very high
Noise (most dominant)	Sun, ambient light sources	Ambient light sources	Electronic appliances
Data rate	11.28 Gbps using LED [26] 100 Gbps using LD [21]	100.8 Tbps [27]	6.93 Gbps [28]
Security	High	High	Low
Mobility	Limited	Limited	Good
Main purpose	Illumination Communication Localization	Communication	Communication Localization
Main limitation	Short distance communication Mobility connection Outdoor communication	Atmospheric influence	Interference

Table 1.1: Comparison of different wireless communication technologies.

Based on these properties, different OWC technologies can be used as key links within 5G wireless communication systems. Table 1.1 summarizes and clearly shows the differences in application scenarios among wireless technologies.

Implementation of OWC systems can be deployed easily. Consequently, a massive expansion of FSO technology has been developed, including applications [20, 29, 30] such as high-definition television (TV), medical video transmission, campus connectivity, backhaul for cellular networks, chip interconnection, satellite connectivity, underwater communications and many others. As is clear from the applications, FSO is predominantly a long-range outdoor technology. On the other hand, RF-based communications are undesirable in places, such as hospitals or airports, where LEDs can be used as a suitable alternative for fulfilling the role of data transmission technology, and even for providing illumination. Smart lighting, using a combination of illumination, communication and control, can significantly reduce costs and energy consumption. Moreover, VLC is being deployed in many other applications, including car to car (C2C), underwater communication, M2M, location-based services, local area networks and many other [24, 31].

This thesis focuses on the FSO and VLC hybrid interconnection of end users. The scenario for such a connection is depicted in Figure 1.1 and shows FSO technology acting as a node for the outdoor interconnection of a network access provider to an access point. On the other hand, VLC provides an indoor last meter access network connection.

In the first part of the doctoral thesis, state-of-the-art OWC is presented, containing an overview and application of FSO and VLC technologies. The objectives of the thesis are given in chapter 3. Then, the thesis core is demonstrated in chapter 4 by a collection of journal papers presenting a description of their contributions and relevance to the thesis topic. In the end, the achieved results and future research topics are summarized.

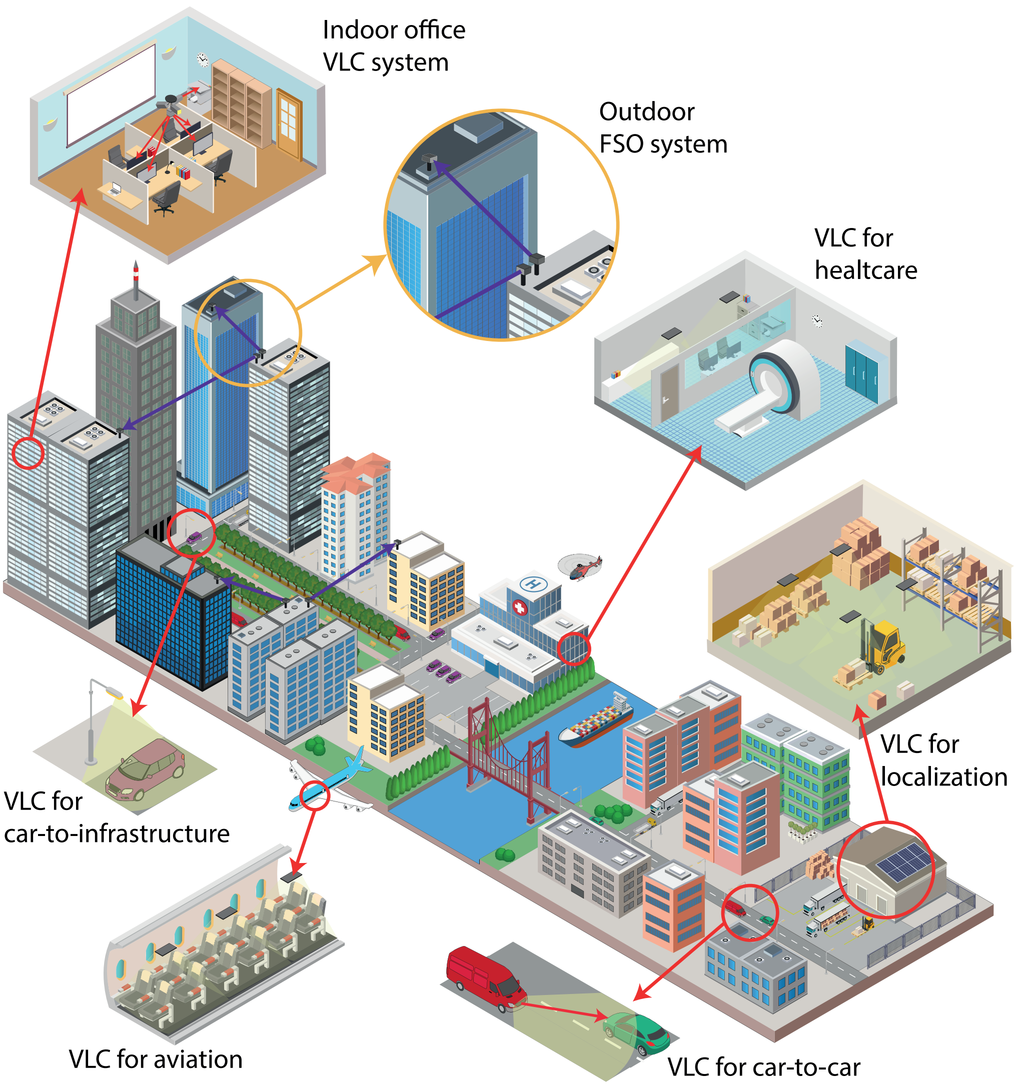

Figure 1.1: Selected VLC and FSO applications

CHAPTER

2 State-of-the-Art

Motivated by RF spectral congestion, OWC has been offered as a promising substitute for conventional RF communication systems, especially for short and medium range systems. OWC has undergone significant development, mainly in its transmission properties, over recent decades as OWC technologies have evolved from single-user to multi-user or hybrid networking.

The following subsections describe the state-of-the-art as it relates to the goals of this thesis.

2.1 Relay-Assisted Free Space Optical System

Due to tremendous data traffic growth of the network edge, FSO technology offers an efficient solution for overcoming the gap between provider's fiber infrastructures and the end users [29, 32, 33]. In recent years, many private companies and research groups have focused on significant data rate progress with the aim of reaching an order of Tb/s [34, 35]. FSO is generally used for LOS applications achieving similar properties as optical fibers.

Despite the many advantages of FSO, it is very challenging to reach the high level of reliability required by users primarily due to tremendously varying atmospheric channel conditions, such as absorption, scattering and turbulence, thus resulting in phase wandering, waveform distortion and optical attenuation [36–38]. An outdoor FSO channel can be significantly influenced by atmospheric turbulence caused by inhomogeneities in temperature and the atmospheric pressure produced by wind and solar heating, leading to variations of the air refractive index along the transmission path [39]. They cause random fluctuations in the amplitude, as well as the phase of the received signal, resulting in system performance degradation [40]. The intensity fluctuation of the received signal is known as scintillation and is measured in terms of a scintillation index (normalized variance of the intensity fluctuations) [39]. However, the scintillation index is a function of the refractive index structure parameter C_n^2 (main measure of turbulence), which varies at different times of day and is altitude dependent, increasing at lower altitudes due to the heat transfer between the ground and air [41]. However, the power fluctuation of the received optical signal is generally described by statistical models.

The development of the statistical models has evolved over several decades. A log-normal model was derived based on a first-order Rytov approximation and was accepted for weak turbulence regimes [42, 43]. However, measurements over several kilometer-long paths have proved the inaccuracy of the model for moderate and strong turbulence [44]. A number of statistical models has been derived to describe scintillation, for instance, the K model in a regime of strong turbulence [45], or the Gamma-Gamma model, which adopts all regimes [39]. Double Weibull distribution is another universal model that has been proven to be more accurate than the Gamma-Gamma model, particularly for cases of moderate and strong turbulence [46]. One of the latest models proposed in [47] is Double Generalized Gamma distribution, which is suitable for all regimes of turbulence.

One possible solution to maintain high reliability and the required data rate is to design a network topology, such as a ring or mesh structure. Nonetheless, recent optical networks have been built to allow transmission between two static points, which is, generally, not the case of end users. Moreover, wireless transmission aims to do the opposite: to transmit as much data information as possible among the maximum number of end users under certain constraints. In RF wireless communication networks, and especially in 5G, a user is no longer the final point of the wireless network, but the user is expected to participate in the storage, relaying, content delivery and computation within the network [48].

The idea of a relay-based system offers many advantages and results in a number of challenges: (*i*) a trade-off between throughput and reliability; (*ii*) the question of bandwidth versus power efficiency; (*iii*) compatibility and (*iv*) re-routing [15]. Recently however, relay-assisted FSO systems have garnered attention as a tool for the mitigation of channel fading [49]. Relay-assisted systems, though, can be designed to feature many options, such as: (*i*) a relay channel; (*ii*) a user cooperation scheme; (*iii*) an ad-hoc network or (*iv*) as a multi-relay channel. This thesis focuses mainly on the relay channel.

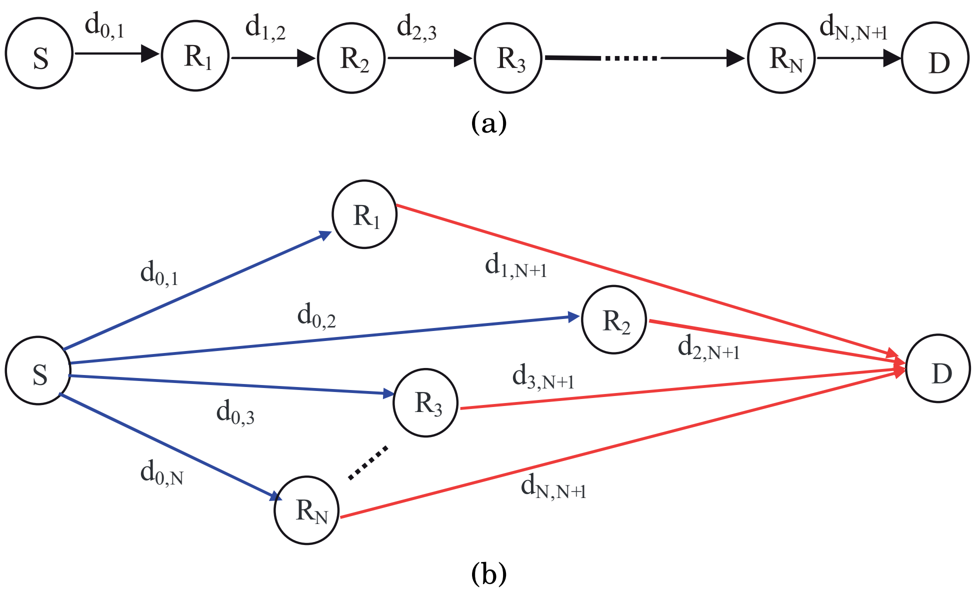

Figure 2.1: FSO relaying techniques: a) serial, b) parallel [49]

A relay-assisted link addresses the solution related to the shortcomings of conventional point-to-point systems in terms of extending transmission length and mitigating channel fading. The utilization of a relay-assisted link for an RF system was demonstrated as an alternative solution for the implementation of spatial diversity without using antenna arrays [50, 51]. This technique is highly effective for FSO technology because it offers a low-cost and efficient solution when compared to a MIMO system and it does not require additional transmitters and receivers [3].

Any network topology can be divided into a combination of serial or parallel links. The communication link can, therefore, be separated into several access points known as relays (R_n), or, in the case of FSO, as hops. Single or multiple R_n can be placed between the source (S) and destination (D), as depicted in Figure 2.1. In general, the relay node does not transmit any additional information, acting as it does as an intermediary between S and D, and, therefore, can be classified as a case of a channel with general feedback [52].

A relay-assisted-based FSO system was first proposed for communication in [53], where the authors investigated network capacity performance of a mesh FSO system. This idea led to the evaluation of the outage probability for a multi-hop FSO system. Considering K and Gamma-Gamma turbulence fading models, the relay-based model was demonstrated to be an effective method for the extension of the coverage area [54, 55]. Unlike RF technology, small-scale fading is distance-dependent for FSO systems, which provides the opportunity to reduce path loss by shortening the distance of relay-based systems, which cause the improvement of small-scale fading channel statistics [56]. Relay-based FSO technology offers many additional advantages, including lower initial costs, higher capacity and extended coverage while keeping sufficient reliability [57]. The outage probability is minimized when consecutive nodes are placed equidistantly along the channel from S to D [58]. In such a scheme, amplify and forward (AF), and decode and forward (DF) transmission protocols are the most commonly used techniques for a relay-based system.

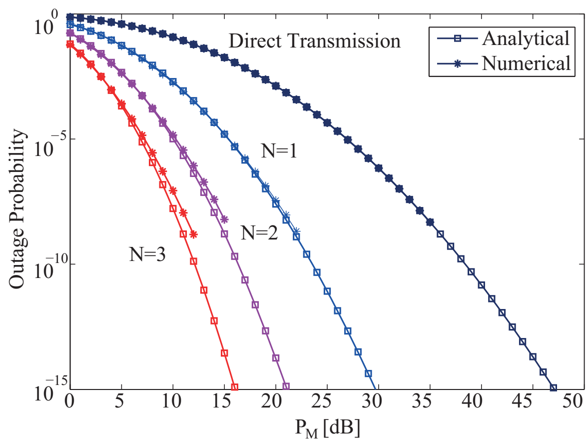

(a)

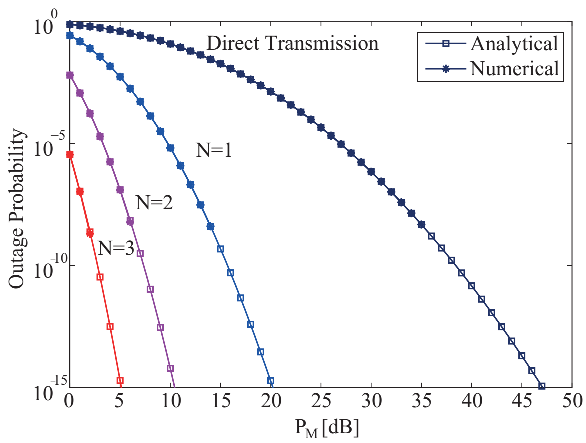

(b)

Figure 2.2: Outage probability of a serial FSO system a) AF and b) DF schemes [49]. N is the number of hops and P_M denotes power margin.

Traditional AF relaying FSO systems were built on the assumption that the relay used optical to electrical (OE) conversion, amplification and electrical to optical (EO) conversion [49, 59]. Whereas, for DF protocol, after conversion following decoding and re-encoding of the signals to improve the SNR [60, 61]. DF systems offer better performance, but require clock recovery and synchronization at each relay node which significantly increases the complexity of the system [62]. A performance comparison of AF and DF systems can be seen in Figure 2.2.

Current relay systems are built on OE/EO high-speed conversion modules which increase the complexity, latency and cost of the system [62]. Nonetheless, currently there is a strong desire for an all-optical network structure to emerge because of higher bandwidth and improved security. This is possible by keeping a signal in the optical domain by using optical amplifiers and low-speed electrical circuits for gain control.

The concept of all-optical FSO relaying was demonstrated for the first time in 2002 [63]. In this work, a 4-channel dense wavelength division multiplexing (DWDM) system was tested over 250 m reaching a bit rate up to 10 Gb/s. An outage performance of dual hop configuration using erbium doped fibre amplifier (EDFA) and considering the effect of amplified spontaneous emission (ASE) was analyzed in [56]. Moreover, a comparison of outage performance between conventional OE and EO conversion and all-optical relaying with EDFA while taking into account the effect of the optical degree of freedom (DoF) presents a favourable trade-off between complexity and performance and can be used as a low-complexity solution [64]. In ideal cases the power performance gain can reach 14.7 dB in comparison to the direct transmission. Optical DoF quantifies the ratio of the bandwidth of the optical filter to the electrical bandwidth. Due to noise accumulation at each R_n, link performance significantly degrades. As a solution, the all-optical regenerate and forward system (consisting of a highly nonlinear fiber and a Gaussian band pass filter) was proposed to suppress the ASE and background noise at each R_n for the next re-transmission [62]. It is shown that the all-optical regenerate and forward system outperforms the AF system for dual hop configuration by about 73% at a bit error rate

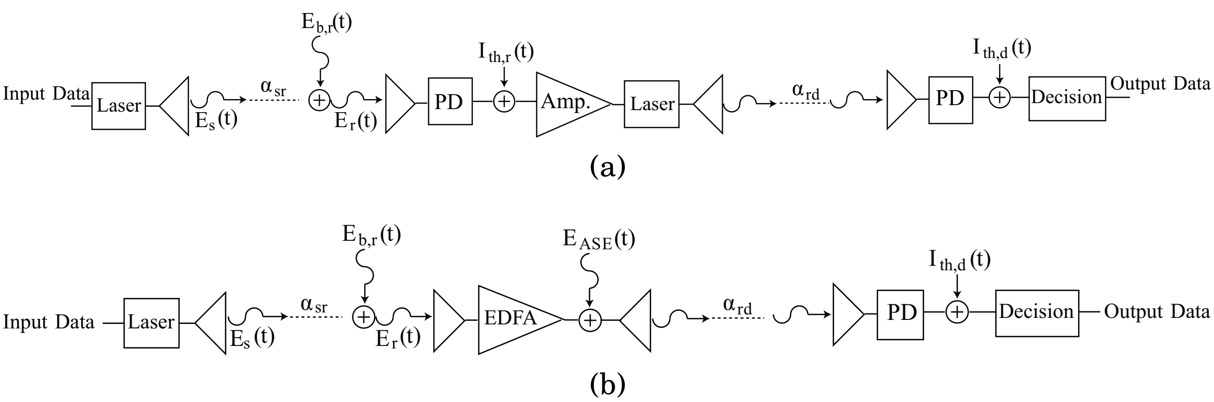

Figure 2.3: Block diagram of FSO AF relay systems with (a) electrical amplification and (b) optical amplification using an EDFA (PD: photodetector) [56].

(BER) of 10^{-5}. However, work in [62] presents BER performance through a Monte Carlo simulation with no taking into account the effect of ASE noise. On the other hand, a cooperative diversity approach adopting parallel relaying schemes offers an effective way to mitigate atmospheric turbulence-induced fading [65]. However, distance-dependent turbulence fading is still the main concern for the assessment of system performance.

Many studies have investigated multihop all-optical FSO systems using EDFA [56, 64, 66–70]. Increasing the number of hops to infinity could not improve system performance. For instance, the experimental setup for a 5 km link span and $C_n^2 = 1.7 \times 10^{-14}$ m$^{-2/3}$, the best system performance was reached with 8 relay nodes, but upon increasing to more than 10 nodes, system performance actually degraded [56]. A dual-hop FSO system working over a Gamma-Gamma turbulence channel was reported in [67], showing that the required transmitted power is reduced proportionately to the amplifier gain. However, it is necessary to take into account the influence of optical DoF that can significantly alter the performance of EDFA [64].

The performance of all-optical FSO relaying can be significantly improved by a combination of EDFA and an optical hard-limiter [69, 70], whereby the optical hard-limiter is used to mitigate accumulated background noise. Nevertheless, the drawback of the proposed solution is that system performance is dependent on the threshold level of the optical hard-limiter. It is therefore essential to set an optimal threshold based on the strength of the turbulence and background noise level. For instance, it is possible to reach a distance of 6 km with 4 relays, while 8 relays are required for the same system including EDFA. For even better BER performance, the idea based on the Mamyshev method with an ultrashort pulse was experimentally demonstrated in [71]. The dual hop Mamyshev all-optical system improved upon the performance by a factor of hundred when compared to the non-regenerate AF scheme in terms of BER.

2.2 Relay-Assisted Visible Light Communication System

The VLC system consists of three building blocks (a transmitter, a channel and a receiver). Although, illumination has made great strides from incandescent lamp to LED-based light, light sources still represent the main limitation of current VLC technology. Nonetheless, developments in the industry and the production of LEDs offer higher switching abilities, higher transmission power and wider illumination angles.

In general, white light is the most available source for indoor and outdoor environments. Two approaches are widely used to produce white light: (*i*) The combination of a blue Indium Gallium Nitride (InGaN) chip and Yttrium Aluminum Garnet (YAG) coating. The coating transforms the blue parts of light to lower frequencies to create a white color [72] when the amount of the phosphor layer is essential, as it defines the color temperature of the light source. (*ii*) White light is obtained as a combination of more chips of different colors, typically red-green-blue (RGB) colors. The resulting color is defined based on the intensity of the individual color components. Multi-color LEDs are attractive as they create the possibility of a parallel transmission using wavelength division multiplexing (WDM) which can significantly increase system throughput [73].

However, with the rapid emergence of display applications and an increase in their resolutions, the dimension of LED chips is becoming too large. It has led to the development of micro-scale LED structure (μ-LED) with dimensions of less than 100 μm × 100 μm and an organic light emitted diode (OLED). However, μ-LEDs have the potential to improve luminescence efficiency for high-intensity lighting, together with better current spreading and the lowering of the self-heating effect [74]. Recently, μ-LEDs, based on an AlGa structure with diameters of 24 μm, can overcome the 800 MHz bandwidth [75]. Such a bandwidth is possible due to the extremely low capacitance of LEDs.

An alternative approach is to use OLEDs which offer several benefits including mechanical flexibility, a long lifetime and low heat dissipation. Due to their organic structure, OLED panels have a limitation in brightness and stability. The main limitation present in OLED panels is a very narrow bandwidth reaching only hundreds of kHz which limits the data rate compared with an LED-based system. To overcome these challenges it will be necessary to move from large thin panels with high capacitance toward the nano-fabrication of large matrices with small OLEDs featuring a large bandwidth [76]. Table 2.1 presents a comparison of parameters and applications of different types of LEDs.

Equalization, MIMO, implementation of WDM and multi-carrier modulations have contributed to achieving the high data rate development of signal processing techniques. These techniques have increased data rates from Mb/s to dozens of Gb/s [77] over the past few years.

	white LED	RGB LED	μ-LED	OLED
Bandwidth	few MHz	dozens of MHz	hundreds of MHz	hundreds of kHz
Efficiency	> 250 lm/W	90 lm/W [72]	N/A	220 lm/W
Cost	low	high	high	very low
Application	illumination	illumination	automotive, display	display

Table 2.1: Comparison of different types of LEDs.

Unlike RF, VLC technology uses an intensity modulation and direct detection (IM/DD) approach. In the case of the IM/DD system, the signal must be real and non-negative. In most cases, baseband or multicarrier modulations are applied to VLC systems. However, most early works on VLC used on off keying (OOK) modulation techniques because of their simplicity. In [78], a non-return-to-zero (NRZ) OOK modulation was introduced for the transmission of 10 Mb/s over the VLC link. To upgrade data rate, the slow yellow phosphor effect has been mitigated by a blue filter resulting in an increase of the data rate to 40 Mb/s [79]. Similarly, in [80] a combination of blue filtering with an equalization technique at the receiver was proposed to achieve a data rate of 125 Mb/s. In [81] it was proven that the avalanche photodiode offers almost 2× data performance improvement over a PIN photodiode. The next improvement was attained by combining RGB frequencies to produce white light. However, the RGB white LEDs need three independent driver circuits to generate white light. A different approach was presented in [82] where the simplest NRZ OOK system with a single RGB LED (only red to transmit) was demonstrated achieving a bit rate of 477 Mb/s and a duo binary technique with bandwidth enhancement (using transmitter and receiver equalization) was employed to achieve 614 Mb/s [83]. The transmission setups for the configurations of RGB sources are shown in Figure 2.4.

Pulse width modulation (PWM) offers an efficient way to achieve modulation and dimming control. In PWM, the width of the pulse is adjusted to the desired level of dimming while the pulse carries the signal. The modulated signal is transmitted during the pulse duration and the LED operates at full brightness during the pulse. One benefit

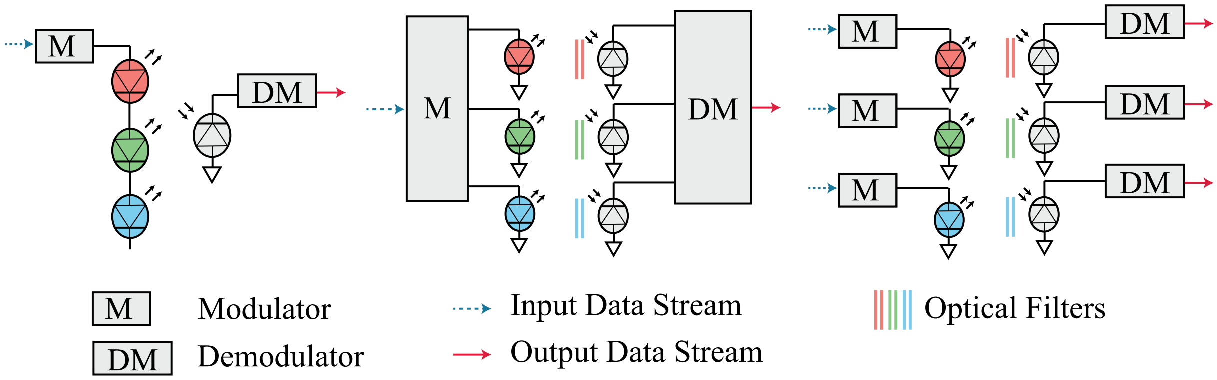

Figure 2.4: Possible configurations for utilizing light sources in VLC [84]

of PWM is that it accomplishes dimming without changing the intensity level of the pulses, therefore a color shift does not occur as in the case of OOK. The drawback of PWM is its limited data rate. To overcome the limited data rate, a combination of discrete multitone modulation (DMT) and mapped quadrature amplitude modulation (QAM) symbols into DMT carriers has been used in [85] to achieve a link rate of 513 Mb/s.

The main limitation of the previously discussed single carrier modulation schemes is that they suffer from high inter symbol interference (ISI) due to the nonlinear frequency response of the VLC channel. Multi-carrier modulation, nonetheless, can significantly improve bandwidth efficiency at the expense of reduced power efficiency due to the DC offset [15].

Multicarrier modulation formats as orthogonal frequency division multiplexing (OFDM) have been widely adopted in RF communication due to their ability to effectively combat the ISI and multipath fading. The authors in [86] first proposed the use of OFDM for VLC whereby the data stream is divided into multiple orthogonal subcarriers and the data is sent into parallel sub-streams modulated over the subcarriers. OFDM for VLC can reduce ISI and does not require a complex equalizer. There are, however, multiple challenges regarding its implementation [87]. First, the OFDM technique needs to be adapted for IM/DD systems such as VLC because OFDM generates a complex signal which needs to be converted to real-valued signals. This can be achieved by using a Hermitian symmetry constraint on the subcarriers and then converting the time domain signals to unipolar signals.

Since the inverse fast Fourier transform (IFFT) block independently sums modulated subcarriers, these components in a DC biased orthogonal frequency division multiplexing (DCO-OFDM) signal could sum constructively, increasing signal amplitude and the chance of signal distortion, causing overheating at high peaks due to the nonlinear operation of the LED chip [88]. The scheme of the DCO-OFDM VLC system is depicted in Figure 2.5. Some of the subcarriers could reach below the threshold of the voltage limit of the LED. This random variation results in a high peak-to-average power ratio (PAPR) which is a significant issue of OFDM [88]. Several methods have been proposed to mitigate the effect, such as the use of a linear amplifier or a power back-off. But the most common method to overcome the problem is to clip the signal at peak levels [89]. An asymmetrically clipped

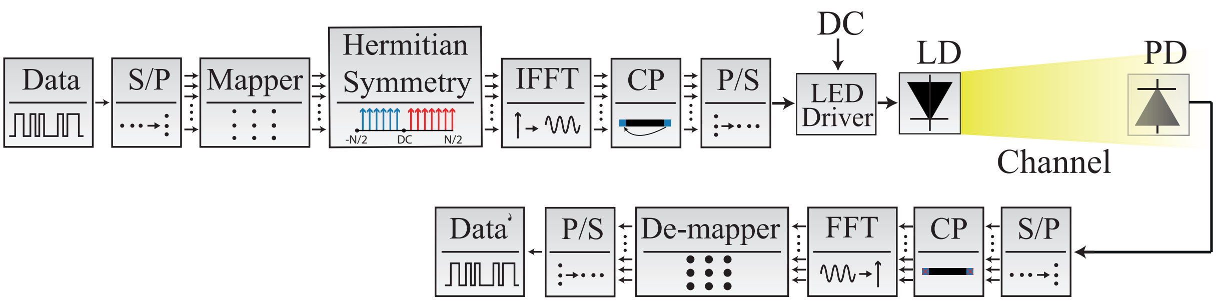

Figure 2.5: Schematic diagram of DCO-OFDM system

optical orthogonal frequency division multiplexing (ACO-OFDM) [90] clips the OFDM signal at zero level, while data is carried in odd subcarriers only. The method reduces the amplitude of the transmitted OFDM signal and is far more power efficient than DCO-OFDM for a given bandwidth, albeit at the expense of losing half of the available bandwidth [91].

Despite these challenges, OFDM for VLC offers great potential in terms of achievable link data rates, such as in [92] where a data speed of 1.6 Gb/s over a 1 m link employing a combination of 16-QAM and OFDM was reported. For instance, a 3 Gb/s VLC system was reported in [93] using a bit and power-loading technique applied to compensate for performance degradation at frequencies outside the 3 dB modulation bandwidth. In 2019, a system reaching 35 Gb/s for a 4 m link span with a four-color multiplexed high-speed VLC system using a micro-electro-mechanical system was designed [77].

Recently, the research community has turned its attention to the carrierless amplitude phase modulation (CAP) format as an alternative to OFDM [94, 95]. CAP is a similar modulation technique to QAM with the main difference being that CAP uses finite impulse response (FIR) filters to generate carrier frequencies unlike QAM, which utilizes a local oscillator. This results in a simpler solution for CAP receivers since time-reversed matched filters are deployed. The schematic diagram of the CAP VLC system is depicted in Figure 2.6.

In previous research, it was experimentally shown that CAP outperforms OFDM in VLC when using the same experimental setup. The improvement in achieved transmission speed was 22% [95]. Nevertheless, CAP requires a flat channel frequency response, which is rare in VLC networks, due to the LEDs acting as a low pass filter. To overcome this, a new approach called multi carrierless amplitude phase modulation (m-CAP) was proposed for short range optical fiber links [96]. The available bandwidth was split into 6 sub-bands and a 6-CAP system outperformed the traditional single CAP system. Splitting the bandwidth into m sub-bands has two key advantages over a single CAP: (*i*) relaxing the flat frequency response requirement and (*ii*) allowing for the adjustment of a number of bits-per-symbol for each sub-band. For instance, in [97] the authors showed that for

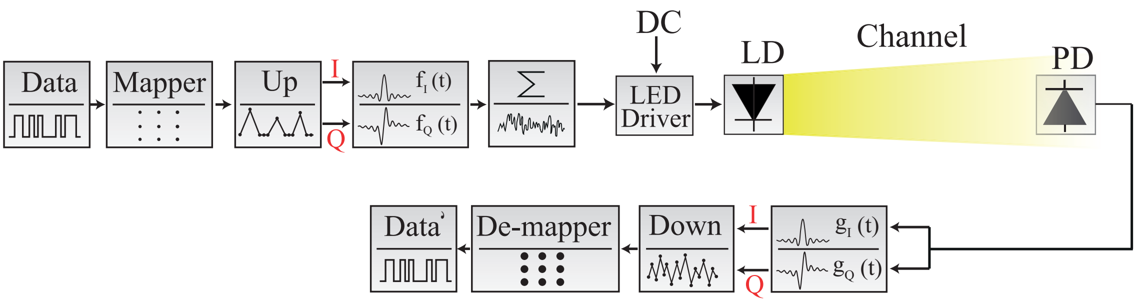

Figure 2.6: Schematic diagram of CAP system

a higher number of sub-bands, a higher transmission capacity can be supported. The highest data rate ~31.5 Mb/s was achieved in the 10-CAP system, using an LED with a very low 4.5 MHz modulation bandwidth. Increasing the number of sub-bands results in a lower bandwidth occupied by each subcarrier. Thus, they are less prone to frequency dependent attenuation caused by the first order low pass filter behavior of an LED and, hence, can support higher throughput. A highly band-limited VLC link was investigated in [98]. The low pass filter cut-off frequency was set to 0.1 of the signal bandwidth and it was shown that the 10-CAP system can support up to a 40% improvement in the bit rate compared to the traditional CAP for the same BER target. By using a high order of CAP modulation, together with four-color multiplexed and hybrid equalizer (see the depicted scheme in Figure 2.7), a data rate of 8 Gb/s was experimentally achieved over a 1 m indoor free-space transmission [99].

VLC technology offers many essential advantages, but also endures several drawbacks. The disadvantages are caused predominantly by the properties of light [100]. Excluding the relatively limited transmission bandwidth mentioned earlier, there are three fundamental limitations (*i*) the LOS condition, (*ii*) limited transmission range and (*iii*) ambient light interference and receiver noise. In indoor environments, the LOS path cannot always be guaranteed due to objects, the movement of people and room layout [101]. To address this problem and to offer seamless communication, as well as to maintain uninterrupted data access, even in temporarily shadowed regions, a number of solutions have been proposed including visible light communication receivers utilizing angular and spatial diversity to enable protection from signal blocking [26]. A combination of MIMO and beamforming can also significantly improve performance under a random shadowing effect [102]. One of the most promising techniques of how to cope with limitations (*i*) and (*ii*) is the implementation of the advanced VLC network system.

VLC networks are still at an early stage of development. To date, there is no VLC-

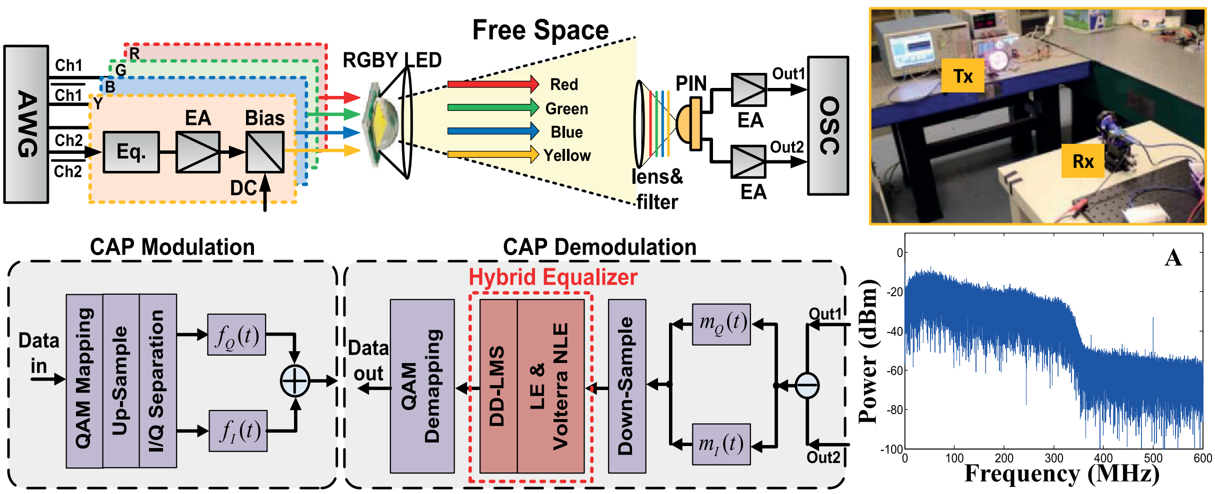

Figure 2.7: Experimental setup of the WDM VLC system employing high-order CAP and a hybrid post equalizer [99].

based networking cross-layer protocol. The vast majority of recent research focuses on partial segments of individual layers [24, 84, 100]. Moreover, the current IEEE 802.15.7 standard [103] does not cover relay-based VLC systems and does not address the full-duplex communication problem. However, IEEE standard 802.15.7 supports three network topologies, namely peer-to-peer, star and broadcast, as shown in Figure 2.8.

In order to improve connectivity, a relay-based VLC employing an LED lighting triangular system topology was analytically investigated in [104]. In the case of light from an LED source mounted on the ceiling and not reaching the user directly, information can be transmitted via a relay node. In [105], connectivity performance of mobile users, based on mobile optical relays in a cooperative multi-hop VLC, was investigated. Improvement doubled in mobile connectivity performance by using the multi-hop scenario due to the user's density, coverage range ratio between hop regions, relay probabilities, and velocity of the mobile users.

The access methods are derived based on purely RF communication systems, without consideration of VLC benefits or channel characteristics. Moreover, the current systems are considered predominantly as a point-to-point link which results in a complicated implementation as regards ad-hoc networking. The current IEEE standard 802.15.7 supports a wireless medium access control (MAC) protocol, such as carrier sense multiple access with collision avoidance (CSMA/CA) access scheme. The idea of CSMA/CA is that a node should be able to listen while transmitting data to detect a possible collision from other nodes. Unfortunately for the VLC system, this access scheme suffers from delays and energy inefficiency [106, 107]. Moreover, in the case of CSMA/CA, a hidden node problem occurs when a node cannot see other nodes in the field of view (FOV). The influence of a hidden node on system performance was investigated in [108].

However, current research adheres to the activities of cellular technology. Nonetheless, the vast majority of conventional RF access schemes cannot be directly used without modifications. One example of an access scheme is orthogonal frequency division multiplexing access (OFDMA) adopted in fourth generation (4G) systems. The OFDMA scheme

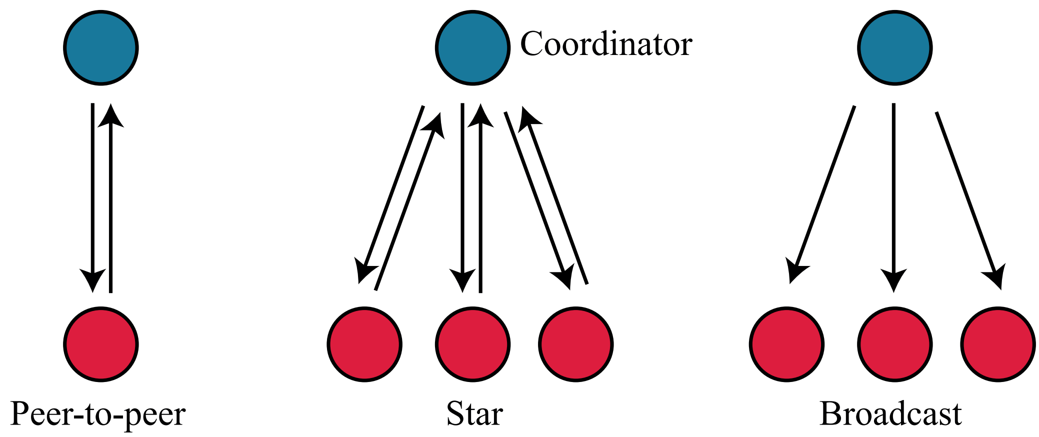

Figure 2.8: IEEE 802.15.7 network MAC topologies

serves multiple users by dividing bandwidth into allocated subcarriers and shares power resources among users. In the case of the VLC system with IM/DD, the DCO-OFDM and ACO-OFDM are the most common modulation formats for the multi-access scheme. A comparison of BER performance, receiver complexities, as well as PAPR, for two versions of OFDMA was investigated in [109]. An interleave division multiple access OFDMA with ACO-OFDM reaches higher power efficiency than the conventional OFDMA method, especially for higher bit rates. To enhance the signal to interference plus noise ratio (SINR) of edge users, joint multiple LEDs for transmission were proposed in [110] which can achieve a 68% throughput system improvement compared to a single system. The next method on how to improve the performance of an edge user is frequency reuse. A combination of DCO-OFDM and fractional frequency reuse significantly reduces interchannel interference (ICI) and offers a good balance between average spectral efficiency and system complexity [111].

However, the current 5G mobile standard supports non orthogonal multiplexing access (NOMA), which is capable of significantly increasing system throughput and user connectivity in VLC networks [112]. Generally, the NOMA system is separated into three versions, namely power-domain, code-domain and spatial domain (beamforming) [113]. In VLC systems, power-domain NOMA is mostly adopted, in which appropriate power levels are allocated to end users due to corresponding channel conditions [114]. The adaptation of the NOMA scheme for usability in VLC systems is motivated predominantly by: *(i)* it is efficient and flexible in multiplexing only a small number of users, *(ii)* the VLC system offering high SNR where NOMA outperforms orthogonal schemes and *(iii)* receivers relying on channel state information (CSI), which can be estimated relatively accurately due to the quasi-static mobility of end users. For power allocation NOMA, the majority of works have investigated the optimization of the throughput in VLC networks. A single LED VLC system, using the Karush-Kuhn-Tucker optimality conditions, outperforms a conventional

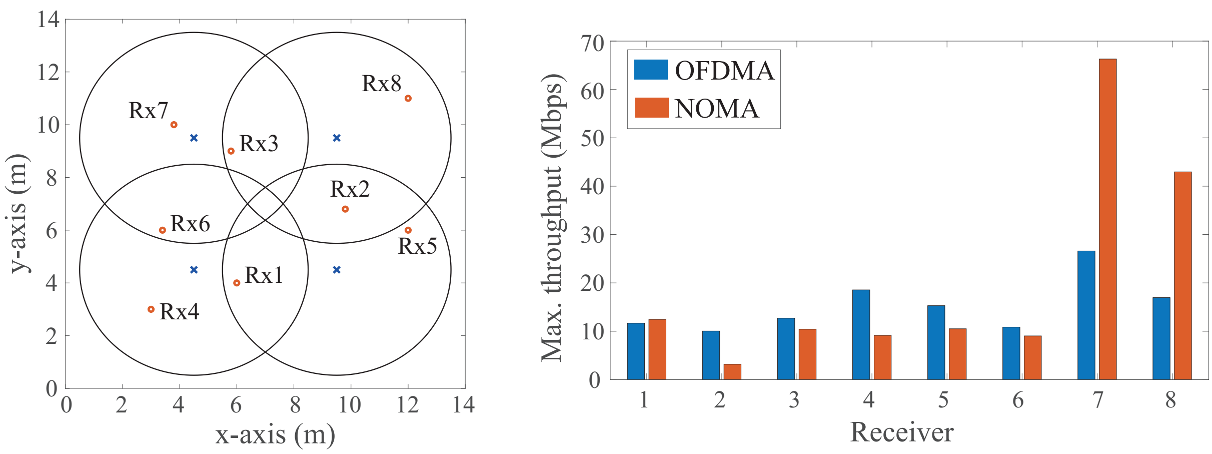

Figure 2.9: Illustration of the room scenario with maximum achievable throughput using the NOMA and OFDMA approaches, where × and ∘ refer to access points and user locations, respectively [115]

OFDMA scheme [116]. Extending the previous work by combining OFDM-power line communication (PLC) and a NOMA system makes it capable of attaining an increase in higher data rate of about 20% [117]. The system can be improved by an optimally and computationally efficient optimization algorithm [118] outperforming the conventional NOMA VLC system for both LOS and non line of sight (NLOS) systems [119].

A multi-LED system can outperform an OFDMA NOMA system for edge users and highly interference users as is shown in Figure 2.9 [115]. On the other hand, when using a gradient projection algorithm, the NOMA scheme achieves higher sum throughput than the time division multiplexing access (TDMA) and OFDMA schemes [120]. Moreover, NOMA can also be used for the MIMO VLC system. An experimental investigation of a single carrier 2×2 MIMO VLC system using frequency interference cancellation has been done in [121], however, the authors do not consider the power allocation issue. A normalized gain difference power allocation algorithm has been proposed for reducing the complexity and improving the efficiency of the NOMA-MIMO system with multiple users [122].

2.3 Hybrid Wireless Communication Systems

Hybrid wireless systems can integrate two or more technologies (*e.g.*, FSO/RF, VLC/RF, VLC/FSO, VLC/WIFI and many other combinations) into a hybrid network and exploit their advantages. Hybrid systems can play a key role in link reliability, wireless connectivity and interference reduction [14]. As was mentioned in previous chapters, the performance of OWC technologies can be affected by many factors including turbulence, dense fog, or a pointing error in the case of FSO. These factors can significantly influence the reliability and performance of an FSO system. One possible solution to improve link performance is a combination of RF and FSO technologies. By combining these technologies, seamless connections, boasting large range, reliability and bandwidth can be established in current networks [123].

Analyses of the AF dual-hop RF/FSO system combining a Rayleigh distributed RF link and the FSO part simulated as a Gamma-Gamma turbulence channel was introduced for the first time in [124]. Extending the previous work considered the pointing error in the FSO link [125]. The dual-hop system outage performance, where RF was modeled as Rayleigh fading and FSO as M-distributed fading, was investigated in [126]. The effect of turbulence and the pointing error on the channel capacity of the RF/FSO system with a Nakagami-m distributed RF link was studied in [127]. However, similar work for a DF-scheme was performed in [128]. Heterodyne detection with variable gain and a fixed relay scheme was considered in [129] and achieved a higher capacity of about 1.5 b/s/Hz compared to IM/DD.

For data rate improvement, the combination of the dual hop MIMO-RF/FSO system with a Gamma-Gamma distributed link was presented in [123]. The multi-user hybrid DF-

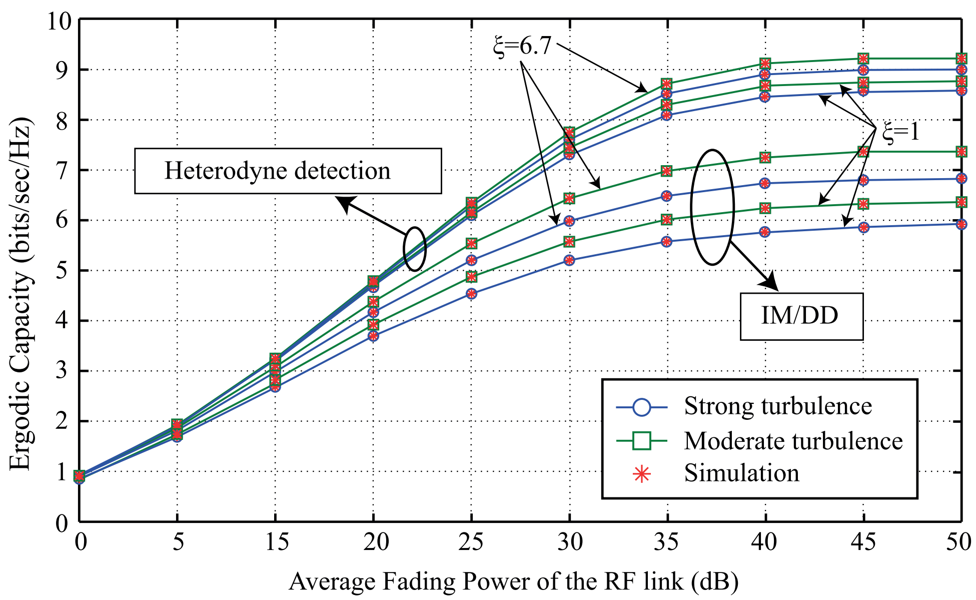

Figure 2.10: Ergodic capacity results showing the performance of heterodyne and IM/DD techniques under turbulence conditions for varying pointing errors (ξ) [129]

based system was analyzed in [130] with the derivation of symbol error probability of each user. The idea of extending the previous work about an optimal power allocation scheme for a multi-user system was proposed in [131] to optimize overall system performance.

In the case of VLC technology, the constraints mentioned in previous chapters lead to the use of predominantly RF hybrid technologies to mitigate LOS blockages, inter-cell interference and handover issue, which results in finding a solution to distribute users among the RF and VLC access points to improve system performance with acceptable fairness of the system [132]. Access point assignment was first studied in [133] and found an optimal load balance between one RF access point and one VLC access point. A method where all traffic is at first assigned to a VLC network, followed by users receiving a lower data rate than the defined RF threshold are re-allocated to the RF access point [134]. Dynamical user distribution, based on channel conditions for multiple VLC and RF access points, was proposed in [135]. This implementation improved system performance by about 40%, compared to a single VLC or RF network. The implementation of centralized and distributed algorithms for resource allocation among both types of access points was analyzed in [136].

To limit the number of handovers and their hard implementation in VLC, in [137], a dynamic load balance algorithm which assigns quasi static users to VLC access points and moving users to RF access points was proposed. Based on previous work, two types of load balancing algorithms were proposed in [138]. A joint optimization algorithm achieves more than a 1.5 times higher data rate than a separate optimization algorithm. However, with significantly higher computation complexity, it reaches even more than a 1000 times of the separate optimization algorithm. A different approach is proposed in [139] based on users' statistical information of channel blockage: the users which are influenced by channel blockages should switch to RF access points. To decrease optimization complexity, a load balance fuzzy logic-based system was proposed in [140]. A user scores an access point based on several conditions (throughput, SNR and interference) and then, based on score, decides whether to connect to RF or VLC access points.

Recently, the hybrid FSO/VLC communication system has gained wide popularity due to its properties, such as high data rate, security and relatively low interference. A cascaded FSO-VLC system consisting of multiple VLC access points using a DF relaying scheme was proposed in [141]. The FSO link is characterized by path-loss, pointing error and atmospheric conditions while the SNR for both links is statistically characterized, taking into account the randomness of end user positions for indoor and outdoor environments. The achieved results provide a compelling solution for current broadcasting systems. Following the extension of the previous work on parallel RF/FSO, an outdoor link was proposed in [142]. The effect of the outdoor parallel link significantly improves system performance, especially in very strong turbulence conditions where outage probability can be improved approximately 58 times. The performance of the hybrid DF relaying

VLC/FSO/VLC system is derived in terms of a closed-form expression for the outage probability [143] for the VLC modeled as the Lambertian emission model and the FSO link as a Gamma-Gamma channel under the impact of turbulence, semi-angle and FOV of a detector. The first experimental application of the hybrid FSO/VLC system was presented for space-air-ground-ocean-integrated communication in [144]. A simple network mechanism for identification, user mobility control and network routing is designed for the interconnection of VLC access points. The system was designed to transfer data rate 450 Mb/s over a 1 m long OFDM-based VLC interconnection and a 960 Mb/s OOK-based FSO over 430 m without a turbulence condition.

CHAPTER

3 Objectives of the Thesis

Relaying techniques and OWC technology, in particular, have recently received increasing attention amongst researchers. Nevertheless, there are still many challenges awaiting theoretical, analytical and experimental verification. Therefore, the dissertation thesis has the following main goals:

- Proposal and experimental verification of an all-optical FSO relaying scheme for a last mile outdoor link
- Analytical description of relaying schemes for VLC technology and their development
- The methodology of design and analysis of a hybrid OWC system for last mile and last meter interconnection

In order to meet the main goals of the thesis, the following specific milestones have been set:

- To analyze the performance of the FSO system under atmospheric conditions.
- To investigate the performance of non-relaying and relaying all-optical FSO schemes.
- To develop a theoretical model of the VLC-based relaying system and to evaluate link performance via analytical and numerical simulations.
- To experimentally verify relaying VLC schemes based on the analytical and numerical simulations.
- To propose a VLC multi-user data allocation system for an indoor environment.
- To design and verify the performance of a hybrid OWC communication system consisting of FSO and VLC links.

CHAPTER 4 Achieved Results

The core of this thesis is based on published papers in scientific journals with impact factor and papers in international conference proceedings. The original papers with bibliographic citations contributing to the thesis are provided in the following sections.

Section 4.1 presents analyses of long term evolution (LTE) signal transmission over combined fiber and FSO systems. The proposed scenario offers an effective utilization for hybrid FSO/RF architecture providing simple signal conversion for a base station. Moreover, the impacts of atmospheric conditions are discussed providing an extended description of noise conditions.

Section 4.2 provides the concept of an all-optical FSO relaying system under turbulence conditions for scenarios combining a single FSO link and a dual-hop FSO link. The results show that the dual-hop link produces improved BER performance in comparison to the single link. Moreover, it is shown that such a system, with all optical switching for intermediate transfer in ad-hoc networks, can considerably mitigate turbulence-induced fading.

Section 4.3 focuses on the utilization of relaying schemes for VLC technology. The behavior of a mobile user acting as a relay considering realistic locations of receivers and transmitters on a standard mobile phone within an indoor environment is investigated. I derived a new analytical description of BER performance on the azimuth and elevation angles of the mobile relay device.

In section 4.4, the relaying scheme model was verified and extended as defined in section 4.3. I experimentally investigated performance for AF and DF relaying techniques for a range of indoor link spans. I showed that the relaying scheme can outperform a single VLC link by more than 60% over a transmission distance of 7 m.

Section 4.5 focuses on the utilization of the CAP scheme for multi-user inter-connectivity. I developed a modified version of m-CAP, called allocated multi-CAP (Am-CAP), which provides significantly higher allocation flexibility for 4-users with the same or less computational complexity, compared to conventional counterpart.

Following previous research in separated VLC and FSO areas, section 4.6 focuses on the performance of joint last mile hybrid interconnection of FSO and VLC technologies. The system performance of the VLC part is influenced by the effect of the band-limited system and caused by a real limitation of the LED frequency response. It is shown how the performance of the m-CAP modulation scheme is strongly dependent on the parameters of the pulse shaping filters. On the other hand, the impact of atmospheric turbulence on the FSO part is also discussed to propose the best performance of a joint FSO- and VLC-based system.

4.1 Experimental Verification of Long-Term Evolution Radio Transmissions over Dual-Polarization Combined Fiber and Free-Space Optics Optical Infrastructures

This chapter is a version of the published manuscript:

J. Bohata, S. Zvanovec, **P. Pesek**, T. Korinek, M. M. Abadi, Z. Ghassemlooy, "Experimental verification of long-term evolution radio transmissions over dual-polarization combined fiber and free-space optics optical infrastructures," Applied Optics, vol. 55(8), pp. 2109–2116, 2016.

Connection to my Ph.D. thesis:

With the immense development of 5G technologies and gigabit services, the current requirements on network infrastructure are growing rapidly. A radio over fiber (RoF) or radio over free space optics (RoFSO) may offer a spare option to the challenges of future high data rate fronthaul networks. Furthermore, by avoiding the digitization process, the complexity and energy consumption of the base station hardware are significantly reduced. For such a system, FSO involving a dual polarization (DP) multiplexed link has been investigated, especially in terms of SNR performance under atmospheric conditions. Moreover, the proposed technique can be adopted for other radio services such as WIFI or worldwide interoperability for microwave access (WiMAX), thus leading to improved network convergence.

applied optics

Experimental verification of long-term evolution radio transmissions over dual-polarization combined fiber and free-space optics optical infrastructures

J. Bohata,[1,*] S. Zvanovec,[1] P. Pesek,[1] T. Korinek,[1] M. Mansour Abadi,[2] and Z. Ghassemlooy[2]

[1]CTU in Prague, Department of Electromagnetic Fields, Technicka 2, Prague, Czech Republic
[2]Optical Communications Research Group, NCRLab, Northumbria University, Newcastle upon Tyne NE1 8ST, UK
*Corresponding author: bohatja2@fel.cvut.cz

Received 30 November 2015; revised 28 January 2016; accepted 29 January 2016; posted 1 February 2016 (Doc. ID 254703); published 10 March 2016

This paper describes the experimental verification of the utilization of long-term evolution radio over fiber (RoF) and radio over free space optics (RoFSO) systems using dual-polarization signals for cloud radio access network applications determining the specific utilization limits. A number of free space optics configurations are proposed and investigated under different atmospheric turbulence regimes in order to recommend the best setup configuration. We show that the performance of the proposed link, based on the combination of RoF and RoFSO for 64 QAM at 2.6 GHz, is more affected by the turbulence based on the measured difference error vector magnitude value of 5.5%. It is further demonstrated the proposed systems can offer higher noise immunity under particular scenarios with the signal-to-noise ratio reliability limit of 5 dB in the radio frequency domain for RoF and 19.3 dB in the optical domain for a combination of RoF and RoFSO links.

OCIS codes: (060.2605) Free-space optical communication; (060.5625) Radio frequency photonics; (010.1330) Atmospheric turbulence; (060.2310) Fiber optics.

http://dx.doi.org/10.1364/AO.55.002109

1. INTRODUCTION

The deployment of small cells and the use of higher radio frequency (RF) bands (e.g., millimeter-wave) are two possible options to fulfill the demand for higher data rates in next-generation wireless access networks. The third-generation partnership project (3GPP) of long-term evolution (LTE) with low latency, also known as the fourth-generation technology, supporting high data rates of up to 300 and 75 Mbps for the downlinks and uplinks, respectively, has been proposed and developed [1,2]. LTE intended for urban areas and operating at a carrier frequency of 2.6 GHz imposes higher loss in wireless transmission, which limits the cell radius due to the degradation of the signal-to-noise ratio (SNR) [3]. In small-cell-based systems, optical fibers are considered as an ideal backhaul medium to provide sufficient bandwidth as well as a future-proof capacity upgrade. More recently, cloud-based radio access networks (C-RAN) technology has been proposed as a cost-effective and power-efficient option for deploying small cells to meet the capacity demand of future wireless access networks. C-RAN decouples the digital baseband processing unit (BBU) from the largely analog remote antenna unit (RAU) and moves it to the BBU pool or BBU hotel, thus allowing for the centralized operation of BBUs and a scalable deployment of RAUs as small cells [4]. In such schemes, optical fiber (OF) communications technology plays a significant role when developing network infrastructures, particularly for connections between adjacent cells, RAUs, and a central unit pool. OF technology covers approximately 35% of the connections between base stations (BSs), while the remaining 55% are based on RF wireless technology [5]. This will rise to over 60% of fiber-connected base stations making fourth and upper generations of mobile communications, resulting in optical infrastructures becoming the most suitable medium for transportation of radio signals from/to RAUs. The functions of RAUs can be further simplified by transmitting analog RF signals over OF backhaul networks. Unlike the conventional digital baseband transmission schemes supporting only one service at a time, the radio-over-fiber (RoF) transmission network [6] enables the coexistence of multiple services and multiple operators in shared resources, thereby offering increased link capacity, advanced networking (i.e., dynamic resources and allocations), and features such as wavelength division multiplexing (WDM)

1559-128X/16/082109-08 Journal

[7] without the need for frequency up- or down-conversion. Transmission of the LTE signals over OFs was presented in [8] and highlighted improvements of the OF backhaul in terms of power and cost effectiveness. A field trial demonstration of high-capacity optical super-channel transmission, based on optical orthogonal frequency division multiplexing with hybrid dual-polarization (DP) quadrature amplitude modulation (QAM)/phase-shift-keying modulations, was reported in [9], providing up to 21.7 Tb/s transmission capacity over long-haul optical links. Polarization division multiplexing (PDM) of two distinctive orthogonal frequency division multiplexing (OFDM) signals, based on ultrawide band standards over the RoF system in passive optical networks, was experimentally demonstrated recently in [10] and effectively doubled the capacity of the system. In [11], an experimental investigation of the RoF system over 100 km of fiber was demonstrated using PDM and the RF frequency bands of 2.6 GHz and 800 MHz, with the highest polarization discrimination of ∼30 dB.

However, the application of RoF depends on the availability of installed OFs between various network facilities to connect BBU and RAU within the C-RAN architecture, and therefore it is possible to considerably extend multiple services over one fiber by using several frequency channels or the WDM technique as showed in [12]. Installation of OF cables can be challenging and costly, especially in urban areas with dense building structures. Once OF cables are installed, rewiring then becomes a difficult and time-consuming task when the distribution of wireless users (WU) and the number of WUs are changed. Therefore, a limited amount of installed OFs highlights the usefulness of free space optics (FSO) [13] technology as it offers the same features as OFs, but with considerably reduced deployment cost and significantly higher capacity [14] compared to conventional RF wireless approaches.

The concept of radio over FSO (RoFSO) has been experimentally introduced by combining a full optical FSO system (employing a 1 km FSO turbulent link at a wavelength of 1550 nm) with a digital TV RF signal without any signal conversion in [15,16]. In [17], a Dense WDM system with RoFSO technology was used to transmit a range of various radio services over 1 km of FSO link under turbulence conditions offering a similar bandwidth to OF for both indoor and outdoor (short-range) applications with 99.9% of link availability. Therefore, it is desirable to extend the existing RoF concepts to RoFSO so as to cover the entire optical transmission technology within future C-RAN. In such scenarios, it is essential to determine system statistics under various channel configurations (i.e., OF, FSO, or a hybrid OF–FSO). A typical scenario employing combined RoF and RoFSO systems is shown in Fig. 1. Among the number of challenges encountered in FSO systems, the atmospheric-induced fading effects (both amplitude and phase) of the received optical signal are the most important [18]. RoFSO can transmit all types of RF signals without interference, and therefore increasing the number of independent channels and expanding the capacity in the optical domain becomes highly desirable. WDM based on an optical power allocation scheme, with consideration of the optical modulation index under a total optical transmission power limitation for an adaptive RoFSO link design, was proposed

Fig. 1. Example of RoF and RoFSO scenario adopting C-RAN architecture.

in [19]. A novel wireless network architecture using RoFSO for WLANs, together with an RF assignment mechanism based on RoFSO, was proposed and investigated in [20] and offered efficient frequency utilization in terms of both the throughput and fairness index. A coherent multilevel polarization shift keying transceiver using spatial diversity detection in the FSO channel was theoretically investigated in [21] for different turbulence regimes. The authors reported a predicted power penalty of ∼25 dB at a symbol error probability of 10E-8 for the strong turbulence regime (Rytov variance σ_R^2 of 3.5). The first concept of the dual-polarization-multiplexing RoFSO system proposed for the LTE radio signal was investigated in [22].

In this paper, an optical dual-polarization LTE RoF and RoFSO system for C-RAN networks using the PDM scheme is proposed. Novel experimental results in terms of the measured and simulated error vector magnitude (EVM) statistics are presented and evaluated. We consider four typical channel configurations using combinations of RoF and RoFSO. The performance of the RoFSO system is highly influenced by environmental factors, and thus we focus on the FSO channel under the turbulence regime. Based on the investigation of the channel dynamic range and noise immunity tests, we have extended the measurement results to include EVM characteristics and have derived specific limits of utilizations of RoF and RoFSO systems. We show that the performance of the proposed link based on the combination of RoF and RoFSO for 64 QAM at 2.6 GHz is more affected by the turbulence based on the measured difference EVM value of 5.5%. We further show that the proposed systems can offer higher noise immunity under particular scenarios with the SNR limit of 5 dB in the RF domain for RoF and 19.3 dB in the optical domain for the combination of RoF and RoFSO links.

The rest of the paper is structured as follows: Section 2 introduces the properties of the proposed system with different configurations and atmospheric turbulence. Results from the measurements and simulations are discussed in Section 3, and the conclusions are presented in Section 4.

2. EXPERIMENTAL SETUP

A. Main Setup Description

The experimental setup consists of transmitter (Tx), channel, and receiver (Rx) parts as shown in Fig. 2. On the Tx side, both branches are modulated by two independent RF signals prior to

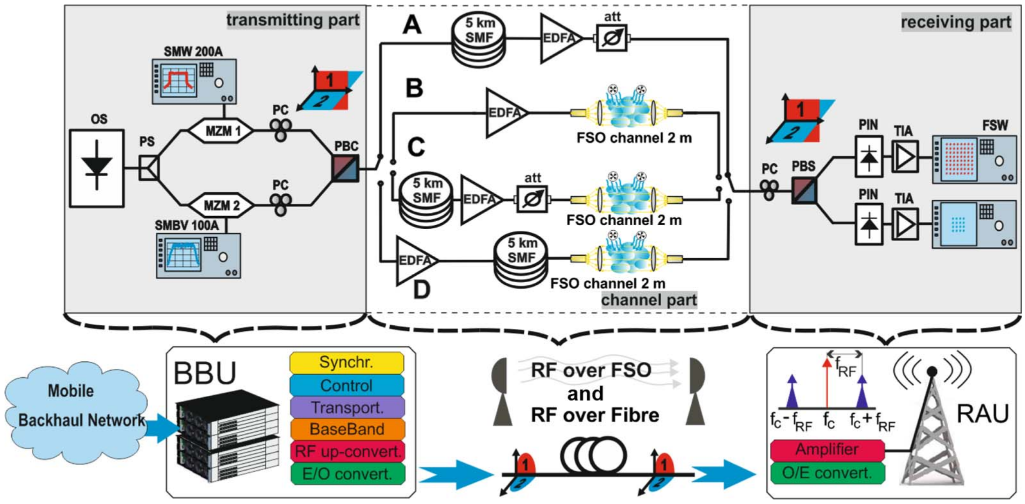

Fig. 2. Schematic diagram of DP-LTE over optical communications for C-RAN architecture (upper part shows laboratory setup; the corresponding network structure is illustrated below).

the application of a polarization-multiplexing technique for transmitting over the optical channel (OF and FSO).

A distributed feedback (DFB) laser diode (ID-Photnonics TL CoBrite Dx4) at a wavelength of 1550 nm was used as the optical source (OS). The output of the OS, passing through a power splitter (Opneti PBS 15-L-1-1-FA), is externally modulated with two digital RF signals (vector signal generators R&S SMBV 100 A and SMW 200 A) of the same carrier frequency and equal bandwidth using Mach–Zehnder modulators (MZMs) (Thorlabs LN81S). For a detailed description of the influence of MZMs on RoF, please refer to [23]. The two orthogonal polarization states of the modulated light beams were controlled using two polarization controllers (PCs) and combined via the polarization beam combiner prior to being launched into standard SMFs. As shown, erbium-doped fiber amplifiers (EDFAs) (Keopsys KPS-BT2-C-10-LN-SA) were used to compensate for the channel loss. Four types of the RoF/RoFSO-based channel configurations were investigated:

(i) Setup A: 5 km of SMF and EDFA
(ii) Setup B: EDFA and the FSO channel
(iii) Setup C: 5 km of SMF, EDFA, and the FSO channel
(iv) Setup D: EDFA, 5 km of SMF (representing the typical transmission span for RoF links), and the FSO channel.

Since the focus in this work was only on the RoF and RoFSO parts of the RAN system, we did not consider retransmission or signal recovery between the OF and FSO parts, which is typically done by the remote RoF units. At the Rx, a PC was used to adjust the polarization states of the incoming optical signal before being fed into a polarization beam splitter (PBS) according to [10] and [11]. PDM optical signals can be potentially demultiplexed by coherent detection and digital signal processing. Polarization dependence of coherent detection can then be managed by means of optical dynamic polarization control or a polarization diversity Rx [24,25]. In a conventional polarization diversity Rx, two sets of Rxs are used to independently detect signal components in the two orthogonal polarization states and the original signal is recovered after combining two components, which is rather inefficient in terms of hardware. However, when two PDM channels are simultaneously transmitted at orthogonal polarization states, a polarization diversity Rx in principle can receive both channels—for example, by using optical dynamic polarization control at the Rx. An all-optic scheme for PDM systems using a dynamic PC has been proposed in [26]. It has been suggested that PDM optical signals can potentially be demultiplexed by combining coherent detection and polarization/phase diversity [27].

The Rx is composed of a pair of encapsulated balanced PIN photodiodes (PDs) and a transimpedance amplifier (TIA, Newport 1544-B50). The output of the TIA was captured for further processing using a signal analyzer (R&S FSV). We used LTE-evolved universal terrestrial radio access (E-UTRA) test models with 16 and 64 QAM in polarization state 1 (noted as Pol 1). An independent digital mobile radio service with 16 QAM, having the same parameters (frequency, bandwidth, and power) as the signal in Pol 1, was launched to polarization state 2 (Pol 2).

The polarization orthogonality was continuously verified by monitoring the parameters at the Tx for one polarization state (i.e., Pol 1) while the signal in the second polarization state (i.e., Pol 2) was switched off and on with no influence observed on either the original power magnitude, SNR, optical signal to noise ratio (OSNR), or the corresponding EVMs. In the experimental setup, we used two commonly adopted LTE frequency bands of 800 MHz and 2.6 GHz with the bandwidth set to 10 MHz. We also set the peak envelope power below the limit of 15 dBm to avoid harmonic distortions at the recovered RF spectrum. All key adopted system parameters are listed in Table 1. For the FSO links, graded-index lenses (Thorlabs 50-1550A-APC) with an aperture of 1.8 mm and convex lenses with a diameter of 25.4 mm (SMPF_115-APC) were used to launch and couple light from/into the SMF. FSO links were subjected to atmospheric turbulence in order to assess the performance of the proposed system.

Table 1. Setup Parameters

Parameter	Value
Carrier frequencies	800 MHz and 2.6 GHz
System bandwidth	10 MHz
OFDM subcarriers	667
OFDM symbols/subframe	7
RF output power	–5 dBm
Modulation scheme	16 and 64 QAM
LTE test models	E-TM2 and E-TM3.2
DFB	
-laser output power	8 dBm
-wavelength	1550 nm
FSO channel length	2 m
FSO channel loss	15 dB
Fiber 5 km loss	1.7 dB
EDFA	
-noise figure	<5 dB
-return loss	> – 40 dB
PIN responsivity	0.75 A/W
TIA bandwidth	10–12 GHz

B. Noise Conditions

In this section, we outline the noise sources associated with the link, in particular the shot noise, thermal noise, and relative intensity noise (RIN).

The power of the shot and thermal noise sources can be expressed as the fundamental noise [28],

$$N_{\text{fund}} = (g_{\text{rf}} + 1)k_B T f + \frac{1}{2} q I_{\text{DC}} f R_{\text{out}}, \tag{1}$$

where g_{rf} is the RF gain, k_B is Boltzmann's constant, T is the temperature, q is the electronic charge constant, I_{DC} is the average PD DC current, and R_{out} is the matching load resistance.

Additionally, there is the excess photon noise due to fluctuations of the intensity of the light source as a result of the beating of various spectral components having random phases. For a purely spontaneous source, it is given as [29]

$$\Delta i_{\text{ex}}^2 = \left(\frac{(1+\alpha^2) I^2 \Delta f}{\Delta v_{\text{eff}}} \right), \tag{2}$$

where α is the degree of polarization and Δv_{eff} is the effective bandwidth. Though all three noise sources can be used to estimate the RIN, it should be noted that Δi_{ex}^2 should only be used for optical sources with a purely spontaneous emission profile.

The RIN, associated with the optical devices, represents the total amount of photon noise per unit bandwidth and is defined as

$$\text{RIN}_{\text{total}} = \frac{P_f^2}{P^2} = \frac{\Delta i_{\text{th}}^2 + \Delta i_{\text{sh}}^2}{I^2 \Delta f} = \frac{4 N_{\text{total}}}{I_{\text{dc}}^2 R_{\text{out}}}, \tag{3}$$

where P_f^2 is the autocorrelated value of the optical power fluctuation at frequency f, which can be measured using an electrical spectrum analyzer to represent the total output noise power spectral density N_{total} delivered to R_{out}. P is continuous wave optical power, which contributes to I_{DC}.

Note that the shot noise is divided into two branches (matching circuit and load). With the links employing optical amplifications, there are additional noise contributions. The primary noise source in optical amplifiers (e.g., EDFA) adopted in optical communications is amplified spontaneous emission (ASE), with a spectrum almost the same as the gain spectrum of the amplifier. When detected, these spontaneously generated photons result in signal-spontaneous (sig-sp) and spontaneous-spontaneous (sp-sp) beat noise currents. The sp-sp beat noise power density is inversely proportional to the OSNR^2, whereas the sig-sp beat noise power density is inversely proportional to the OSNR. The sp-sp beat noise also depends on the baseband frequency, with the noise density decreasing with increase of the baseband frequency. In principle, the sp-sp beat noise intensity spectrum could be as wide as the optical amplifier bandwidth in the absence of optical filtering. From a practical point of view, the excess noise regime is highly important, where the noise level is higher than the level of shot noise due to the influence of sig-sp beat noise, etc. Therefore, here we only consider the sig-sp beat noise, which is given as [28]

$$RIN_{\text{sig-sp}} = \frac{4 n_{\text{sp}} h\nu}{g_{\text{opt}} P_{\text{sig}}}, \tag{4}$$

where n_{sp} is the spontaneous emission factor, h is Planck's constant, ν is optical frequency, g_{opt} represents the optical power gain of the EDFA, F_{opt} is the noise factor of the EDFA, and P_{sig} stands for average optical signal power input to the EDFA. Assuming that $g_{\text{opt}} \gg 1$, Eq. (4) can be expressed as

$$\text{RIN}_{\text{sig-sp}} \approx \frac{2 F_{\text{opt}} h\nu}{P_{\text{sig}}}. \tag{5}$$

F_{opt} is related to the shot noise and the detection scheme. For an ideal detector, $F_{\text{opt}} = 2n_{\text{sp}}$. The degradation of SNR in RoF and RoFSO links is represented by the RF noise factor F_{rf} with respect to thermally limited input and is defined in terms of the RoF link output noise power N_{out} as [28]

$$F_{\text{rf}} \equiv \frac{N_{\text{out}}}{g_{\text{rf}} k_B T}. \tag{6}$$

Typically, F_{rf} is enumerated under $T = 290$ K. We can rewrite the definition of the noise factor by using Eq. (3) and the RF gain as

$$F_{\text{rf}} \equiv \frac{V_\pi^2 \text{RIN}_{\text{total}}}{\pi^2 R_{\text{in}} k_B T}, \tag{7}$$

where R_{in} is the input resistance of the MZM and V_π is a convenient parameter to specify the efficiency of an electro-optic intensity modulator, which is defined as the voltage required to change the optical power transfer function from the minimum to the maximum.

In the experimental test setup, the SNR was set in the RF domain directly via the signal generator by including an additional noise source while the OSNR was controlled by adding a variable optical attenuator placed directly behind the EDFA in setups A and C to avoid the amplifier's gain-induced OSNR fluctuations as depicted in Fig. 2. In setup C, we positioned the optical attenuator in front of the optical link to maintain the desired OSNR level over the FSO channel. OSNR was measured using an optical spectrum analyzer. Here, we have adopted the intensity modulation with direct detection (IM/DD) scheme and used single-drive MZMs which were biased at their maximal transmission point. At the input of the MZM, the field waveform (in time t) can be expressed as [28]

$$E_{IN}(t) = \kappa\sqrt{2P_{laser}}e^{j\omega_0 t}, \quad (8)$$

where P_{laser} is average laser power at angular frequency ω_0 and κ is a constant relating field and average power. The input voltage to the MZM is defined by

$$V_{IN}(t) = V_{dc} + V_{RF}\sin(\omega_0 t), \quad (9)$$

where V_{dc} stands for bias voltage and the expression $V_{RF}\sin(\omega_0 t)$ defines the modulating RF signal V_{RF}. Among other factors, IM/DD introduces additive noise to the hybrid radio and photonic system.

C. FSO Turbulence Effects

There are a number of methods for generating turbulence within an indoor controlled environment, including near-index matching, liquid-filled chambers, spatial light modulators, ion-exchange phase screens, surface etching, and hot air chambers [30]. For assessing the performance of the proposed scheme, we have adopted the latter and used an artificial turbulence generator with known, realistic, and repeatable characteristics. Two fans were used to blow hot air into the channel perpendicular to the propagating optical beam. To measure the temperature profile and determine the temperature gradient along the channel, we placed 20 thermal sensors at an interval of 10 cm along the FSO channel. We used Rytov variance and the refractive index structure parameter to characterize strength of the turbulence according to [22]. The variance of the log-intensity signal fluctuation defined by Rytov variance σ_R^2 is given by [31]

$$\sigma_R^2 = 1.23k^{\frac{7}{6}}C_n^2 L^{\frac{11}{6}}, \quad (10)$$

where $k = 2\pi/\lambda$ is the wavenumber and λ is the transmission wavelength.

C_n^2 is the refractive index structure parameter (the main measure of the turbulence scale), which is given as [18]

$$C_n^2 = \left(79 \times 10^{-6}\frac{P_a}{T^2}\right)^2 C_T^2, \quad (11)$$

where P_a is the atmospheric pressure in millibars. C_T^2 is the temperature structure constant, which is defined as [18]

$$C_T^2 = (T_1 - T_2)^2/L_p^{2/3}. \quad (12)$$

T_1 and T_2 are temperatures at two points separated by distance L_p. Knowing the thermal distribution along the FSO propagation path, it is possible to determine C_T^2 and then C_n^2.

3. EXPERIMENTAL AND SIMULATION RESULTS

The experimental section is divided into three parts. In part A, the transmission properties of four selected scenarios (setups A–D; see Fig. 2) were tested under the steady-state condition with no turbulence. Part B describes the detailed investigation of the dynamic range and noise conditions of the RoF system compared to the hybrid RoF and RoFSO (setups A and C) systems. Finally, part C outlines the comparison of the links including the FSO channel under turbulence regimes (setups B–D).

A. System Properties

We have tested the suitability of proposed scenarios A–D using the polarization multiplexed technique for RF signals. Two standardized E-UTRA test models were selected for the investigation of the channel quality: Test models 2 and 3.2 [32]. Both test models are specified for testing E-UTRA systems with an emphasis on either the dynamic range or the quality of the transmitted signal using 64 and 16 QAM, respectively.

Scenarios A and B evinced EVM around 1%, while scenarios C and D evinced EVM between 2% and 3%. It can be observed that scenarios A and B offer roughly two or three times better EVM performance when compared to the hybrid RoF and RoFSO systems (C and D). Nevertheless, all scenarios show EVM values dramatically below the maximal 3GPP LTE EVM threshold of 8% recommended for high-data-rate systems [33]. Note that for setup A, with 5 km of SMF, the output power of EDFA had to be decreased in order to ensure that the PIN PD was not saturated or damaged. The gain of the EDFA was preserved throughout the experimental work in order to maintain similar conditions. Last but not least, we simulated the conditions of a real system by employing an EDFA in order to further increase the transmission span.

B. Noise Parameters

Next, we carried out several tests focusing on the quality of the E-UTRA signals transmitted over the optical channels for a range of OSNR and SNR values. These tests were focused on the hazard noise effects described in Section 2B, which can significantly reduce both OSNR and SNR, thus degrading the performance of RoF and RoFSO systems. At first, we carried out simulations for the EVMs for the proposed system featuring SMF and FSO sections (setups A and C). Subsequent measurements using a frequency of 2.6 GHz and 64 QAM were also carried out to validate the simulated results. The constellation diagrams of the 64 QAM and the evolution of the EVM parameter were evaluated both experimentally and by means of simulation, which was then correlated. Figures 3 and 4 depict the predicted and measured EVM as a function of the OSNR for setups A and C, respectively. For setup A, there is a mismatch between the measured and predicted EVMs, with the maximum difference of <2% at an OSNR of 28 dB. This is, in all probability, caused by the slightly different properties of simulated and real behavior of EDFAs, which

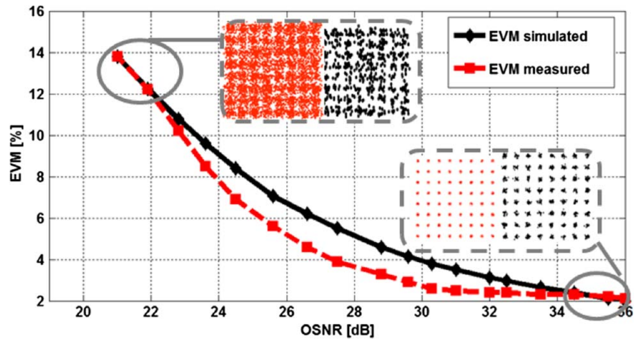

Fig. 3. Simulated and measured EVM as a function of OSNR for 64 QAM at a frequency of 2.6 GHz for 5 km of SMF (setup A). Inset shows the constellation diagrams.

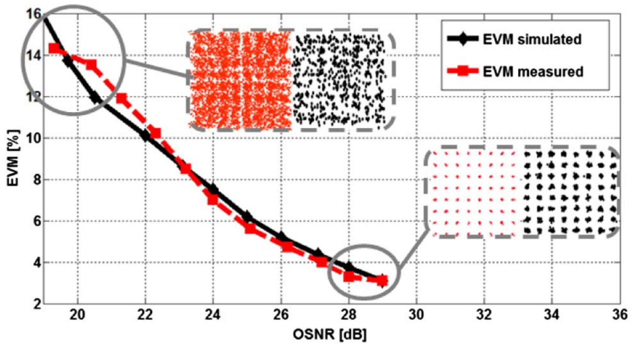

Fig. 4. Simulated and measured EVM as a function of OSNR for 64 QAM at a frequency of 2.6 GHz for 5 km of SMF + FSO channel (setup C). Inset shows the constellation diagrams.

are due to the ASE being the main noise source in the optical domain. For setup C, there is a good match between the measured and predicted plots. The measured (red) and simulated (black) constellation diagrams are also shown in Figs. 3 and 4. These plots show that the RoF with 5 km of fiber can operate over a wide range of OSNR (i.e., from 36 to 21 dB) whereas, for the hybrid RoF and RoFSO links, the OSNR range is only 10 dB (from 29 to 19.3 dB). In the case of the FSO channel, this can be attributed to the power budget being significantly lower and the noise floor belonging to a particular scenario. The experimental and simulated EVM curves for setup C show the same trend for OSNR values of 29 and 21 dB as in setup A, with the only difference being the initial EVM values. In addition, as just described, the EDFA power had to be reduced while using setup A, which resulted in a minimal OSNR value of ~21 dB. It can be observed that the proposed systems even operate over the recommended 8% EVM limit when using 64 QAM, but at the cost of higher error probability.

Next we investigated the EVM as a function of the SNR, which was measured on the Rx side, for setup C for 64 QAM at a frequency of 2.6 GHz with no turbulence, as shown in Fig. 5. The insets illustrate the corresponding constellation diagrams. The plots demonstrate a good agreement between the measured and simulated results. The SNR dynamic range shows a decrease of ~5 dB compared to setup A (while employing only 5 km of SMF). Both scenarios meet dynamic range requirements for home, local, and wide-area BSs specified by [32].

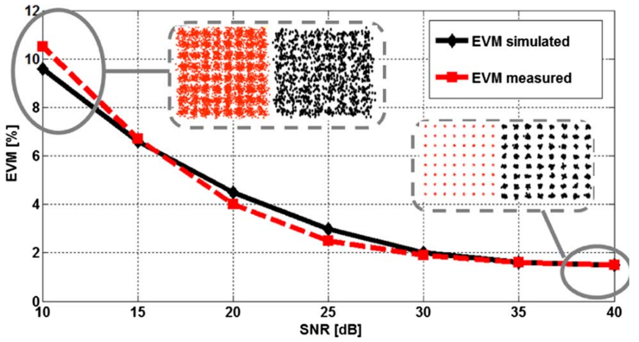

Fig. 5. Simulated and measured EVM as a function of SNR for 64 QAM at a frequency of 2.6 GHz for 5 km of SMF (setup C). Insets show the constellation diagrams.

C. Turbulence

Finally, we compared the performance of both RoFSO (setup B) and the hybrid RoF and RoFSO (setups C and D) systems under the influence of atmospheric turbulence. The average values of ΔEVM for these particular scenarios were captured for a range of the refractive index structure parameter C_n^2. Since the initial magnitude of EVM was different for particular scenarios, all EVM values were aligned by showing the ΔEVM. We have adopted the frequency of 2.6 GHz for further detailed investigations since the performance of the systems for 800 MHz and 2.6 GHz are almost the same. We compare all optical-based systems including the FSO part (setups B, C, and D from Fig. 2) at 2.6 GHz for 64 QAM for different turbulence regimes in terms of changes in EVM, as illustrated in Fig. 6.

The higher C_n^2 is, the larger the fluctuation of the power magnitude and its corresponding EVM values, which can exceed the reliability limits of the RAN system. The proposed LTE test model for 64 QAM fulfills the reliability and the high data-rate limit of EVM (i.e., <8%). Results indicate that a RoFSO scenario evinces the best properties comparable to the hybrid RoF and RoFSO setups C and D, where tolerable limits were exceeded approximately beyond the threshold C_n^2 of ~7.0E – 11 $m^{-2/3}$, in particular because of high fluctuations observed in EVM. In other words, the use of the RoF technology, together with RoFSO under the turbulence condition, resulted in slightly reduced performance compared with the RoFSO link in terms of increased mean value of ΔEVM by 2.5% and 5.5% in setups C and D, respectively, at C_n^2 of ~1E – 10 $m^{-2/3}$. This cannot be attributed only to added SMF (with an average EVM of 1%), and therefore the overall EVM system has to be determined. The hybrid setups (C and D) offer a reliable, high data rate transmission for the C_n^2 value up to ~7E – 11 $m^{-2/3}$, which corresponds to C_n^2 of 5.37E – 14 $m^{-2/3}$ in the case of a 100 m long FSO link extrapolated through the Rytov variance expression in Eq. (11). The predicted values largely fall into the moderate turbulence regime, thus representing typical maximal turbulence strength according to [18] and [34], where a 1 km long FSO link under a real turbulence condition was investigated. By placing the EDFA between the RoF and RoFSO systems so as to compensate

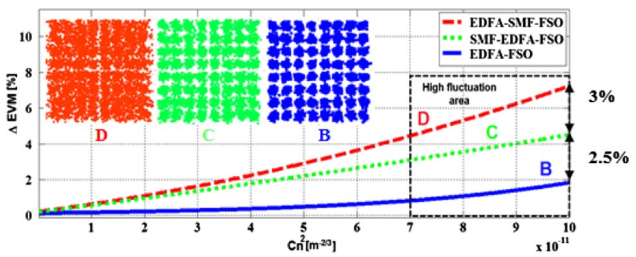

Fig. 6. ΔEVM as a function of the refractive index structure parameter C_n^2 for setups B, C, and D for 64 QAM at 2.6 GHz and OSNR corresponding to maximal values for each particular scenario.

for the loss in the RoF link and boost the incoming signal prior to the RoFSO link, the EVM is improved by ∼3%, as shown within the high fluctuation region in Fig. 6. Note that the optical output power (OS and EDFA) levels were kept at a relatively low level to avoid the more significant role of nonlinear effects in OF.

4. CONCLUSION

Having proposed an optical dual-polarization LTE RoF and RoFSO system for C-RAN networks and having evaluated its performance in terms of the measured and simulated EVM statistics, we showed the configuration of radio systems for 64 QAM at 2.6 GHz, incorporating FSO under the turbulence regimes, which lead to EVM values below 8% for C_n^2 of up to 5.37E – 14 $m^{-2/3}$ when considering a 100 m long FSO link. We also showed that the performance of the proposed link based on the combination of RoF and RoFSO was more affected by the turbulence, with the measured ΔEVM value increased to 5.5%. However, the EVM was reduced by ∼3% when placing an EDFA between the RoF and RoFSO links. The proposed systems can offer higher noise immunity under particular scenarios, with SNR reliability limits of 5 dB in the RF domain for RoF and 19.3 dB in the optical domain for RoFSO links. There were no significant changes in the polarization of the radio PDM system while propagating through the fiber and FSO channels, thus illustrating proposed system attributes to a higher transmission capacity. The employment of the dual-polarization solutions, as part of the C-RAN infrastructures, creates a dense network between the RF base-end parts and central cloud pools, thus making the infrastructure simpler and more robust. Moreover, the proposed technique can be adopted for other radio services such as WiFi or Wimax, thus leading to improved network convergence.

Funding. European Cooperation in Science and Technology (COST) (IC 1101); SGS (SGS14/190/OHK3/3T/13).

Acknowledgment. Authors would like to thank Rohde and Schwarz–Praha, S.R.O., for their technical support.

REFERENCES

1. S. Seung-Chul and L. Young-Poong, "Testing of early applied LTE-advanced technologies on current LTE service to overcome real network problem and to increase data capacity," in *Proceedings of 15th Annual Conference on Advanced Communication Technology* (IEEE, 2013), pp. 275–281.
2. S. Kanchi, S. Sandilya, D. Bhosale, A. Pitkar, and M. Gondhalekar, "Overview of LTE-A technology," in *Proceedings of IEEE Global High Tech Congress on Electronics* (IEEE, 2013), pp. 195–200.
3. T. Wirth, V. Venkatkumar, T. Haustein, and E. Schulz, "LTE-advanced relaying for outdoor range extension," in *Proceedings of IEEE 70th Vehicular Technology Conference Fall* (IEEE, 2009), pp. 1–4.
4. A. Checko, H. L. Christiansen, Y. Yan, L. Scolari, G. Kardaras, M. S. Bertger, and L. Dittman, "Cloud RAN for mobile networks-a technology overview," Commun. Surveys Tuts. **17**, 405–426 (2015).
5. J. Segel, "Lightradio portfolio: white paper 3," Technical Report p.17 (Alcatel-Lucent Bell Labs, 2011).
6. S. Ting, J. Zheng, J. Wang, M. Zhu, Z. Dong, M. Xu, M. Zhang, X. Chen, and G. K. Chang, "Multiservice wireless transport over RoF link with colorless BS using PolM-to-IM convertor," IEEE Photon. Technol. Lett. **27**, 403–406 (2015).
7. H. Al-Raweshidy and S. Komaki, *Radio Over Fiber Technologies for Mobile Communications Networks* (Artech, 2002).
8. S. Aleksic, M. Deruyck, and W. Joseph, "Energy efficiency of optically backhauled LTE: a case study," in *Proceedings of Electromagnetics in Advanced Applications* (IEEE, 2013), pp. 390–393.
9. H. Y. Huang, M. F. Huang, E. Ip, E. Mateo, P. N. Ji, D. Qian, A. Tanaka, Y. Shao, T. Wang, Y. Aono, T. Tajima, T. J. Xia, and G. A. Wellbrock, "High-capacity fiber field trial using terabit/s all-optical OFDM superchannels with DP-QPSK and DP-8QAM/DP-QPSK modulation," J. Lightwave Technol. **31**, 546–553 (2013).
10. M. Morant, J. Perez, and R. Llorente, "Polarization division multiplexing of OFDM radio-over-fiber signals in passive optical networks," Adv. Opt. Technol. **2014**, 269524 (2014).
11. M. Morant, J. Prat, and R. Llorente, "Radio-over-fiber optical polarization-multiplexed networks for 3GPP wireless carrier-aggregated MIMO provision," J. Lightwave Technol. **32**, 3721–3727 (2014).
12. C. Liu, L. Zhang, M. Zhu, J. Wang, L. Cheng, and G. K. Chang, "A novel multi-service small-cell cloud radio access network for mobile backhaul and computing based on radio-over-fiber technologies," J. Lightwave Technol. **31**, 2869–2875 (2013).
13. Z. Ghassemlooy, W. Popoola, and S. Rajbhandari, *Optical Wireless Communications: System and Channel Modelling with MATLAB®* (Taylor & Francis, 2012).
14. G. Parca, A. Shahpari, V. Carrozzo, G. M. Beleffi, and A. L. J. Teixeira, "Optical wireless transmission at 1.6-Tbit/s (16 × 100 Gbit/s) for next-generation convergent urban infrastructures," Opt. Eng. **52**, 116102 (2013).
15. C. Ben Naila, K. Wakamori, M. Matsumoto, and K. Tsukamoto, "Transmission analysis of digital TV signals over a radio-on-FSO channel," in *Proceedings of ITU Kaleidoscope: the Fully Networked Human?—Innovations for Future Networks and Services* (ITU, 2011), pp. 1–7.
16. C. B. Naila, K. Wakamori, and M. Matsumoto, "Transmission analysis of digital TV signals over a radio-on-FSO channel," IEEE Commun. Mag. **50**(8), 137–144 (2012).
17. D. Pham Tien, A. M. Shah, K. Kazaura, and K. Wakamori, "A study on transmission of RF signals over a turbulent free space optical link," in *Proceedings of International Topical Meeting on Microwave Photonics, Jointly Held with the Asia-Pacific Microwave Photonics Conference* (IEEE, 2008), pp. 173–176.
18. L. C. Andrews and R. L. Phillips, *Laser Beam Propagation through Random Media* (SPIE, 2005).
19. K. Kyung-Hwan, T. Higashino, K. Tsukamoto, and S. Komaki, "WDM optical power allocation method for adaptive radio on free space optics system design," in *Proceedings of International Topical Meeting on Microwave Photonics & Microwave Photonics Conference* (IEEE, 2011), pp. 361–364.
20. P. Yue, X. Yi, and Z. Li, "Research on radio frequency assignment mechanism of the distributed antenna system based on radio over free space optics technology," in *Proceedings of IEEE Services Computing Conference* (IEEE, 2010), pp. 526–530.
21. X. Tang, Z. Ghassemlooy, S. Rajbhandari, W. O. Popoola, and C. G. Lee, "Coherent heterodyne multilevel polarization shift keying with spatial diversity in a free-space optical turbulence channel," J. Lightwave Technol. **30**, 2689–2695 (2012).
22. J. Bohata, S. Zvanovec, T. Korinek, M. A. Abadi, and Z. Ghassemlooy, "Characterization of dual-polarization LTE radio over a free-space optical turbulence channel," Appl. Opt. **54**, 7082–7087 (2015).
23. T. Kanesan, W. Pang Ng, Z. Ghassemlooy, and C. Lu, "Investigation of optical modulators in optimized nonlinear compensated LTE RoF system," J. Lightwave Technol. **32**, 1944–1950 (2014).
24. B. Glance, "Polarization independent coherent optical receiver," J. Lightwave Technol. **5**, 274–276 (1987).
25. Y. Han and G. Li, "Coherent optical communication using polarization multiple-input-multiple-output," Opt. Express **13**, 7527–7534 (2005).

26. X. Steve Yao, L.-S. Yan, B. Zhang, A. E. Willner, and J. Jiang, "All-optic scheme for automatic polarization division demultiplexing," Opt. Express **15**, 7407–7414 (2007).
27. M. G. Taylor, "Coherent detection method using DSP for demodulation of signal and subsequent equalization of propagation impairments," IEEE Photon. Technol. Lett. **16**, 674–676 (2004).
28. C. H. Lee, *Microwave Photonics*, 2nd ed. (Taylor & Francis, 2013).
29. Y. Wang, I. Tomov, J. S. Nelson, Z. Chen, H. Lim, and F. Wise, "Low-noise broadband light generation from optical fibers for use in high-resolution optical coherence tomography," J. Opt. Soc. Am. A **22**, 1492–1499 (2005).
30. R. Rampy, D. Gavel, D. Dillon, and S. Thomas, "Production of phase screens for simulation of atmospheric turbulence," Appl. Opt. **51**, 8769–8778 (2012).
31. R. L. Fante, "Electromagnetic beam propagation in turbulent media," Proc. IEEE **63**, 1669–1692 (1975).
32. "The 3rd generation partnership project," http://www.3gpp.org/.
33. B. Bangerter, S. Talwar, R. Arefi, and K. Stewart, "Networks and devices for the 5G era," IEEE Commun. Mag. **52**(2), 90–96 (2014).
34. C. B. Naila, A. Bekkali, K. Wakamori, and M. Matsumoto, "Performance analysis of CDMA-based wireless services transmission over a turbulent RF-on-FSO channel," J. Opt. Commun. Netw. **3**, 475–486 (2011).

4.2 Experimental Verification of an All-Optical Dual-Hop 10 Gbit/s Free-Space Optics Link under Turbulence Regimes

This chapter is a version of the published manuscript:

J. Libich, M. Komanec, S. Zvanovec, **P. Pesek**, P. Popoola, Z. Ghassemlooy, "Experimental verification of an all-optical dual-hop 10 Gbit/s free-space optics link under turbulence regimes," Optics Letters, vol. 40(3), pp. 391–394, 2015.

Connection to my Ph.D. thesis:

To achieve greater diversity and data rates, it was necessary to investigate an all-optical FSO switching system for intermediate transfer in ad-hoc networks. Relaying systems support optical interconnection between source and destination which cannot be reached by a direct LOS link. Compared with an electrical relaying scheme, where the relays use OE/EO converters, all-optical relaying avoids requiring high-speed electronics and EO devices. We have proved that the proposed system can considerably mitigate turbulence-induced fading. Moreover, a dual-hop FSO link can provide up to four orders of magnitude improvement in BER under the presence of atmospheric turbulence against a single FSO link.

Experimental verification of an all-optical dual-hop 10 Gbit/s free-space optics link under turbulence regimes

Jiri Libich,[1,*] Matej Komanec,[1] Stanislav Zvanovec,[1] Petr Pesek,[1] Wasiu O. Popoola,[2] and Zabih Ghassemlooy[3]

[1]Department of Electromagnetic Field, Czech Technical University in Prague, Prague 166 27, Czech Republic

[2]Institute for Digital Communications, School of Engineering, University of Edinburgh, Edinburgh, EH9 3JL, UK

[3]OCR Group, Northumbria University, Newcastle-upon-Tyne NE1 8ST, UK

*Corresponding author: libicjir@fel.cvut.cz

Received November 12, 2014; revised December 22, 2014; accepted December 22, 2014; posted December 23, 2014 (Doc. ID 226740); published January 29, 2015

This Letter presents original measurement results from an all-optical 10 Gbit/s free-space optics (FSO) relay link involving two FSO links and an all-optical switch. Considering the fact that reported analyses of relay links are dominated by analytical findings, the experimental results represent a vital resource for evaluating the performance of relay FSO links in the presence of atmospheric turbulence. Bit-error-rate (BER) performance of the relay system is tested for single and dual-hop links under several turbulence regimes. Furthermore, results from this measurement are used to ascertain real parameters of the outdoor links and to improve the accuracy of simulation results. Results show that using a dual-hop FSO link against a single FSO link could result in up to four orders of magnitude improvement in BER in the presence of atmospheric turbulence.

OCIS codes: (060.2605) Free-space optical communication; (010.1330) Atmospheric turbulence.
http://dx.doi.org/10.1364/OL.40.000391

Free-space optical (FSO) communications, as part of optical wireless communications (OWC) systems, is an emerging complementary technology for addressing the last-mile bottle neck in future access networks. FSO technologies are nowadays capable of transferring up to 1.6 Tbit/s over a single link by employing dense wavelength division multiplexing (DWDM) [1]. The huge unlicensed bandwidth and its ability to deliver high data rates make FSO very attractive for the backbone segments of 5G mobile infrastructures and *ad hoc* hybrid networks.

Although recent Letters provide a strong analytical background for multihop links within *ad hoc* and mesh networks, experimental validations of such schemes are yet to be reported. We aim to address this by studying an all-optical two-hop FSO system in a laboratory environment. This Letter considerably extends our previous experiments devoted to routing techniques and *ad hoc* network diversity segments [2] where only parallel OWC links were characterized.

As in radio frequency-based systems, FSO link performance is also affected by the atmospheric conditions including turbulence [3]. In the turbulence channel, the variation in the received optical signal power is typically expressed by the Rytov variance, which depends on the refractive index structure parameter C_n^2. Several statistical models have been developed for intensity variation due to turbulence. The most widely used of these models are the log-normal distribution, which well describes the weak turbulence regime and the gamma-gamma distribution that is most suitable for medium to strong turbulence regimes [4].

The performance degradation of an outdoor FSO link in terms of the optical signal fades due to the atmospheric turbulence is very well reported both theoretically and experimentally. To reduce the effect of atmospheric turbulence on the FSO link, a number of techniques have been proposed including aperture averaging [5] and spatial diversity [6] at the receiver, and novel modulation schemes [7].

In complex *ad hoc* networks with short link spans between nodes, the path-routing approach could be adopted to avoid paths that are severely affected by turbulence or minimize the effect of turbulence as illustrated in Fig. 1. Outdoor experimental evaluation of a real FSO mesh network communication system was performed by Kaneko *et al.* in 2002 in the Tokyo metropolitan area [8]. This was the first report on ascertaining the effectiveness of routing in a FSO mesh network.

The mechanism of turbulence spread over several internode links introduces quite a complex task especially in terms of the evaluation of joint fading statistics. Karagiannidis *et al.* have considered K-distribution atmospheric-induced fading models for the multihop FSO system under the strong turbulence regime in [9]. The outage probability involving statistically independent, but not necessarily identically distributed, Nakagami relay channels was evaluated in [10]. The outage probability of relay-assisted links was derived in [11,12].

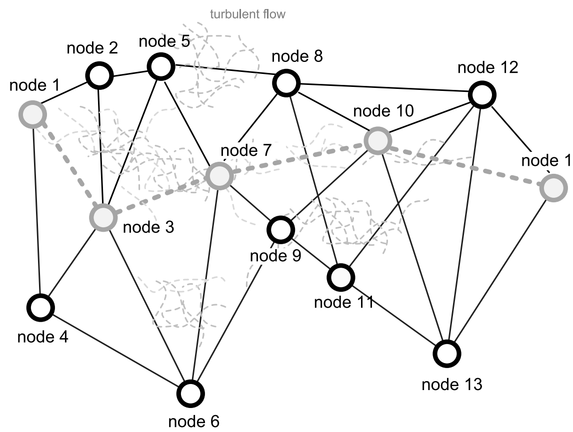

Fig. 1. Multihop scheme within the *ad hoc* network.

Both amplify-and-forward and decode-and-forward methods were analytically tested for multihop configurations showing power margin improvements of 12.2 and 18.5 dB, respectively, at a link-span of 5 km. The analysis assumed channel-independent small turbulence-induced fading characterized by the log-normal distribution. In [12] further analyses and optimizations of serial and parallel nodes together with quantification of advantages relating to the number of relays and channel parameters were presented. Algorithms for optimal node locations based on the outage statistics were proposed.

Transmission protocols without the need for synchronization in relay-assisted FSO systems were proposed by Chatzidiamantis *et al.* in [7]. Numerical tests for the outage probabilities and optimal power allocation were accomplished for all-active (worst tested case), select-max, and distributed switch and stay relay (DSS) selection protocols while considering the gamma-gamma channel model. The effect of employing erbium-doped fiber amplifier (EDFA) amplifiers within the FSO relay network has been investigated by Bayaki *et al.* in [13].

In order to validate analytical approaches, we have carried out an experimental measurement campaign using a real state-of-the-art dual-hop wireless optical system setup [see Fig. 2(a)]. The link is composed of two FSO channels connected in series with an all-optical switching unit in between. A detail of the FSO link is depicted in Fig. 2(b).

The signal generator (and simultaneously a BER tester–BERT) was formed by a VeEX VePAL TX300/e network analyzer using a 1550 nm Finisar FTRX-3661-334 XFP transceiver, which was modulated by a 10 Gbit/s on–off keying (OOK) pseudo-random binary sequence (PRBS). The output of the signal generator was launched into a conventional single-mode fiber (SMF) via a gradient-index (GRIN) lens (GRIN2315-Thorlabs) to form the first FSO transmitter (Tx1). An optical attenuator (ATT) is used to control the level of transmitted optical

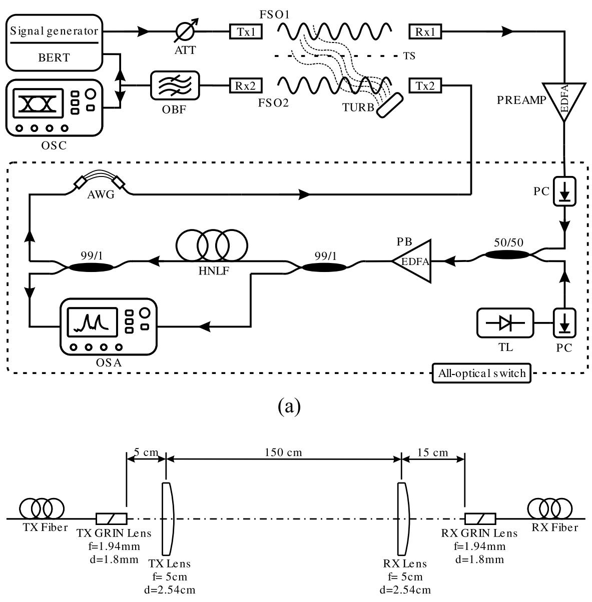

Fig. 2. (a) Block diagram of the laboratory experiment with (b) a detail of the dual-hop FSO link.

power. The GRIN lens enabled lower divergence of the output field in contrast to bare SMF facet, with focal length $f = 1.94$ mm and numerical aperture $\mathrm{NA} = 0.46$. A second plano–convex lens (N-BK7, Thorlabs) with $f = 50$ mm was placed in the transmitter segment to focus the beam on the receiver segment. The receiver is composed of a plano–convex lens (N-BK7) with a focal length f of 150 mm, a GRIN lens, and a SMF. The output of the SMF was then passed though an EDFA prior to detection. The EDFA ensured a stable power level and was set to 0 dBm.

The total length of the experimental FSO channel for each link was 1.5 m. The turbulence within the channel was created using a heater with an adjustable built-in fan. Ten temperature sensors (TS) were equidistantly placed along each FSO channel at a distance of 0.15 m to precisely capture temperature profiles along both channels. Refractive index structure parameter C_n^2 was determined to be associated with thermal fluctuations by Obukhov [14] and Corrsin [15] from temperature T and pressure P as

$$C_n^2 = \left(79 \cdot 10^{-6} \frac{P}{T^2}\right)^2 C_T^2, \tag{1}$$

where temperature structure parameter C_T related to the 2/3 power law of temperature variation along the path can be obtained from temperature structure function $D_T(R)$ by [3]

$$D_T(R) = \langle (T_1 - T_2)^2 \rangle = C_T^2 R^{2/3}, \qquad l_0 < R < L_0. \tag{2}$$

T_1 and T_2 stand for temperatures measured at two points separated by distance R, and l_0 and L_0 represent the inner and outer scales of turbulence, respectively.

The FSO1 link experienced correlated turbulence with the FSO2 link. The insertion loss of the complete FSO1 was measured to be 5.5 dB, and the FSO2 link experienced a similar loss (also having a length of 1.5 m).

The switching setup was based on our previous work [16]. We have used a polarization controller (PC) to set the polarization state of the preamplified input data signal from the FSO1 link. The polarized signal was combined, using a 50/50 coupler, with the pump signal at 1556 nm, generated by a tunable laser (TL), which also passed through a PC. The TL covers the entire C- and L-band, thus enabling signal switching within the C-band. The signal was amplified using an EDFA to a total output power level of 21 dBm. A small fraction of the amplified signal was captured by an optical spectrum analyzer (OSA) for monitoring purposes. The remaining part of the signal passed through a highly nonlinear fiber (HNLF), a 99/1 power splitter, and an arrayed-waveguide grating (AWG) to Tx2.

Figure 3 shows the measured four-wave mixing wavelength conversion efficiency (CE), for better illustration fitted by polynomial curves, as a function of the SNR at the output of FSO1 for a range of C_n^2. The best CE obtained is −10.4 dB for the case of no turbulence and no applied attenuation at an SNR of 37 dB.

By gradually decreasing the SNR and/or increasing the turbulence strength, the CE value reduces (also caused

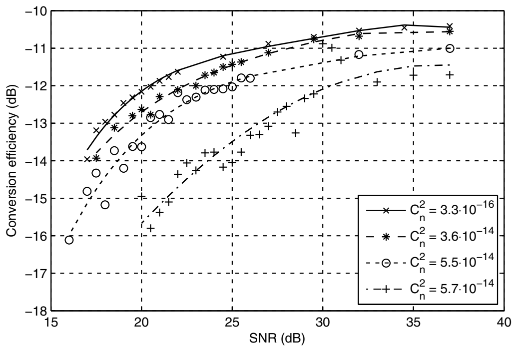

Fig. 3. All-optical switching conversion efficiency plots with respect to SNR of the input signal for a range of C_n^2.

by higher added noise in the PREAMP/PB stage). For instance, the two curves for $C_n^2 = 5.5 \cdot 10^{-14}\ \mathrm{m}^{-2/3}$ (marked with circles) and $C_n^2 = 5.7 \cdot 10^{-14}\ \mathrm{m}^{-2/3}$ (marked with crosses) in Fig. 3 imply that with stronger turbulence level, the fluctuations of the data signal power levels affect the CE significantly.

At first we carried out a test on the single 10 Gbit/s optical wireless link and used it as a reference for further tests with a dual-hop FSO link and in combination with the all-optical switching method. Figure 4 depicts the measured BER performance of a single FSO link with and without the turbulence effect. This figure also includes the analytical BER plot without turbulence as presented in [3]. As expected, the plots show degradation of the link's BER in the presence of turbulence. It can be seen that for a particular SNR value, turbulence degrades the BER performance by orders of magnitude. For instance, at an SNR of 20 dB and with very weak turbulence ($C_n^2 = 6.3 \cdot 10^{-16}\ \mathrm{m}^{-2/3}$), the BER is $5 \cdot 10^{-7}$ increasing by three orders of magnitude to $8 \cdot 10^{-4}$ in the presence of turbulence ($C_n^2 = 4.1 \cdot 10^{-14}\ \mathrm{m}^{-2/3}$). For smaller SNR, results of analytical analysis differ from measured data owing to noise generated by the optical amplifier, because amplification of a low signal to the particular level decreases SNR.

Next, we carried out tests and measurements on the dual-hop FSO configuration. As in the first measurement, two FSO channels with 1.5 m lengths were used as a common turbulent channel. Following amplification, the output signal from the FSO1 link was optically switched to the wavelength of 1547.6 nm (37th channel of the DWDM 100 GHz ITU-grid) and propagated

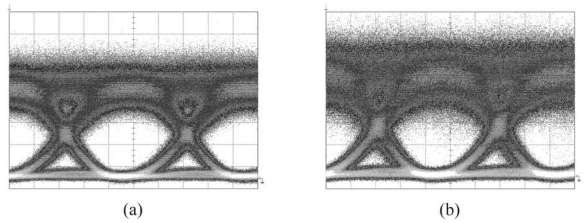

Fig. 5. Eye diagram for the dual-hop FSO link under (a) weak turbulence $C_n^2 = 10^{-16}\ \mathrm{m}^{-2/3}$ and (b) medium turbulence $C_n^2 = 10^{-14}\ \mathrm{m}^{-2/3}$. Here, x axis is time, 20 ps/div; y axis is voltage, 38 μV/div.

backward via the FSO2 link to the BERT receiver. The FSO2 link turbulence was highly correlated with that of FSO1. The impact of this turbulence on the dual link is depicted in the measured eye diagram of Fig. 5. The eye SNR dropped from 8.3 to 7.3 dB owing to turbulence.

To further quantify the impact of turbulence on this dual-hop system, we present the measured BER for several turbulence regimes in Fig. 6. Comparing both measurement configurations, it is important to note that at a BER of around 10^{-3} and with the same turbulence level the SNR requirements are 19 and 12 dB for the single link and the dual-hop link, respectively. Also, if we consider, say, an SNR of 20 dB, BER for the single and dual-hop links are about $8 \cdot 10^{-4}$ (for turbulence with $C_n^2 = 4.1 \cdot 10^{-14}\ \mathrm{m}^{-2/3}$) and $9 \cdot 10^{-9}$ ($C_n^2 = 3.6 \cdot 10^{-14}\ \mathrm{m}^{-2/3}$), respectively. These values represent a considerable improvement in the dual-hop link performance over the single hop.

We also carried out simulations of BER performance (based on the work reported in [3] and [4]) using a setup that models exactly the components used in the experimental measurements. Simulation was optimized using data from experimental measurements and then was used for the simulation of the real FSO link. The simulation software enabled both fiber optics (with precise parameter settings for, e.g., the nonlinear fiber) and the FSO link including atmospheric turbulence, beam divergence, etc. We performed the simulation for both the single and dual-hop FSO links with varying link lengths. The parameters of both FSO transceivers were set identical with a beam diverge of 2.16 mrad, transmitter aperture of 1 cm, receiver aperture of 10 cm, data rates of 10 Gbit/s using OOK with the nonreturn-to-zero pulse pattern, and a link length of 500 m to correspond a real FSO link [17].

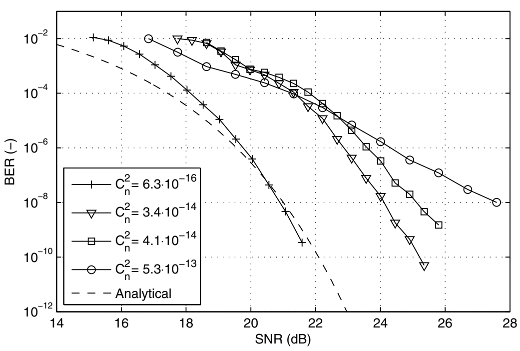

Fig. 4. Measured and predicted BER performance against the SNR for a range of C_n^2 for a single FSO.

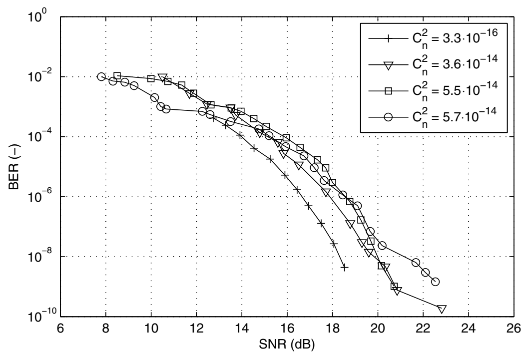

Fig. 6. Measured BER performance against SNR for a range of C_n^2 for a dual-hop link.

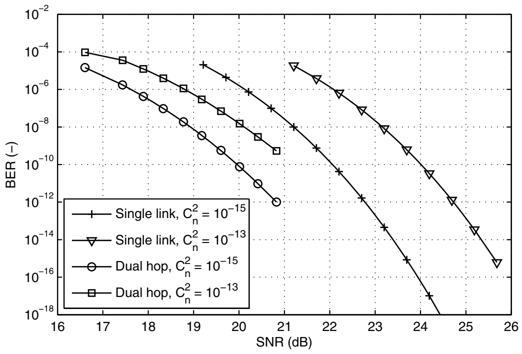

Fig. 7. Simulated BER performance of single FSO and dual-hop FSO links with a total length of 500 m.

Figure 7 shows the simulation results for BER performance of a single 500 m long FSO link and dual-hop FSO link (the link was divided into two 250 m long links) under turbulence with C_n^2 of 10^{-15} and 10^{-13} $m^{-2/3}$. It can be seen that by separating the wireless optical link into two shorter paths, the impact of the turbulence on the BER performance can significantly be reduced by up to four orders of magnitude.

To summarize this Letter, we have experimentally analyzed the concept of a 10 Gbit/s dual-hop FSO link under turbulence regimes. We have performed several parametric studies of the single FSO and dual-hop FSO links under turbulence conditions for a link span of 100 to 500 m. The results show that the dual-hop link has a better BER performance than the single link. Moreover, we have successfully shown that such a system with all-optical switching for intermediate transfer in *ad hoc* networks can considerably mitigate turbulence-induced fading. To the best of the authors' knowledge, this represents the first ever demonstration of an all-optical dual-hop FSO system at 10 GBit/s bit rates with optical switching. This demonstration further strengthens the argument in favor of FSO as a very promising technology for the emerging generation of adaptive heterogeneous networks. Further tests are, however, needed to validate the dual-hop/relaying features within large-scale turbulence regimes and to incorporate other advanced modulation formats.

The joint research was supported by EU COST ICT Action IC1101 and by the MEYS CR grant LD12058. Research of J. Libich is supported by the European social fund within the framework of the project CZ.1.07/2.3.00/30.0034.

References

1. G. Parca, A. Shahpari, V. Carrozzo, G. M. Tosi Beleffi, and A. L. J. Teixeira, Opt. Eng. **52**, 116102 (2013).
2. S. Zvanovec, J. Perez, Z. Ghassemlooy, S. Rajbhandari, and J. Libich, Opt. Express **21**, 7641 (2013).
3. Z. Ghassemlooy, W. Popoola, and S. Rajbhandari, *Optical Wireless Communications: System and Channel Modelling with MATLAB* (CRC, 2012).
4. L. C. Andrews and R. L. Phillips, *Laser Beam Propagation through Random Media* (SPIE, 2005).
5. M. A. Khalighi, N. Schwartz, N. Aitamer, and S. Bourennane, J. Opt. Commun. Netw. **1**, 580 (2009).
6. S. M. Navidpour, M. Uysal, and M. Kavehrad, IEEE Trans. Wireless Commun. **6**, 2813 (2007).
7. N. D. Chatzidiamantis, D. S. Michalopoulos, E. E. Kriezis, G. K. Karagiannidis, and R. Schober, J. Opt. Commun. Netw. **5**, 92 (2013).
8. S. Kaneko, T. Hamai, and K. Oba, J. Opt. Netw. **1**, 414 (2002).
9. G. K. Karagiannidis, T. A. Tsiftsis, and H. G. Sandalidis, Electron. Lett. **42**, 994 (2006).
10. X. Tang, Z. Xu, and Z. Ghassemlooy, *IEEE 8th Conference on Network and Optical Communications* (IEEE, 2013), pp. 199–202.
11. M. Safari and M. Uysal, IEEE Trans. Wireless Commun. **7**, 5441 (2008).
12. M. A. Kashani, M. Safari, and M. Uysal, J. Opt. Commun. Netw. **5**, 37 (2013).
13. E. Bayaki, D. S. Michalopoulos, and R. Schober, IEEE Trans. Commun. **60**, 3797 (2012).
14. A. M. Obukhov, Izv. Akad. Nauk. SSSR, Ser. Geogr. i Geofiz **13**, 58 (1949).
15. S. Corrsin, J. Appl. Phys. **22**, 469 (1951).
16. M. Komanec, P. Skoda, J. Sistek, and T. Martan, Radioengineering **23**, 768 (2014).
17. J. Libich, S. Zvanovec, and M. Mudroch, Proc. SPIE **8246**, 82460O (2012).

4.3 Mobile User Connectivity in Relay-Assisted Visible Light Communications

This chapter is a version of the published manuscript:

P. Pesek, S. Zvanovec, P. Chvojka, M. R. Bhatnagar, Z. Ghassemlooy, P. Saxena, "Mobile User Connectivity in Relay-Assisted Visible Light Communications," Sensors, vol. 18, pp. 1125, 2018.

Connection to my Ph.D. thesis:

Cooperation techniques for an indoor VLC interconnection of end users are much more challenging, due to the movement of people, objects and equipment within the room which can block the LOS. Moreover, VLC systems for reliable communications are limited to a range of only a few meters, due to regulated transmission power. In order to increase a viable communication range, relay communications can be used. Therefore, it was necessary to determine the dependency of BER performance on azimuth and elevation angles of the mobile VLC relay device moving inside an office space. Moreover, it was necessary to derive an analytic model for comparing relaying techniques. The results show a significant improvement in the VLC link performance using cooperative schemes when compared to a direct NLOS transmission.

sensors

Article

Mobile User Connectivity in Relay-Assisted Visible Light Communications

Petr Pešek [1,*], Stanislav Zvanovec [1], Petr Chvojka [1], Manav R. Bhatnagar [2], Zabih Ghassemlooy [3] and Prakriti Saxena [2]

1 Department of Electromagnetic Field, Faculty of Electrical Engineering, Czech Technical University in Prague, 2 Technicka, 16627 Prague, Czech Republic; xzvanove@fel.cvut.cz (S.Z.); chvojpe8@fel.cvut.cz (P.C.)
2 Department of Electrical Engineering, Indian Institute of Technology Delhi, Hauz Khas, IN-110016 New Delhi, India; manav@ee.iitd.ac.in (M.R.B.); prakriti1192@gmail.com (P.S.)
3 Optical Communications Research Group, NCRLab, Faculty of Engineering and Environment, Northumbria University, NE1 8ST Newcastle upon Tyne, UK; z.ghassemlooy@northumbria.ac.uk
* Correspondence: pesekpe3@fel.cvut.cz

Received: 14 February 2018; Accepted: 4 April 2018; Published: 7 April 2018

Abstract: In this paper, we investigate relay-assisted visible light communications (VLC) where a mobile user acts as a relay and forwards data from a transmitter to the end mobile user. We analyse the utilization of the amplify-and-forward (AF) and decode-and-forward (DF) relaying schemes. The focus of the paper is on analysis of the behavior of the mobile user acting as a relay while considering a realistic locations of the receivers and transmitters on a standard mobile phone, more specifically with two photodetectors on both sides of a mobile phone and a transmitting LED array located upright. We also investigate dependency of the bit error rate (BER) performance on the azimuth and elevation angles of the mobile relay device within a typical office environment. We provide a new analytical description of BER for AF and DF-based relays in VLC. In addition we compare AF and DF-based systems and show that DF offers a marginal improvement in the coverage area with a BER $< 10^{-3}$ and a data rate of 100 Mb/s. Numerical results also illustrate that relay-based systems offer a significant improvement in terms of the coverage compared to direct non-line of sight VLC links.

Keywords: amplify-and-forward relaying; cooperative communication; decode-and-forward relaying; visible light communications

1. Introduction

With the enormous growth of data traffic over wireless infrastructures due to increased demands for video and audio streaming, file sharing, data and voice over Internet protocol (VoIP) [1], the lack of available radio-frequency (RF) spectrum is becoming the limiting factor for high-speed data transmission. One possible solution to address this problem, mostly in an indoor environment at the moment, is the visible light communications (VLC) offering attractive capabilities such as vast unregulated spectrum (∼380–780 nm), inherent security and high energy efficiency [2,3].

The rapid growth of VLC is due to the development in solid-state lighting (SSL) and highly efficient white light-emitting diodes (LEDs) [4]. White LEDs offer a longer life span and much higher power efficiency (∼60–80 %) than the conventional fluorescent and incandescent lamps, as well as the possibility to be used in safe and secure applications (e.g., in hospitals, gas stations and airplanes) where RF-based technologies cannot be used [5].

Indoor VLC can be categorized into the line-of-sight (LOS) and diffuse systems. Data rates in the order of Gb/s over a very short transmission span can be achieved using LOS VLC links [6].

For instance, in [7] a 4.5 Gb/s VLC system employing carrier-less amplitude and phase (CAP) modulation and a recursive least square (RLS) based adaptive equalizer over a link span of 1.5 m was experimentally demonstrated. In [8] a data speed of 1.6 Gb/s over a 1 m link employing a combination of 16-quadrature amplitude modulation (QAM) and orthogonal frequency division multiplexing (OFDM) was reported. On the other hand, diffuse VLC systems are robust to blocking and shadowing. However, they suffer from higher losses and offer much lower data rates than LOS links due to multipath induced dispersion [9,10].

In indoor environments, the LOS path cannot always be guaranteed due to objects, people's movement and the layout of the room [11]. To address this problem and offer seamless communications as well as to maintain an uninterrupted data access even in temporarily shadowed regions a number of solutions have been proposed [12,13]. One of the most promising techniques is the relay-assisted VLC system. Note that, the current IEEE 802.15.7 standard does not cover the relay based VLC systems, but the standard supports device discovery mechanisms in homogeneous networks [14]. In order to improve the connectivity, a full-duplex relay based VLC employing an LED lighting triangular system topology was analytically investigated in [15]. In the case of the light from an LED source mounted on the ceiling not reaching the user directly, the information can be retransmitted via a relay node (RN). In [16], the connectivity performance of mobile users based on the optical mobile relays in cooperative multi-hop VLC was investigated. An improvement in the network performance was reported by using the multi-hop scenario, which was dependent on the users' density, coverage range ratio between hop regions, relay probabilities, and velocity of the mobile users. A number of existing works also analyzed the multi-hop VLC systems using a combination of RF and VLC links [17,18]. In order to improve the quality of service, in [17] hybrid VLC and power line communications (PLC) with a backup parallel RF link were proposed. In [18] the authors investigated the scenario, where data is transmitted from the base station to the relay via the RF link and the signal is then amplified and re-transmitted to the user over the VLC channel.

OFDM VLC over frequency-selective indoor channels was analyzed in [19] providing the first analytical statistics for pure VLC relaying using amplify-and-forward (AF) or decode-and-forward (DF) relaying schemes. In [20] a relay based DC-biased optical OFDM (DCO-OFDM) VLC was investigated for two test cases using a desk lamp and a ceiling light lamp to provide optimal power allocation and improved bit error rate (BER) performance when employing relays compared to the direct transmission.

However, none of the existing works reporting on the relay-assisted VLC systems have investigated the use of a mobile phone (MP) as a relay. In this paper, for the first time, to the best of authors' knowledge, we provide results for performance evaluation of a relay-based VLC system employing MP as an RN for miscellaneous configurations. We give distinctive statistics of AF and DF-based relays for ceiling mounted light sources via MP, taking into account MP node orientation and a range of channel parameters. It is very important in such cases to estimate the area where such a node can be searched for, which is fully dependent on the elevation and the azimuth of MP and the required BER or the allocated optical power level. All these aspects are studied in following sections.

The rest of the paper is organized as follows. Section 2 discusses the indoor VLC channel model and the specific functionality of the MP for utilization in a relay-assisted system. Section 3 outlines a channel model for the VLC relay system and describes the cooperation techniques for the relay-assisted systems and provides analytical model for BER of AF and DF VLC. In Section 4 numerical results for the BER performance of the relay-assisted network with AF and DF modes are summarized. Finally, the summary and conclusions are given in Section 5.

2. Relay-VLC Deployment in the Indoor Environment

In this paper, we consider a typical office room with a dimensions of 5 m × 5 m × 3 m with no furniture as depicted in Figure 1a. The system consists of a transmitter (Tx), which provides both illumination and data transmission, located at the center of the ceiling at the height of 2.8 m pointing downwards with an elevation angle of –90°, and a MP is used as either a receiver (Rx) or an RN. The Tx is realized an LED array with Lambertian radiation pattern. The power of LEDs is adjusted to meet the light illumination requirement of 200 to 1500 lx for an office environment as defined by International Organization for Standardization (ISO) [21].

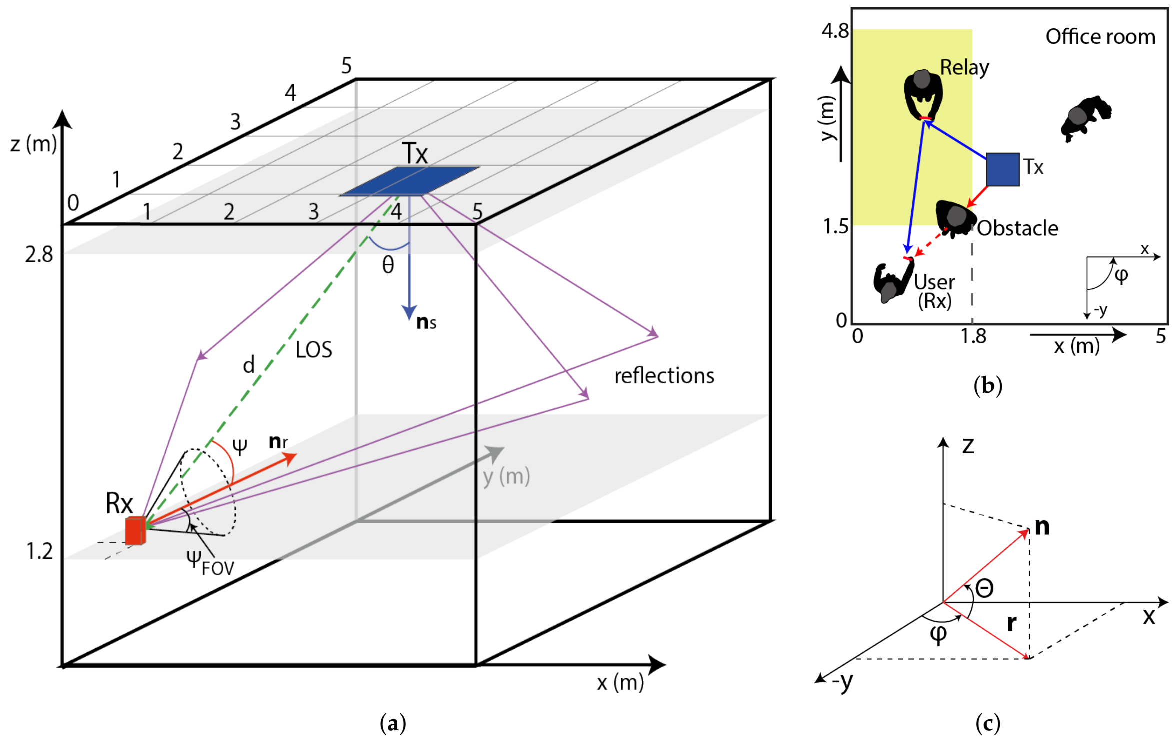

Figure 1. Room model: (**a**) Tx and Rx geometry model; (**b**) users' situation in the room; and (**c**) the coordinate system.

Furthermore, we assume that a relay-based user holding a MP at the height of 1.2 m above the floor level is randomly moving around within the room. The walls, floor, and ceiling of the room are modeled as general Lambertian reflectors as in vast majority of publications [22,23]. We investigate an office environment including people where we consider shadowing between the Tx and the Rx, see Figure 1b. The LOS path between the Tx and the Rx will be blocked due to shadowing, and therefore the Tx will select a non-shadowed mobile user as an RN, which is located in the yellow area (see Figure 1b) to re-establish the link between the Tx and the Rx via the relay user. Note that, in a real environment the RN must be close to the the user, and such RN scheme would have very limiting application for considerably longer VLC connections. Here we consider an arbitrary orientation of the mobile-based RN.

The coordinates of the proposed system are depicted in Figure 1c. The unit vector $\boldsymbol{n}$ is specified in terms of conventions followed by room coordinates. The Tx and the Rx directions (i.e., elevation and azimuth angles) can be converted to unit vectors $\boldsymbol{n_s}$ and $\boldsymbol{n_r}$, respectively (see Figure 1a). An elevation of the Tx is an angle that $\boldsymbol{n_s}$ makes with the xy plane, therefore if the Tx is directly pointing downwards, the elevation angle will be –90°. An azimuth angle of the Tx is defined with 0° oriented along the negative y-axis in the projection of $\boldsymbol{n_s}$ on the xy and it increases with the counter-clockwise orientation (i.e., the positive x-axis has an azimuth of +90°). All the key system parameters are summarized in Table 1 [21,24]. According to [25], the majority of mobile data usage (close to 80%) is in indoor environments, which are rather static, unlike the outdoor environments. Even though the location of RNs or users may change before it is initiated to retransmit the data, without loss of generality we can consider the device is stationary during the relaying process due to the slow movement of the users.

Table 1. Key System Parameters.

Parameter	Symbol	Value
Room size	-	$5 \times 5 \times 3$ m
No. of rays	-	100,000
No. of reflection	-	5
Time resolution	Δt	0.2 ns
Bit rate	-	100 Mb/s
Reflectivity of walls	ρ_{wall}	0.74
Reflectivity of ceiling	$\rho_{ceiling}$	0.38
Reflectivity of floor	ρ_{floor}	0.61
Smoothness of the reflecting material	u	1
Tx position	-	$2.5 \times 2.5 \times 2.8$ m
Tx power per LED	-	20 mW
Size of the LED array	-	60×60
Semiangle at half power	$\theta_{1/2}$	60°
Tx elevation	-	–90°
Tx azimuth	-	0°

3. System Model

3.1. VLC Channel

We consider the Tx to be a monochromatic point source with a Lambertian radiation pattern. The LOS link gain is given by [21]:

$$H = \begin{cases} \frac{(m+1)A_r}{2\pi d^2} \cos^m(\theta)\cos(\Psi)g(\Psi)T_s(\Psi) & ,0 \leq \Psi \leq \Psi_{FOV} \\ 0 & ,\Psi > \Psi_{FOV} \end{cases} \quad (1)$$

where A_r is the effective area of the Rx photodiode, d represents the distance between the Tx and the Rx, θ stands for the irradiance angle with respect to $\boldsymbol{n_s}$, and Ψ is the incident angle with respect to $\boldsymbol{n_r}$ (see Figure 1). $T_s(\Psi)$ is the optical filter gain, $g(\Psi)$ the optical concentrator gain, Ψ_{FOV} is the field of view (FOV) of the Rx and m represents the Lambertian emission, which is given by:

$$m = \frac{-\ln(2)}{\ln(\cos(\theta_{1/2}))} \quad (2)$$

where $\theta_{1/2}$ is the half-power angle of the LED.

By adopting Lambert-Phong method [9], the diffuse paths are assumed to be represented by scattered rays, re-radiated from the wall to the Rx, which are being attenuated (i.e., based on the surface reflection coefficient). We define the reflection scattering using a generalized Lambert radiation pattern as:

$$P_{rWall} = \frac{P_i(u+1)}{2\pi}\rho\cos^u(\delta) \quad (3)$$

where P_i is the incident normalized unit power at the wall, P_{rWall} is the reflection power from the reflected surface, u is the smoothness of the reflecting material, ρ is reflection coefficient, and δ is the randomly uniformly distributed angle between reflected rays and the diffusely reflected ray. Note that, in this paper, we study a practical scenario of VLC system with mobile users being used as RNs. To be as much as illustrative, we have used the average reflectivity over the entire visible spectrum defined by [22] and the nonlinearity of LED sources is not considered. However, model presented in this work can be extended to include non-LOS configuration (NLOS) (i.e., reflections) as part of the future studies, by considering spectral dependency of reflective surfaces [26] and non-Lambertian reflections [27,28].

3.2. Mobile User

Research work on direct VLC links using mobile devices as Rxs has been reported e.g., in [29]. In contrast to work reported in the literature, in this paper, we investigate the use of MP acting as the Rx and an RN as a part a relay-based VLC system, see Figure 2a. Let's assume that the MP has (i) two photodetectors (PDs) on both sides, thus providing the MP with spatial diversity using a selection of the strongest received signal; and (ii) the Tx LED array placed perpendicular to the Rx planes as depicted in Figure 2b. Note that within the MP elevation plane, an azimuth angle remains the same as in the case of the Rx. The MP parameters are summarized in Table 2.

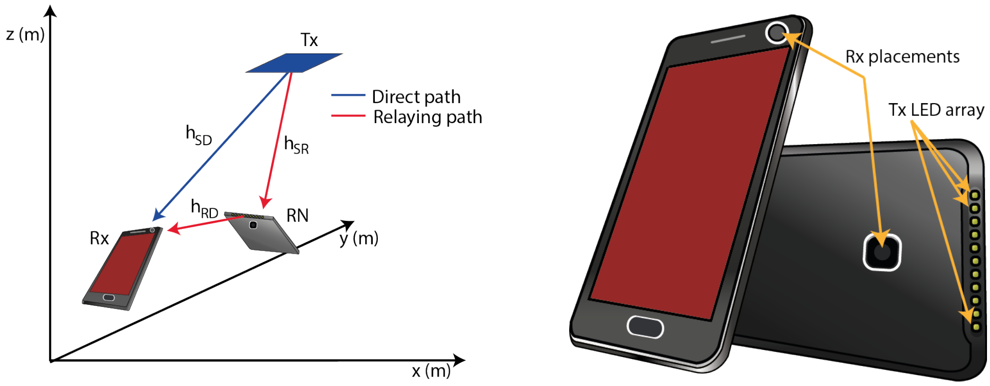

(**a**) (**b**)

Figure 2. (**a**) Mobile user position in a room; and (**b**) the positions of the Rx and Tx on a mobile device.

Table 2. Mobile Device Parameters.

Parameter	Symbol	Value
Rx area	A_r	1 cm^2
Effective area of a photodiode	Ψ_{FOV}	50°
Photodetector responsivity	γ	0.53 A/W
Optical filter concentrator	Ts	1
Optical concentrator gain	g	3
User position	-	0.5 × 0.5 × 1.2 m
Rx elevation	-	50°
Rx azimuth	-	90°
Tx_{RN} power per LED	-	200 mW
Size of LEDs	-	1 × 10, 1 × 14
Semiangle at half power	$\theta_{1/2}$	60°
Background dark current	I_{bg}	10 nA
Noise bandwidth factors	I_2, I_3	0.562, 0.0868
Absolute temperature	T_k	295 K
Open-loop voltage gain	G	10
Capacitance	η	112 × 10^{-8} F/m^2
FET channel noise factor	Γ	1.5
FET transconductance	g_m	0.03 S

In this work we investigate the orientation of the MP within the indoor environment. Based on 1300 observations of people using their MPs on the street, airports, on trains and buses, 49% of them used their MPs with only one hand and up to 90% held it vertically facing upwards [30]. Based on our tests, people were reading messages and surfing the Internet by holding the MP typically with the elevation angle within the range of 5°–65°. Therefore, without any loss of generality, we have adopted the same elevations in this study. Note that, the download traffic (mostly data) is significantly higher than the upload and other forms of traffic as reported in [31], therefore we have focused only on the download case.

Let us have an example of a NLOS transmission when the Rx (i.e., the MP) is located near the corner of a room (i.e., the position of 0.5 m × 0.5 m × 1.2 m), see Figures 1b and 2b. The upper edge of the user's MP is oriented in azimuth and elevation angles of 180° and 50°, respectively. The impulse responses of the link with no LOS path and using a MP-based Rx with front and rear cameras are depicted in Figure 3a,b, respectively. The impulse responses are calculated using the first five reflection components from walls. As can be seen from the figures, using the rear camera oriented to the Tx, the received power is higher and the impulse response is slightly less dispersive compared to the front photodiode.

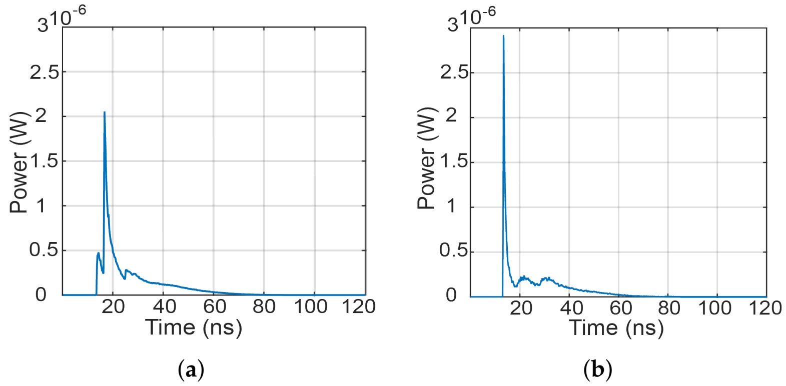

Figure 3. Impulse response of the link with MP acting as a Rx when using: (**a**) front camera; and (**b**) rear camera.

3.3. Noise

At the Rx, there are three dominant noise sources: shot noise, thermal noise and intersymbol interference caused by an optical paths difference. The total noise variance is calculated as:

$$\sigma_{total}^2 = \sigma_{shot}^2 + \sigma_{thermal}^2 + \gamma^2 P_{rISI}^2 \tag{4}$$

where γ is the photodiode responsivity (A/W) and P_{rISI} is the received power by intersymbol interference (ISI) given by:

$$P_{rISI} = \int_T^{\infty} (h(t) \otimes s(t))dt \tag{5}$$

where $h(t)$ is the impulse response, $s(t)$ represents the transmitted optical pulse and the symbol $\otimes$ denotes convolution. The shot noise is defined in terms of its variance as [21]:

$$\sigma_{shot}^2 = 2q\gamma(P_r + P_{rISI})B + 2qI_{bg}I_2B \tag{6}$$

where q is the electric charge, P_r is the received optical power, B is the equivalent noise bandwidth, I_{bg} is the background dark current and I_2 is the bandwidth noise factor. The thermal noise variance is independent of the incident power and is given by [21]:

$$\sigma_{thermal}^2 = \frac{8\pi k T_k}{G} \eta A_r I_2 B^2 + \frac{16\pi^2 k T_k \Gamma}{g_m} \eta^2 A_r^2 I_3 B^3 \tag{7}$$

where the two terms represent feedback-resistor noise and field effect transistor (FET) channel noise, respectively. Here, k is the Boltzmann's constant, T_K is the absolute temperature, I_3 is the noise bandwidth factor, G is the open-loop voltage gain, η is the fixed capacitance of a PD per unit area, Γ is the FET channel noise factor and g_m is the FET transconductance.

3.4. Modulation

Along with illumination, LEDs can be also used for data communications. Here, we have adopted the most common data format of on-off keying (OOK) for intensity modulation of LEDs. However, other modulation formats could also be used. The information bits of an LED are denoted by $\{b^j\}_{j=-\infty}^{\infty}$ where b^j is a uniformly distributed sequence of {0,1}. The LED is 'on' when $b^j = 1$ and is 'off' when $b^j = 0$. Let $rect(t)$ be a unit amplitude rectangular pulse of duration T (i.e., data rate $R_d = T^{-1}$). The transmitted optical signal is given by:

$$s(t) = P_p \sum_{j=-\infty}^{\infty} b^j rect(t - jT) \tag{8}$$

where P_p is the peak optical power of the emitted light wave. The received electrical signal at the photodiode is given by:

$$y(t) = \gamma h(t) \otimes s(t - \tau) + n(t) \tag{9}$$

where $n(t)$ is the additive white Gaussian noise (AWGN) and τ denotes the transmission delay.

A standard matched filter is adopted at the Rx in order to recover the transmitted data. The impulse response of the filter at the Rx is a rectangular pulse of a unity amplitude and duration T. Let us assume $\tau = 0$, i.e., the matched filter of the Rx is synchronized to the arrival signal transmitted by an LED as in [24].

3.5. Relay Assisted Models

Among the various possible strategies available for user-based relay assisted cooperation [19,20], in this paper we have adopted: the AF and DF schemes. In this case, the source transmits a packet (or symbol) in one time slot and the RN re-transmits it in the next time slot, which are then combined at the destination prior to decision making. The scheme like in [18] consists of two phases. At first, the Tx sends data to both the relay and the Rx. In the relaying phase, the Tx remains silent and the relay terminal forwards the data to the Rx.

3.5.1. Analytical Performance of AF Relaying

In the AF mode, the RN amplifies the received signal and forwards it to the Rx. Here we assume that the power of the signal retransmitted by the RN is scaled uniformly with respect to all bits in the packet with the average retransmission energy of E_S. In the 1st time slot/phase the sampled signals received at the RN ($y_R(t)$) and at the Rx (destination) ($y_D(t)$) are given by:

$$y_R(t) = \sqrt{E_s} h_{SR}(t) \otimes s(t) + n_R(t) \tag{10}$$

$$y_D(t) = \sqrt{E_s} h_{SD}(t) \otimes s(t) + n_D(t) \tag{11}$$

where h_{SR} and h_{SD} denote the VLC impulse responses for the Tx-RN and the Tx-Rx links, respectively, and n_R and n_D are AWGN noises. During the 2nd time slot/phase the signals at the output of the RN and received by the Rx are, respectively, given by [32]:

$$x_R^{AF}(t) = \sqrt{\frac{E_S}{E_S h_{SR}^2(t) + \sigma_{total}^2}} h_{SR}(t) \otimes s(t) + \sqrt{\frac{1}{E_S h_{SR}^2(t) + \sigma_{total}^2}} n_R(t) \tag{12}$$

$$y_D^{AF}(t) = \sqrt{E_s} h_{RD}(t) \otimes x_R^{AF}(t) + n_D^{'}(t) \tag{13}$$

where $n_D^{'}$ is the AWGN noise.

Combining (12) and (13), the *sampled signal* (from sampled signal we mean that the time varying signal is passed through a matched filter and it is sampled to maximize the signal-to-noise ratio, therefore, we drop the time index t) can be written as:

$$y_D^{AF} = \sqrt{E_s} h_{RD} \sqrt{\frac{E_S h_{SR}^2}{E_S h_{SR}^2 + \sigma_{total}^2}} s + \sqrt{E_s} h_{RD} \sqrt{\frac{1}{E_S h_{SR}^2 + \sigma_{total}^2}} n_R + n_D^{'} \quad (14)$$

From Equation (14) it is clear that $y_D^{AF} \sim \mathcal{N}(\mu_1, \sigma_1^2)$ where
$\mu_1 = \sqrt{E_s} h_{RD} \sqrt{\frac{E_S h_{SR}^2}{E_S h_{SR}^2 + \sigma_{total}^2}} s$ and $\sigma_1^2 = \left(\frac{E_s h_{RD}^2}{E_S h_{SR}^2 + \sigma_{total}^2} + 1 \right) \sigma_{total}^2$

Log-Likelihood Detector

At destination, the receiver has two copies of the transmitted signal. Employing the equal gain combining scheme at the Rx. The *sampled signal* is given as:

$$y_D^{'} = y_D + y_D^{AF} \quad (15)$$

It can be seen from (11) and (14) that the probability density function (PDF) of the sampled signal is given by:

$$f(y_D^{'}) = \mathcal{N}(\mu_2, \sigma_2^2) \quad (16)$$

where $\mu_2 = \mu_1 + \sqrt{E_s} h_{SD} s$ and $\sigma_2^2 = \sigma_1^2 + \sigma_{total}^2$.

The Rx will detect the transmitted bit from the received signal by using the log-likelihood ratio (LLR) detector, which can be written as:

$$f(y_D^{'} | s = 1) \underset{0}{\overset{1}{\gtrless}} f(y_D^{'} | s = 0) \quad (17)$$

Hence, for the AF cooperative scheme the LLR detector test gives:

$$\frac{1}{\sqrt{2\pi\sigma_2^2}} e^{-\frac{(y_D^{'} - \mu_2^{'})^2}{2\sigma_2^2}} \underset{0}{\overset{1}{\gtrless}} \frac{1}{\sqrt{2\pi\sigma_2^2}} e^{-\frac{(y_D^{'})^2}{2\sigma_2^2}} \quad (18)$$

where $\mu_2^{'} = \mu_2|_{s=1}$.

From (18), we get the following threshold-based detector, which indicates that if the value of received sampled signal is greater than the threshold κ_{th}^{AF}, then the transmitted symbol is estimated as 1, else it is 0:

$$y_D^{'} \underset{0}{\overset{1}{\gtrless}} \kappa_{th}^{AF} \quad (19)$$

where

$$\kappa_{th}^{AF} = \frac{1}{2} \left(\frac{E_S h_{SR} h_{RD}}{\sqrt{E_S h_{SR}^2 + \sigma_{total}^2}} + \sqrt{E_s} h_{SD} \right) \quad (20)$$

Bit Error Rate Calculation:

The overall bit error probability of the considered VLC system with OOK is given as:

$$P_e^{AF} = \frac{1}{2} (P_e(y_D^{'} | s = 0) + P_e(y_D^{'} | s = 1)) \quad (21)$$

Equation (21) can be rewritten as:

$$P_e^{AF} = \frac{1}{2} (Pr(y_D^{'} > \kappa_{th}^{AF} | s = 0) + Pr(y_D^{'} < \kappa_{th}^{AF} | s = 1)) \quad (22)$$

where $Pr(\cdot)$ stands for the probability.

Employing (16) in (22), we get:

$$P_e^{AF} = \frac{1}{2}\left(\int_{\kappa_{th}^{AF}}^{\infty} \frac{1}{\sqrt{2\pi\sigma_2^2}} e^{-\frac{(y_D^{'})^2}{2\sigma_2^2}} dy_D^{'} + \int_{-\infty}^{\kappa_{th}^{AF}} \frac{1}{\sqrt{2\pi\sigma_2^2}} e^{-\frac{(y_D^{'}-\mu_2^{'})^2}{2\sigma_2^2}} dy_D^{'} \right) \tag{23}$$

Substituting $\frac{y_D^{'}}{\sigma_2} = t$ and $\frac{y_D^{'}-\mu_2^{'}}{\sigma_2} = u$ in (21) we can rewrite it as:

$$P_e^{AF} = \frac{1}{2}\left(\int_{\frac{\mu_2^{'}}{2\sigma_2}}^{\infty} \frac{1}{\sqrt{2\pi}} e^{-\frac{t^2}{2}} dt + \int_{-\infty}^{-\frac{\mu_2^{'}}{2\sigma_2}} \frac{1}{\sqrt{2\pi}} e^{-\frac{u^2}{2}} du \right) \tag{24}$$

Again substituting $u = -v$ in the second integral of (24), we have:

$$P_e^{AF} = \frac{1}{2}\left(\int_{\frac{\mu_2}{2\sigma_2}}^{\infty} \frac{1}{\sqrt{2\pi}} e^{-\frac{t^2}{2}} dt + \int_{\frac{\mu_2}{2\sigma_2}}^{\infty} \frac{1}{\sqrt{2\pi}} e^{-\frac{v^2}{2}} dv \right) \tag{25}$$

The integrals of (25) can be written in the form of Gaussian Q function as:

$$P_e^{AF} = Q\left(\frac{\mu_2^{'}}{2\sigma_2}\right) = Q\left(\frac{E_S h_{SR} h_{RD} + \sqrt{E_s} h_{SD} \sqrt{E_S h_{SR}^2 + \sigma_{total}^2}}{2\sqrt{\left(E_s h_{RD}^2 + 2(E_S h_{SR}^2 + \sigma_{total}^2)\right)\sigma_{total}^2}} \right) \tag{26}$$

3.5.2. Analytical Performance of Selective DF Relaying

In the DF scheme the source will transmit the signal to the both relay and the destination within the 1st time slot. Here, the relay will follow the selective DF cooperative scheme. If the relay decodes the signal correctly then it will retransmit the signal to the destination during the 2nd time slot/phase, otherwise it will stay idle. The received signal in the DF scheme is given by:

$$y_D^{DF}(t) = \sqrt{E_s} h_{RD}(t) \otimes s(t) + n_D^{'}(t) \tag{27}$$

The equations for the signal transmitted by the source to the relay and from the source to the destination are same as (10) and (11).

Due to selective relaying, the received sampled signal at the destination is given by:

$$y_D^{'} = \begin{cases} y_D^{DF} + y_D, & \text{when relay decodes correctly} \\ y_D, & \text{when relay does not decode correctly} \end{cases} \tag{28}$$

It can be easily verified from (28) that when relay decodes correctly, then we have:

$$y_D^{'} \sim \mathcal{N}(0, 2\sigma_{total}^2), \ for\ s = 0 \tag{29}$$

$$y_D^{'} \sim \mathcal{N}((h_{SD} + h_{RD})\sqrt{E_s}, 2\sigma_{total}^2), \ for\ s = 1 \tag{30}$$

From (29) and (30) the LLR detection rule can be written as:

$$\frac{1}{\sqrt{4\pi\sigma^2}} e^{-\frac{(y_D^{'})^2}{4\sigma^2}} \underset{1}{\overset{0}{\gtrless}} \frac{1}{\sqrt{4\pi\sigma^2}} e^{-\frac{(y_D^{'}-\sqrt{E_s}(h_{SD}+h_{RD}))^2}{4\sigma^2}} \tag{31}$$

Solving (31) results in the following detection condition:

$$y_D^{'} \underset{0}{\overset{1}{\gtrless}} \frac{\sqrt{E_s}(h_{SD} + h_{RD})}{2} = \kappa_{th}^{DF,1} \tag{32}$$

Similarly, when the relay is in error and remains idle, we have the following detection condition:

$$y_D^{'} \underset{0}{\overset{1}{\gtrless}} \frac{\sqrt{E_s} h_{SD}}{2} = \kappa_{th}^{DF,0} \tag{33}$$

Based on (32) and (33), the destination uses the following detection [33]:

$$y_D + v y_D^{DF} \underset{0}{\overset{1}{\gtrless}} \kappa_{th}^{DF,v} \tag{34}$$

where $v = 1$ when relay transmits and $v = 0$ when relay does not transmit.

The BER for the considered VLC system for the case *when the relay is transmitting* can be given as:

$$P_e^{DF,1} = \frac{1}{2}\left(\int_{\kappa_{th}^{DF,1}}^{\infty} \frac{1}{\sqrt{4\pi\sigma_{total}^2}} e^{-\frac{(y_D^{'})^2}{4\sigma_{total}^2}} dy_D^{'} + \int_{-\infty}^{\kappa_{th}^{DF,1}} \frac{1}{\sqrt{4\pi\sigma_{total}^2}} e^{-\frac{(y_D^{'} - \sqrt{E_s}(h_{SD}+h_{RD}))^2}{4\sigma_{total}^2}} dy_D^{'} \right) \tag{35}$$

Solving (35) in a similar way as (23) the BER is given as:

$$P_e^{DF,1} = Pr\big(y_D + y_D^{DF} < \kappa_{th}^{DF,1} | s = 1\big) = Q\left(\frac{\sqrt{E_s}(h_{SD} + h_{RD})}{2\sqrt{2}\sigma_{total}} \right) \tag{36}$$

Similarly, the BER for the case when the relay is in error and remains idle in the 2nd phase can be found as:

$$P_e^{DF,0} = Pr\big(y_D < \kappa_{th}^{DF,0} | s = 1\big) = Q\left(\frac{\sqrt{E_s} h_{SD}}{2\sqrt{2}\sigma_{total}} \right) \tag{37}$$

Further, the BER of the relay is given by:

$$P_e^{R} = Q\left(\frac{\sqrt{E_s} h_{SR}}{2\sqrt{2}\sigma_{total}} \right) \tag{38}$$

Using (36)–(38), and results given in [33], the overall BER for the proposed VLC system using the selective DF cooperative scheme is given as:

$$P_e^{DF} = Q\left(\frac{\sqrt{E_s} h_{SR}}{2\sqrt{2}\sigma_{total}} \right) Q\left(\frac{\sqrt{E_s} h_{SD}}{2\sqrt{2}\sigma_{total}} \right) + \left(1 - Q\left(\frac{\sqrt{E_s} h_{SR}}{2\sqrt{2}\sigma_{total}} \right) \right) Q\left(\frac{\sqrt{E_s}(h_{SR} + h_{RD})}{2\sqrt{2}\sigma_{total}} \right) \tag{39}$$

Figure 4 provides a comparison of the average BER as a function of SNR for both AF and DF schemes and for different irradiance angles of the relay and the source. The mobile parameters were used from Table 2, a distance between the source and the end user was set to 3 m and the RN was located in the middle of the link. We can clearly see how DF outperforms AF. As the value of irradiance angle increases for a constant FOV, the performance of the considered VLC system degrades. For example at a $BER = 10^{-3}$ the power penalties are 0.8 dB and 0.75 dB for θ = 30° and 50°, respectively.

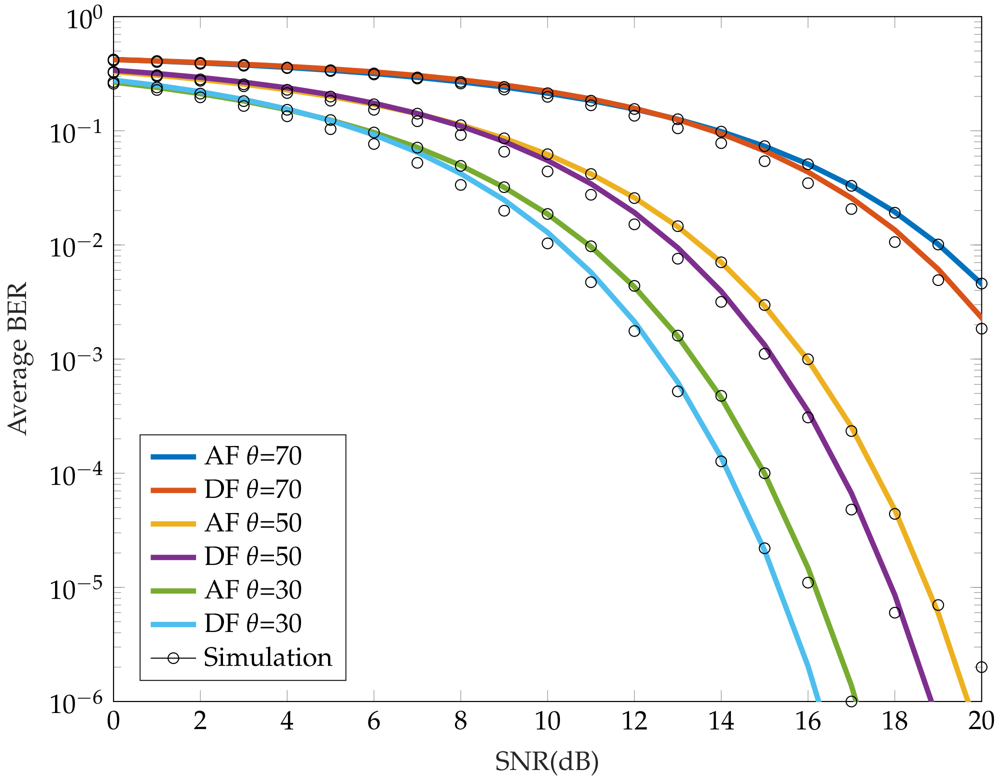

Figure 4. Comparison of average BER for different irradiance angle with constant FOV.

4. Simulation Results

In this section, we present the results for the performance analyses of the proposed VLC relay cooperation system. In order to provide a more accurate comparison between AF and DF modes, we have adopted a simulation model with 5 reflections based on the Monte Carlo ray tracing algorithm using the assumption of a half-duplex OOK cooperation transmission link. For simulations, we have used the key parameters shown in Table 2.

In order to evaluate the azimuthal and angular dependency of the RN, we assessed a scenario where the relay user is located at the coordinates of 2 m × 2 m × 1.2 m with the transmit power of 2 W. Figure 5a,b depict a comparison of the SNR as a function of the azimuth and elevation angles for AF and DF relaying schemes. SNR > 9.8 dB corresponds to a BER of 10^{-3} for the relay user transmission. Note that, the maximum SNR is achieved at the azimuth angle of –15°.

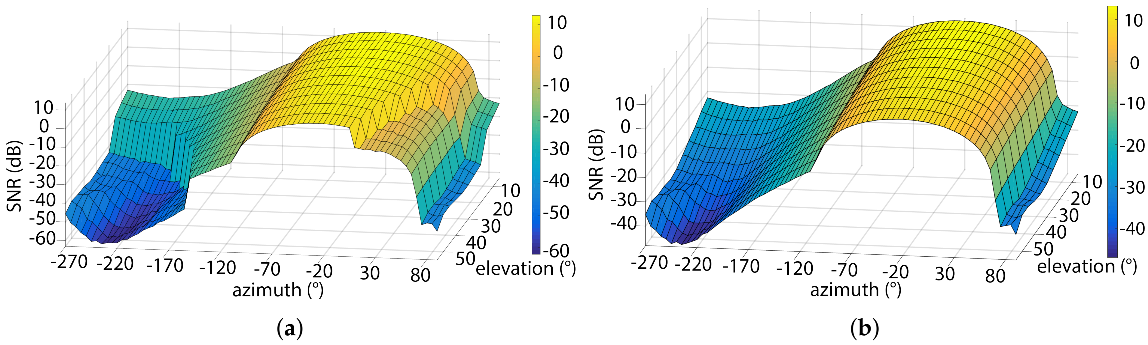

Figure 5. SNR dependency on azimuthal orientation of relay in: (**a**) AF; and (**b**) DF.

To illustrate the position of the mobile relay user within the room, see Figure 1b. We calculated the impulse response of the channel, considering that the mobile relay user can only move around within a specific region in the room, see yellow marked area in Figure 1b. As an example for the relay-assisted DF model, with the RN positioned at the coordinates of 2 m × 2 m × 1.2 m with azimuth and elevation angles of –20° and 5°, respectively, the impulse responses for source-to-RN and RN-to-Rx are depicted in Figure 6a,b, respectively. The channel gains for the source-relay G_{SR} and the relay-user G_{RD} links against the direct source-user link are determined to be 39.1 dB and 4.4 dB, respectively.

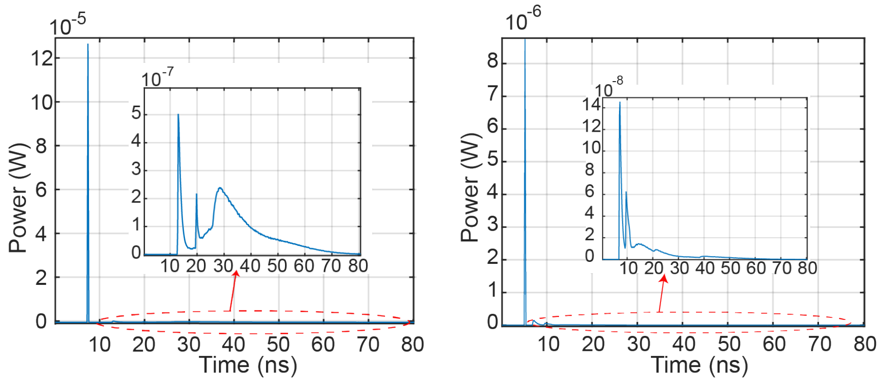

(**a**) (**b**)

Figure 6. Impulse response for VLC with RN for: (**a**) source to RN; and (**b**) RN to the Rx.

Next we considered the azimuthal orientation of the RN against its position within the yellow area of the room, see Figure 1b. In the simulation, we have assumed that the Rx is (i) at the elevation angle of 55°; and (ii) an azimuth angle is –180°. Figure 7 shows the borders of the room covered by the RN for a range of azimuthal angles to ensure a BER of 10^{-3}. Figure 7a is for the case when the RN is oriented more to the opposite direction from the source (negative azimuth). It can be seen that the DF mode offers improved results more specifically at positions further from the source (i.e., x = 0 to 0.8) and close to the wall. For the azimuth of –20°, with the DF the coverage area is only increased by ∼0.2 m^2 compared to AF, therefore less complex AF would be the preferred option to adopt. A difference of 20° in the azimuthal plane results in changes in the coverage area by ∼30 cm and 40 cm in the x- and y-axis, respectively. Note that, RN widens the coverage area by ∼1.9 m^2 for the azimuth angle changed from –80° (orientation to the wall) to –20°. The insets in Figure 7a depict the overall impulse responses of the VLC channel (i.e., from Tx to the Rx via the RN) for given positions and the azimuth of –20°, where SNR is mainly affected by the ISI.

The azimuthal orientation of the RN in the contra-clockwise direction (i.e., from the 0° to 80° towards the Tx) is illustrated in Figure 7b. In the case where the RN rotates in azimuth to the left, the DF cooperative mode offers an improvement of more than 10 cm for all positions in the y-axis. Note that, the relay MP azimuthal oriented in 80° can be used only in small fraction area. For a wider angle of rotation, the difference in the coverage area between AF and DF modes increases from 0.2 m^2 for 20° to 0.4 m^2 for 60°. Whereas, the azimuthal orientations of 0° and 80° result in widening of the coverage area by 2.16 m^2.

In the following, we show how the RN area changes based on the elevation of the MP for both AF and DF-based links for a range of elevation angles θ_{MP}, an azimuth angle of –20°, and a BER of $< 10^{-3}$ as illustrated in Figure 8a. The maximum covered area is achieved for θ_{MP} of 5°, therefore RN can be placed up to 2 m from the Rx. Increasing θ_{MP} to 25° results in the reduced distance between the RN and Rx by ∼10 cm. For θ_{MP} of 65° the maximal RN position in the y-axis is only 1.6 m. Note that, for 25° $< \theta_{MP} <$ to 45° the coverage area is changed by 0.67 m^2.

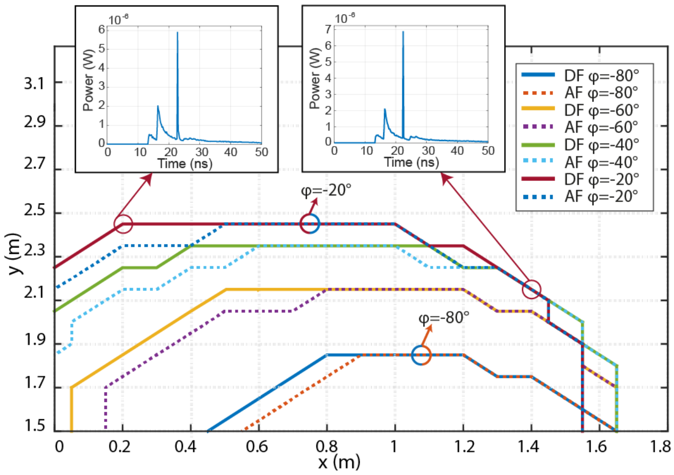

(**a**)

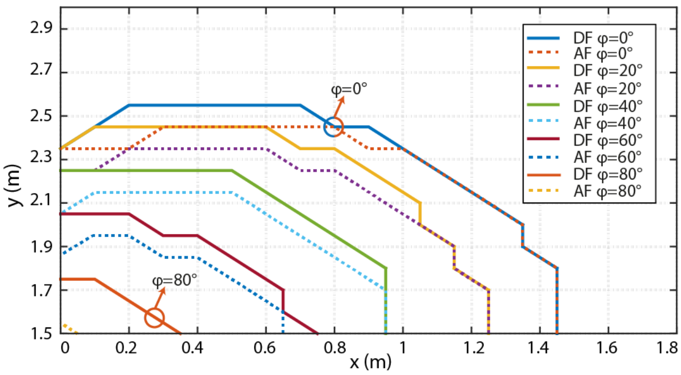

(**b**)

Figure 7. Azimuthal dependency of the RN with an elevation angle of 5° with RN oriented toward the: (**a**) right wall; and (**b**) left wall. Curves show the borders where the RN can be used and ensures a BER of $< 10^{-3}$ for the entire link. Insets in (**a**) illustrate impulse responses of the complete relay-assisted link.

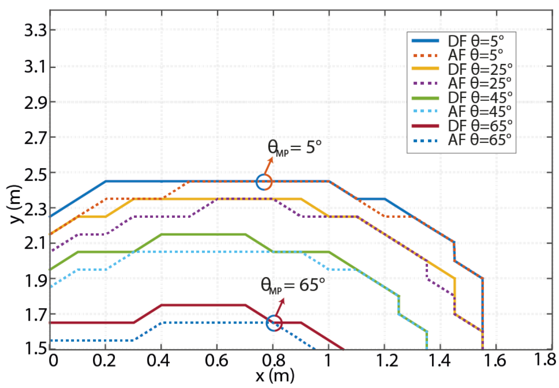

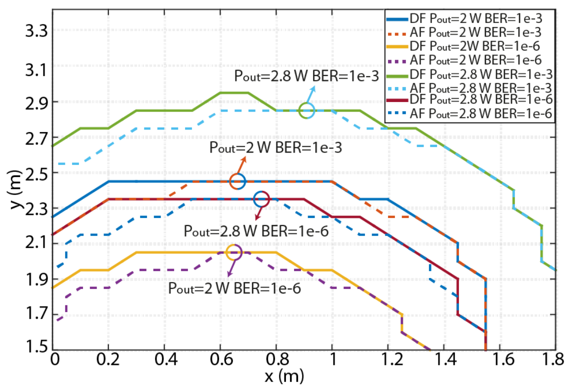

(**a**) (**b**)

Figure 8. (**a**) Elevation angle dependence of RN for both AF and DF-based links for a range of irradiance angle θ_{MP}, an azimuth angle of –20° and a BER of $< 10^{-3}$; and (**b**) RN transmitted power and the BER profiles for both DF and AF-based links.

The final result illustrates how the RN area can be extended either by increasing the transmit power P_{out} (i.e., more LEDs on the MP) at the RN or by changing the target BER. In Figure 8b, we compare the transmit power from the relay MP for both DF and AF modes for the optimum azimuth and elevation angles of –20° and 5°, respectively. For example, for a BER of 10^{-3} using a LED array of 1 × 14 with the P_{out} of ∼2.8 W the coverage area for relay-assisted communications is increased by ∼1.43 m^2 compared to the LED array of 1 × 10. Note that, in case of P_{out} of 2 W and lower BER target 10^{-6} we can observe reduced coverage area as expected.

5. Conclusions

In this paper, we investigated an OOK half-duplex-based VLC link with a mobile unit-based relay node used to improve the link availability and coverage area in a typical office environment. For the first time, the real mobile was considered with two photodetectors on both sides of mobile phone (utilising spatial diversity) and a perpendicular placed transmitting LED array. We considered the case where the receiver was positioned close to the corner of the room and we investigated the optimal position of the relay node based on its azimuthal and elevation orientation. The results showed significant improvement in the link performance using cooperative schemes when compared to direct NLOS transmission. In addition, we derived analytic model that compared DF and AF relay techniques. The results showed that DF outperforms the AF relaying scheme for different irradiance angles. The power penalties at a BER of 10^{-3} were 0.8 and 0.75 dB for θ = 30° and 50°. Numerical results also illustrated that the DF relay-based system offered a wider coverage area compared with the AF scheme.

Acknowledgments: The work was supported by the Czech Science Foundation project GACR 17-17538S, SGS 279 CTU (SGS17/182/OHK3/3T/13) and Engineering and Physical Sciences Research Council (EPSRC) funded MARVEL project (EP/P006280/1).

Author Contributions: P.P. conceived the idea and developed the simulation model, S.Z. supervised the work, M.R.B. and P.S. derived the analytic model and revised the paper, P.C. and Z.G. contributed in the revision of the paper. All authors contributed equally to writing the paper.

Conflicts of Interest: The authors declare no conflict of interest.

References

1. Barnett, T.J.; Sumits, A.; Jain, S.; Andra, U. Cisco Visual Networking in Update Global Mobile Data Traffic Forecast, 2016–2021—White paper. Available online: https://cisco.com (accessed on 28 November 2017).
2. Ghassemlooy, Z.; Alves, L.N.; Zvanovec, S.; Khalighi, M.A. *Visible Light Communications Theory and Applications*; Taylor & Francis Group: New York, NY, USA, 2017; ISBN: 9781498767538.
3. Ghassemlooy, Z.; Arnon, S.; Uysal, M.; Xu, Z.; Cheng, J. Emerging Optical Wireless Communications-Advances and Challenges. *IEEE J. Sel. Areas Commun.* **2015**, *33*, 1738–1749.
4. Elgala, H.; Mesleh, R.; Haas, H. Indoor Optical Wireless Communication: Potential and State-of-the-Art. *IEEE Commun. Mag.* **2008**, *49*, 56–62.
5. Grubor, J.; Randel, S.; Langer, K.D.; Walewski, J.W. Broadband Information Broadcasting using LED-Based Interior Lighting. *J. Light. Technol.* **2008**, *26*, 3883–3892.
6. Rajbhandari, S.; McKendry, J.J.D.; Herrnsdorf, J.; Chun, H.; Faulkner, G.; Haas, H.; Watson, I.M.; O'Brien, D. A Review of Gallium Nitride LEDs for Multi-Gigabit-per-Second Visible Light Data Communications. *Semicond. Sci. Technol.* **2017**, *32*, 23001, doi:10.1088/1361-6641/32/2/023001.
7. Wang, Y.; Huang, X.; Tao, L.; Shi, J.; Chi, N. 4.5-Gb/s RGB-LED Based WDM Visible Light Communication System Employing CAP Modulation and RLS Based Adaptive Equalization. *Opt. Express* **2015**, *23*, 13626–13633.
8. Huang, X.; Wang, Z.; Shi, J.; Wang, Y.; Chi, N. 1.6 Gbit/s Phosphorescent White LED Based VLC Transmission using a Cascaded Pre-Equalization Circuit and a Differential Outputs PIN Receiver. *Opt. Express* **2015**, *23*, 22034–22042.
9. Ding, D.; Ke, X. A New Indoor VLC Channel Model Based on Reflection. *Optoelectron. Lett.* **2010**, *6*, 295–298.
10. Wang, Q.; Wang, Z.; Dai, L. Multiuser MIMO-OFDM for Visible Light Communications. *IEEE Photonics J.* **2015**, *7*, 1–11, doi:10.1109/JPHOT.2015.2497224.

11. Chvojka, P.; Zvanovec, S.; Haigh, P.A.; Ghassemlooy, Z. Channel Characteristics of Visible Light Communications within Dynamic Indoor Environment. *J. Light. Technol.* **2015**, *33*, 1719–1725.
12. Chen, Z.; Tsonev, D.; Haas, H. Improving SINR in Indoor Cellular Visible Light Communication Networks. In Proceedings of the 2014 IEEE International Conference on Communications, Sydney, Australia, 10–14 June 2014; pp. 3383–3388.
13. Burton, A.; Ghassemlooy, Z.; Rajbhandari, S.; Liaw, S.K. Design and Analysis of an Angular-Segmented Full-Mobility Visible Light Communications Receiver. *Trans. Emerg. Telecommun. Technol.* **2014**, *25*, 591–599.
14. *802.15.7-2011—IEEE Standard for Local and Metropolitan Area Networks–Part 15.7: Short-Range Wireless Optical Communication Using Visible Light*; IEEE: Piscataway, NJ, USA, 2011; pp. 1–309, doi:10.1109/IEEESTD.2011.6016195.
15. Yang, H.; Pandharipande, A. Full-Duplex Relay VLC in LED Lighting Triangular System Topology. In Proceedings of the 2014 6th International Symposium on Communications, Control and Signal Processing, Athens, Greece, 21–23 May 2014; pp. 85–88.
16. Chowdhury, H.; Katz, M. Cooperative Multihop Connectivity Performance in Visible Light Communications. In Proceedings of the 2013 IFIP Wireless Days, Valencia, Spain, 13–15 November 2013; pp. 1–4.
17. Kashef, M.; Torky, A.; Abdallah, M.; Al-Dhahir, N.; Qaraqe, K. On the Achievable Rate of a Hybrid PLC/VLC/RF Communication System. In Proceedings of the 2015 IEEE Global Communications Conference, San Diego, CA, USA, 6–10 December 2015; pp. 1–6.
18. Hussain, S.I.; Abdallah, M.M.; Qaraqe, K.A. Hybrid Radio-Visible Light Downlink Performance in RF Sensitive Indoor Environments. In Proceedings of the 2014 6th International Symposium on Communications, Control and Signal Processing, Athens, Greece, 21–23 May 2014; pp. 81–84.
19. Narmanlioglu, O.; Kizilirmak, R.C.; Uysal, M. Relay-Assisted OFDM-Based Visible Light Communications over Multipath Channels. In Proceedings of the 2015 17th International Conference on Transparent Optical Networks, Budapest, Hungary, 5–9 July 2015; pp. 1–4.
20. Kizilirmak, R.C.; Narmanlioglu, O.; Uysal, M. Relay-Assisted OFDM-Based Visible Light Communications. *IEEE Trans. Commun.* **2015**, *63*, 3765–3778.
21. Komine, T.; Nakagawa, M. Fundamental Analysis for Visible-Light Communication System using LED Lights. *IEEE Trans. Consum. Electron.* **2004**, *50*, 100–107.
22. Lee, K.; Park, H.; Barry, J.R. Indoor Channel Characteristics for Visible Light Communications. *IEEE Commun. Lett.* **2011**, *15*, 217–219.
23. Hayasaka, N.; Ito, T. Channel Modeling of Nondirected Wireless Infrared Indoor Diffuse Link. *Electron. Commun. Jpn.* **2007**, *90*, 9–19.
24. Chen, Y.; Sung, C.W.; Ho, S.W.; Wong, W.S. BER Analysis for Interfering Visible Light Communication Systems. In Proceedings of the 2016 10th International Symposium on Communication Systems, Networks and Digital Signal Processing, Prague, Czech Republic, 20–22 July 2016; pp. 1–6.
25. Cisco Service Provider Wi-Fi: A Platform for Business Innovation and Revenue Generation. Available online: https://cisco.com (accessed on 28 November 2017).
26. Miramirkhani, F.; Uysal, M. Channel Modeling and Characterization for Visible Light Communications. *IEEE Photon. J.* **2015**, *7*, 1–16.
27. Rodriguez, S.P.; Perez-Jimenez, R.; Lopez-Hernandez, F.J.; Gonzalez, O.; Ayala, A. Reflection Model for Calculation of the Impulse Response on IR-Wireless Indoor Channels using Ray-Tracing Algorithm. *Microw. Opt. Technol. Lett.* **2002**, *32*, 296–300.
28. Rodriguez, S.P.; Perez-Jimenez, R.; Mendoza, B.R.; Lopez-Hernandez, F.J.; Ayala, A. Simulation of Impulse Response for Indoor Visible Light Communications using 3D CAD Models. *EURASIP J. Wirel. Commun. Netw.* **2013**, *2013*, 1–10.
29. Del Campo-Jimenez, G.; Perandones, J.M.; Lopez-Hernandez, F.J. A VLC-Based Beacon Location System for Mobile Applications. In Proceedings of the 2013 International Conference on Localization and GNSS, Turin, Italy, 25–27 June 2013; pp. 3–6.
30. How Do Users Really Hold Mobile Devices? Available online: http://uxmatters.com (accessed on 20 November 2017).
31. Ding, N.; Wagner, D.; Chen, X.; Hu, Y.C.; Rice, A. Characterizing and Modeling the Impact of Wireless Signal Strength on Smartphone Battery Drain. *ACM SIGMETRICS Perform. Eval. Rev.* **2013**, *41*, 29–40.

32. Yu, M.; Li, J. Is Amplify-and-Forward Practically Better than Decode-and-Forward or Vice Versa? In Proceedings of the 2005 IEEE International Conference on Acoustics, Speech and Signal Processing, Philadelphia, PA, USA, 23 March 2005; pp. 365–368.
33. Bhatnagar, M.R. Performance Analysis of Decode-and-Forward Relaying in Gamma-Gamma Fading Channels. *IEEE Photon. Technol. Lett.* **2012**, *24*, 545–547.

4.4 Experimental Validation of Indoor Relay-Assisted Visible Light Communications for a Last-Meter Access Network

This chapter is a version of the published manuscript:

P. Pesek, S. Zvanovec, Z. Ghassemlooy, N. A. M. Nor, "Experimental validation of indoor relay-assisted visible light communications for a last-meter access network," Optics Communications, vol. 451, pp. 319—322, 2019.

Connection to my Ph.D. thesis:

Based on our previous work reported in section 4.3, we experimentally evaluate the AF, DF relaying schemes and NLOS link for interconnection of the last meter VLC access network. The paper provides the first-ever experimental results and comparisons for relaying VLC systems. I demonstrate that a relay-based VLC scheme improves system performance, especially for link spans longer than 5 meters. The diffuse VLC system is resistant to shadowing and blocking. Nonetheless, due to multipath induced dispersion, the NLOS provides lower data rates and high losses. I also demonstrate that an m-CAP VLC link relay scheme achieves about a 60% higher data rate when compared to a relay-based link and a single VLC link over a transmission distance of 7 m.

Optics Communications 451 (2019) 319–322

Contents lists available at ScienceDirect

Optics Communications

journal homepage: www.elsevier.com/locate/optcom

Experimental validation of indoor relay-assisted visible light communications for a last-meter access network

Petr Pesek [a,*], Stanislav Zvanovec [a], Petr Chvojka [a], Zabih Ghassemlooy [b], Norhanis Aida Mohd Nor [c], Pooria Tabeshmehr [d]

[a] Department of Electromagnetic Field, Faculty of Electrical Engineering, Czech Technical University in Prague, 16627, Czech Republic
[b] Optical Communications Research Group, NCRLab, Faculty of Engineering and Environment, Northumbria University, Newcastle upon, Tyne NE1 8ST, UK
[c] Department of Science, Kulliyyah of Engineering, International Islamic University Malaysia, P.O. Box 10, 50728 Kuala Lumpur, Malaysia
[d] Department of Electrical and Computer Engineering, University of Tehran, Amir Abad St., Tehran, Iran

ARTICLE INFO

Keywords:
Visible light communication (VLC)
Amplitude-and-forward (AF)
Decode-and-forward (AF)
Multiband carrier-less amplitude and phase modulation (*m*-CAP)

ABSTRACT

This paper provides experimental results for a relay-assisted visible light communications (VLC) link using a white light-emitting diode (LED) for a last-meter access network. We demonstrate that a relay-based VLC scheme improves the system performance, especially for link spans longer than 5 meters, in the presence of blocking and shadowing by redirecting the transmitted signal. We also demonstrate a multiband carrier-less amplitude and phase modulation (*m*-CAP) VLC link where the decode-and-forward (DF) relay scheme offers improvement in the data rate by 25% and 60% when compared to the amplify-and-forward (AF) relay-based link and single VLC link over a 7 m transmission distance respectively.

1. Introduction

In recent years, end users have increasingly demanded wireless connectivity with improved flexibility, reliability, scalability, data throughput, as well as significantly reduced latency [1]. Although, radio frequency-based wireless technologies (WTs) have addressed these demands, in particular, improved both the spectral and power efficiencies, end users still face spectrum congestion due to the exponential growth in data being used and generated. To address spectral congestion and allow the use of the radio frequency (RF) spectrum in applications where it is most needed, the focus of this research has been on the utilisation of an alternative complementary WT. Within this context, visible light communications (VLC) have been considered as a possible solution for high-speed communications, especially in indoor environments [2,3].

In VLC systems, white light emitting diode-based lights are used to provide illumination, data communication and indoor localisation within indoor scenarios. VLC links, with a range of data rates R_d over short transmission spans, have been reported in the literature. In [4], a 1 Gb/s real-time line-of-sight (LOS) VLC link based on non-return-to-zero on–off keying (NRZ-OOK), with a bit error rate (BER) of 7.36×10^{-4} using a commercial phosphorescent white light emitting diode (LED) over a transmission distance of 1.5 m, was reported. A VLC system employing a micro-LED with R_d of 3.5 Gb/s and 5 Gb/s using pulse-amplitude modulation (PAM) and DC-biased optical orthogonal frequency division multiplexing (DCO-OFDM) respectively, over a link span 0.5 m, was demonstrated in [5]. In [6], a combination of a DCO-OFDM and a red–green–blue (RGB) LED-based wavelength division multiplexing (WDM) VLC system was used to demonstrate R_d of 11.28 Gb/s (and 10.4 Gb/s with forward error correction (FEC) overhead reduction) over a link span of 1.5 m.

However, the performance of VLC links depends mostly on the transmission distance between the transmitter (Tx) and the receiver (Rx), and the received optical power via the LOS path (i.e., the dominant path in high-speed VLC links). Thus, higher R_d are associated with the availability of an LOS transmission path, which is not always the case in indoor environments due to mobility, shadowing and blocking effects caused by people and objects within the room.

To address this problem and maintain an uninterrupted data transmission with much reduced interference, even within temporarily shadowed regions in an indoor environment, an angular diversity Rx, together with different combining schemes, was proposed in [7,8]. An alternative solution to shadowing is to use a hybrid RF/VLC system to ensure link availability at all times. In [9], the authors investigated an indoor data network composed of multiple VLC and RF access points, whereas in [10], the expression for the outage probability of relay-assisted hybrid RF/VLC link for an indoor application was given. In [11], the effect of human induced shadowing on VLC link performance was investigated, but with no effective solutions being proposed to address the problem. To increase VLC link reliability and availability, a full-duplex (FD) relay link using LED-based triangular topology was

* Corresponding author.
E-mail address: pesekpe3@fel.cvut.cz (P. Pesek).

https://doi.org/10.1016/j.optcom.2019.06.071
Received 23 May 2019; Received in revised form 27 June 2019; Accepted 28 June 2019
Available online 2 July 2019
0030-4018/

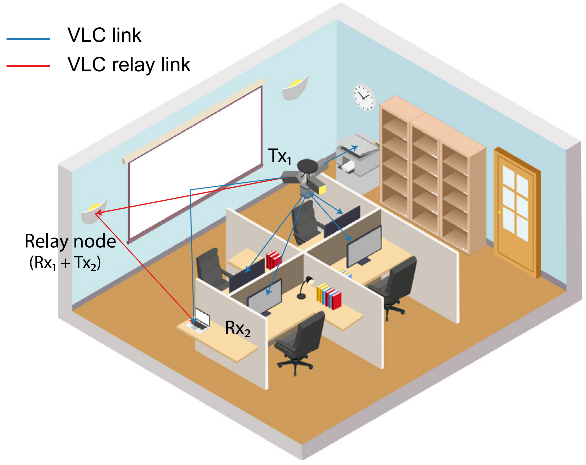

Fig. 1. Schematic diagram of a relay-assisted VLC link for an office.

investigated in [12] and showed improved BER performance compared to LOS VLC. The performance of the cooperative multi-hop relay-based VLC system has been reported in the literature by considering (*i*) the user's mobility and relay probabilities [13]; (*ii*) FD relay compared with a half-duplex (HD) system [14]; (*iii*) OFDM VLC with amplify-and-forward (AF) or decode-and-forward (DF) relay schemes over frequency-selective indoor channels while considering different pulse shaping filters [15]; and (*iv*) DCO-OFDM VLC for optimal power allocation and improved BER performance [16]. In most relay-based VLC links, the use of relay nodes has not been fully exploited since they are treated as auxiliary nodes. In [17], an asymmetrically clipped DCO-OFDM (ADO-OFDM) relay-based VLC system with two power allocation factors was investigated and was shown to offer highly stable communications. In [18], an optical bidirectional beacon, composed of RGB LEDs, photodetectors and colour filters was proposed as an effective scheme to address the performance degradation in a non-LOS VLC system. In [19], we analytically investigated an OOK HD-based VLC link which used a mobile unit-based relay node to improve link availability and coverage area in a typical office environment. A new analytical description of BER for the AF- and DF-based relay VLC links has been provided.

Nonetheless, none of the existing works have reported an experimental comparison single channel and relay-based VLC link performance. In this paper, we experimentally investigate the performance of multiband carrier-less amplitude and phase (m-CAP) modulation scheme AF relay-assisted systems and DF relay-assisted VLC systems for the last meter access network, as can be seen in a typical scheme illustrated in Fig. 1. In an office environment, the link between the end user (i.e., a laptop (Rx_2)) and the Tx can experience shadowing due to partitioning screens and other objects (fixed or mobile) within a room. In this scenario, the link can be re-established via a relay node (i.e., wall mounted lights) or via non-LOS (i.e., reflections), see Fig. 1. The main contributions of this paper are (*i*) a demonstration of results from an experimental testbed for a relay-based *m*-CAP VLC link, and (*ii*) a performance comparison of LOS, non-LOS and relay-assisted VLC links in terms of R_d.

The rest of the paper is organised as follows: in Section 2, the experimental setup and system parameters are outlined, whereas, in Section 3, the results for the relay-assisted VLC system are presented. Finally, the conclusions are given in Section 4.

2. System setup

The system setup for AF and DF relay-assisted VLC systems is depicted in Fig. 2. A (2^{15}−1) long pseudorandom binary sequence

Table 1
VLC system parameters.

Parameter	Value
Pseudorandom binary sequence	$2^{15} - 1$
LED biased current	480 mA
m-CAP signal bandwidth	5 MHz
Biconvex lenses focal length at Rxs	35 mm
Biconvex lenses focal length at Txs	25 mm
VSG peak-to-peak voltage	300 mV
VSG sample frequency	20 MHz
Oscilloscope sample rate	1 GSa/s
BER limit	3.8×10^{-3}
m-CAP order	10
m-CAP roll-off factor	0.2
m-CAP filter length	10 symbols

(PRBS) $x_b(t)$ is generated for each *m*-CAP subcarrier (SC) and mapped into M-ary quadrature amplitude modulation (M-QAM) symbols, where M is the order of modulation. The mapped data is up-sampled and split into its real and imaginary parts prior to being applied to the square root raised cosine pulse shaping (SRRC) filters. Note, the impulse responses form a Hilbert pair, i.e., being orthogonal in the time domain and shifted by 90° in phase; more details of *m*-CAP modulation scheme can be found, e.g., in [20]. The generated signals are loaded to a vector signal generator (VSG) (Rohde & Schwarz SMW200A) the output of which is DC-biased prior to the intensity modulation of two commercially available LEDs (OSRAM Golden Dragon) used for Tx_1 and Tx_2. The white LED 3 dB modulation bandwidth, with no pre-equalisation, is limited to 1.5 MHz. For the measurement, we set the transmitted signal bandwidth to 5 MHz. Biconvex lenses, with focal lengths f_1 and f_2 of 25 mm and 35 mm respectively, are used at the Txs and the Rxs to increase the received optical power level.

The complexity of *m*-CAP depends mainly on (*i*) filter length L_s; (*ii*) roll-off factor β; and (*iii*) the number of SCs (i.e., m). Following our previous works [21,22], we have set L_s to 10 symbols (since for $L_s > 10$ there is marginal performance improvement), β to 0.2 and m to 10, which offers the best trade-off between complexity and R_d.

Following a transmission over the first channel, the relaying schemes are applied. The relay node is composed of an optical Rx_1 (an adjustable gain Si avalanche photodetector with a low noise transimpedance amplifier (Thorlabs APD430A)), an LED driver and the Tx_2. For the AF-scheme, the received signal is amplified to its initial power level and retransmitted over the second channel. Whereas for the DF-scheme, the received signal is captured using a real-time digital oscilloscope (OSC, LeCroy WaveRunner Z640i) and processed (i.e., demodulated) off-line in Matlab. The processed and regenerated signal is loaded to VSG and retransmitted via the Tx_2 over channel 2. At the Rx_2 (Thorlabs PDA10A2), following optical detection, the signal is resampled to the sampling frequency of the transmitted signal, then demodulated to recover the estimated version of $x_b(t)$. All the key parameters adopted in the proposed system are shown in Table 1. An application improvement could be done using biconvex lenses with shorter focal length or by lenses integration on a chip.

3. Experimental results

The primary objective is to analyse the performance of relay-assisted *m*-CAP VLC systems for a range of link spans in terms of R_d. Note, the same conditions were adopted during the experimental measurements to compare both AF and DF schemes (i.e., keeping the same transmit power level and a BER threshold level of 3.8×10^{-3} (corresponding to the 7% FEC limit)).

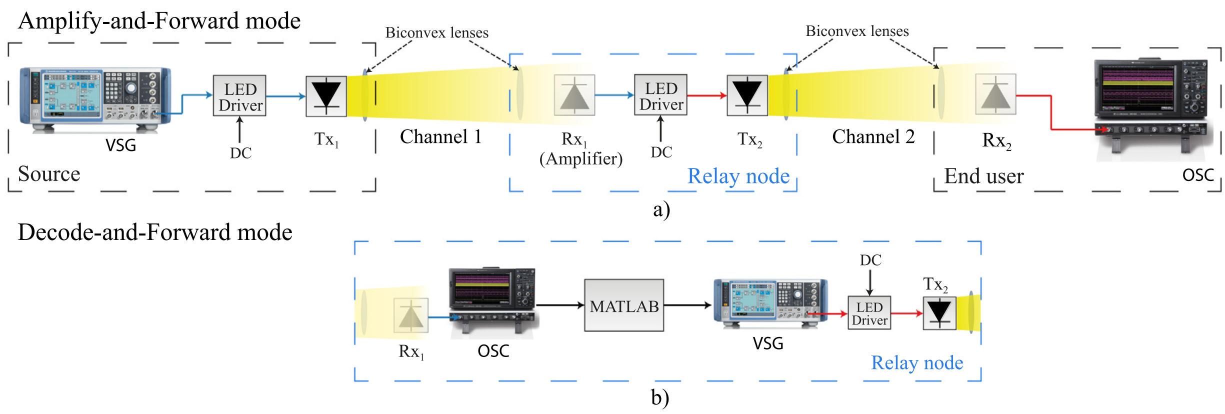

Fig. 2. Experimental setup for the relay-assisted VLC link with: (a) AF, and (b) DF relay nodes.

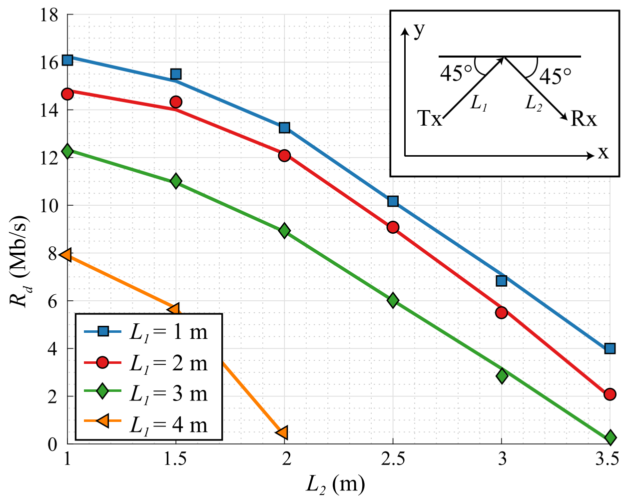

Fig. 3. Measured *m*-CAP VLC link performance with reflections from a whiteboard for a range of L_1 and L_2.

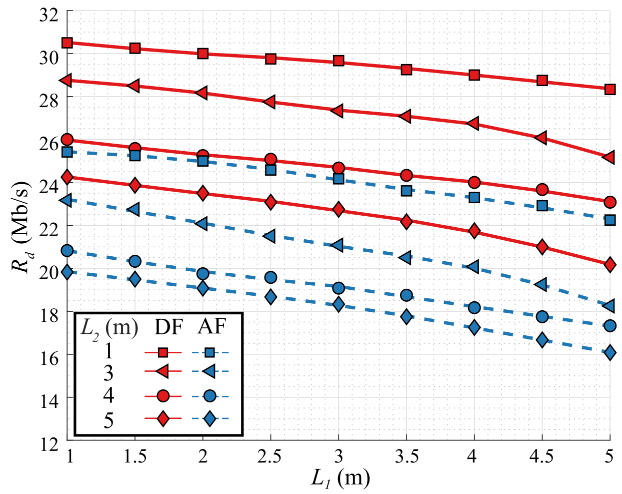

Fig. 4. Measured data rates against L_1 for AF and DF based *m*-CAP VLC for a range of L_2 link spans.

3.1. Reflected link performance

As illustrated in Fig. 1, the signal can reach end users via non-LOS paths by means of reflections from walls or any other surfaces within the room. To this end, an experimental measurement for R_d with reflections from whiteboard for a range of L_1 and L_2 was conducted. Note that both the end user's Rxs and the ceiling-based LEDs (Txs) were pointing to a whiteboard at an angle of 45° as shown in the inset of Fig. 3. For the sake of simplification, the Rx and the Tx were positioned at the same height. The distortion and absorption of the light signal by the whiteboard results in a significant reduction in R_d with respect to L_2. To achieve a maximum R_d, we used a pilot binary phase-shift keying (BPSK) signal to load the appropriate number of bits/symbol to each individual SC based on the measured signal-to-noise ratio (SNR) level. For a 2 m long L_1, increasing L_2 by about 2 m results in R_d being reduced by ~9.5 Mb/s. Nonetheless, in the worst-case scenario, only a 2 m transmission extension can lead to reduced R_d 0.5 Mb/s due to the reflected beam distortion.

3.2. Dependences of relay links spans

Thus, in the next part, R_d was measured as a function of the first channel length L_1 and a range of second channel spans L_2 for both AF and DF relay-based *m*-CAP VLC links.

As shown in Fig. 4, the maximum R_d of 31 Mb/s is achieved for the shortest link with DF and a BER below the 7% FEC threshold level of 3.8×10^{-3}. The extension of the transmission link span (either in channel 1 or channel 2) has resulted in a reduced received optical power level, thus leading to the deterioration of the link's SNR performance. The difference in R_d between the two schemes is from 4 to 6 Mb/s depending on the link span. The performance difference is caused by noise accumulation and amplification at the relay node in AF protocol, while noise is eliminated during processing in the DF scheme. By extending the channels and keeping the same BER value around the FEC limit, the AF scheme is influenced more by the limited received optical power level, i.e., a decrease in the data rates of 3.5 Mb/s and 4.92 Mb/s for DF and AF, respectively for L_2 = 3 m and L_1 increased by 4 m (i.e., from 1 m to 5 m).

3.3. Performance of the entire relay-assisted link

Fig. 5 illustrates the comparison of aggregated *m*-CAP R_d (i.e., maximum achieved performance) of the entire VLC link over link distance for the following scenarios (*i*) with the relay scheme (i.e., AF and DF); note in this case, we plot the best achieved R_d from all combinations of L_1 and L_2; (*ii*) LOS without relay, i.e., a direct link — maximally measured either within channel 1 or channel 2; and (*iii*) NLOS VLC with a reflection. The maximum R_d is reached in the case of the DF-relay VLC link. An LOS link without the relaying scheme can offer improved performance for up to a 5 m link compared to the AF scheme. This is due to the limited 3 dB modulation bandwidth of the OSRAM Golden Dragon LED. Note that with no regeneration, as in

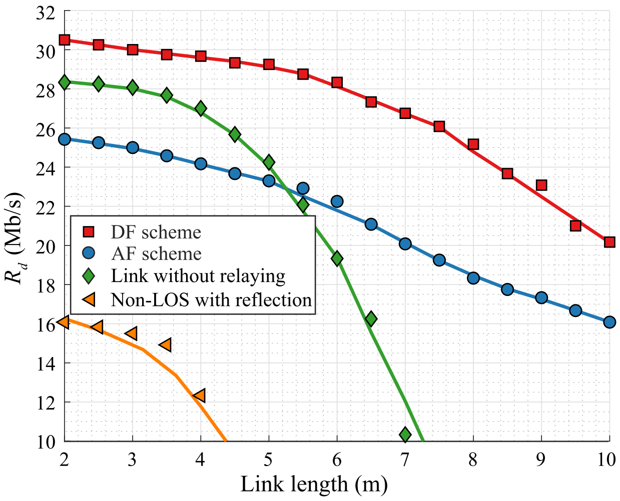

Fig. 5. Experimentally measured data rates of the VLC systems: DF (red), AF (blue), link without relaying (green) and non-LOS with reflection (orange).

the case in AF, the received signal with low SNR is again degenerated by an LED. However, for a transmission range of beyond 5 m, link performance without relaying is marginally decreased due to lower SNR. The measured data rates for the non-LOS link (i.e., reflected) are approximately half that of the DF system for a link span of up to 3.5 m and decreases to less than 10 Mb/s for link spans longer than 4.5 m. For a data rate of 16 Mb/s, the AF scheme offers five times greater transmission length compared to a non-LOS VLC link.

4. Conclusion

In this paper, an *m*-CAP-based relay-assisted VLC system was experimentally investigated. It was demonstrated that relay VLC links can provide higher data rates compared to a direct VLC link. This is particularly important for link distances longer than 5 m. For relay VLC systems, it was shown that *m*-CAP-based DF VLC offered higher data rates of ∼25% over a link span of 10 m when compared to AF VLC.

Acknowledgements

The work was supported by Czech Science Foundation project GACR 17-17538S and the Horizon 2020 MSC ITN Grant 764461 (VISION).

References

[1] Cisco Systems Inc., Cisco Visual Networking Index: Global Mobile Data Traffic Forecast Update, 2016–2021 White Paper. Cisco 2017; URL: https://www.cisco.com/c/en/us/solutions/collateral/service-provider/visual-networking-index-vni/complete-white-paper-c11-481360.pdf.

[2] Z. Ghassemlooy, L.N. Alves, S. Zvánovec, M.A. Khalighi, Visible light communications: Theory and applications, Visible Light Communications: Theory and Applications, ISBN: 9781498767545, 2017, pp. 1–568, http://dx.doi.org/10.1201/9781315367330.

[3] S. Long, M.A. Khalighi, M. Wolf, S. Bourennane, Z. Ghassemlooy, Investigating channel frequency selectivity in indoor visible-light communication systems, IET Optoelectron. 10 (3) (2016) 80–88, http://dx.doi.org/10.1049/iet-opt.2015.0015.

[4] H. Zhang, A. Yang, L. Feng, P. Guo, Gb/s real-time visible light communication system based on white leds using t-bridge cascaded pre-equalization circuit, IEEE Photonics J. 10 (2) (2018) http://dx.doi.org/10.1109/JPHOT.2018.2812759.

[5] R.X.G. Ferreira, E. Xie, J.J.D. McKendry, S. Rajbhandari, H. Chun, G. Faulkner, S. Watson, A.E. Kelly, E. Gu, R.V. Penty, I.H. White, D.C. O'Brien, M.D. Dawson, High bandwidth GaN-based micro-LEDs for multi-Gb/s visible light communications, IEEE Photonics Technol. Lett. 28 (19) (2016) 2023–2026, http://dx.doi.org/10.1109/LPT.2016.2581318.

[6] H. Chun, S. Rajbhandari, G. Faulkner, D. Tsonev, E. Xie, J.J.D. McKendry, E. Gu, M.D. Dawson, D.C. O'Brien, H. Haas, LED based wavelength division multiplexed 10 Gb/s visible light communications, J. Lightwave Technol. 34 (13) (2016) 3047–3052, http://dx.doi.org/10.1109/JLT.2016.2554145.

[7] Z. Chen, D. Tsonev, H. Haas, Improving SINR in indoor cellular visible light communication networks, in: 2014 IEEE International Conference on Communications, ICC 2014, ISBN: 9781479920037, 2014, pp. 3383–3388, http://dx.doi.org/10.1109/ICC.2014.6883844.

[8] A. Burton, Z. Ghassemlooy, S. Rajbhandari, S.K. Liaw, Design and analysis of an angular-segmented full-mobility visible light communications receiver, Trans. Emerg. Telecommun. Technol. 25 (6) (2014) 591–599, http://dx.doi.org/10.1002/ett.2811.

[9] M. Kashef, M. Ismail, M. Abdallah, K.A. Qaraqe, E. Serpedin, Energy efficient resource allocation for mixed RF/VLC heterogeneous wireless networks, IEEE J. Sel. Areas Commun. 34 (4) (2016) 883–893, http://dx.doi.org/10.1109/JSAC.2016.2544618.

[10] M. Namdar, A. Basgumus, T. Tsiftsis, A. Altuncu, Outage and BER performances of indoor relay-assisted hybrid RF/VLC systems, IET Commun. 12 (17) (2018) 2104–2109, http://dx.doi.org/10.1049/iet-com.2018.5389.

[11] Y. Xiang, M. Zhang, M. Kavehrad, M.I.S. Chowdhury, M. Liu, J. Wu, X. Tang, Human shadowing effect on indoor visible light communications channel characteristics, Opt. Eng. 53 (8) (2014) 086113, http://dx.doi.org/10.1117/1.oe.53.8.086113.

[12] H. Yang, A. Pandharipande, Full-duplex relay VLC in LED lighting triangular system topology, in: ISCCSP 2014 - 2014 6th International Symposium on Communications, Control and Signal Processing, Proceedings, ISBN: 9781479928903, 2014, pp. 85–88, http://dx.doi.org/10.1109/ISCCSP.2014.6877822.

[13] H. Chowdhury, M. Katz, Cooperative multihop connectivity performance in visible light communications, in: IFIP Wireless Days, ISBN: 9781479905423, 2013, http://dx.doi.org/10.1109/WD.2013.6686444.

[14] O. Narmanlioglu, R.C. Kizilirmak, F. Miramirkhani, M. Uysal, Cooperative visible light communications with full-duplex relaying, IEEE Photonics J. 9 (3) (2017) http://dx.doi.org/10.1109/JPHOT.2017.2708746.

[15] O. Narmanlioglu, R.C. Kizilirmak, M. Uysal, Relay-assisted OFDM-based visible light communications over multipath channels, in: International Conference on Transparent Optical Networks; Vol. 2015-August, ISBN: 9781467378802, 2015, http://dx.doi.org/10.1109/ICTON.2015.7193338.

[16] R.C. Kizilirmak, O. Narmanlioglu, M. Uysal, Relay-assisted OFDM-based visible light communications, IEEE Trans. Commun. 63 (10) (2015) 3765–3778, http://dx.doi.org/10.1109/TCOMM.2015.2464815.

[17] Z. Na, Y. Wang, M. Xiong, X. Liu, J. Xia, Modeling and throughput analysis of an ADO-OFDM based relay-assisted VLC system for 5G networks, IEEE Access 6 (2018) 17586–17594, http://dx.doi.org/10.1109/ACCESS.2018.2817487.

[18] S.V. Tiwari, A. Sewaiwar, Y.H. Chung, Optical bidirectional beacon based visible light communications, Opt. Express 23 (20) (2015) 26551, http://dx.doi.org/10.1364/oe.23.026551.

[19] P. Pešek, S. Zvanovec, P. Chvojka, M.R. Bhatnagar, Z. Ghassemlooy, P. Saxena, Mobile user connectivity in relay-assisted visible light communications, Sens. (Switzerland) 18 (4) (2018) http://dx.doi.org/10.3390/s18041125.

[20] M.I. Olmedo, T. Zuo, J.B. Jensen, Q. Zhong, X. Xu, S. Popov, I.T. Monroy, Multiband carrierless amplitude phase modulation for high capacity optical data links, J. Lightwave Technol. 32 (4) (2014) 798–804, http://dx.doi.org/10.1109/JLT.2013.2284926.

[21] P. Chvojka, K. Werfli, S. Zvanovec, P.A. Haigh, V.H. Vacek, P. Dvorak, P. Pesek, Z. Ghassemlooy, On the m-CAP performance with different pulse shaping filters parameters for visible light communications, IEEE Photonics J. 9 (5) (2017) http://dx.doi.org/10.1109/JPHOT.2017.2749203.

[22] P. Chvojka, P.A. Haigh, S. Zvanovec, P. Pesek, Z. Ghassemlooy, Evaluation of multi-band carrier-less amplitude and phase modulation performance for VLC under various pulse shaping filter parameters, in: 13th Int. Joint Conf. E-Bus. Telecommun., 2016, pp. 25–31, http://dx.doi.org/10.5220/0005956900250031.

4.5 An Experimental Multi-User VLC System using Non-Orthogonal Multi-Band CAP Modulation

This chapter is a version of the published manuscript:

P. Pesek, P. A. Haigh, O. I. Younus, P. Chvojka, Z. Ghassemlooy, S. Zvanovec, "An Experimental Multi-User VLC System using Non-Orthogonal Multi-Band CAP Modulation," Optics Express, vol. 28(12), pp. 18241–18250, 2020.

Connection to my Ph.D. thesis:

Majority of current OWC systems focus on maximization of point-to-point data rates, however, a multi-user interconnection represents the key parameter of last meter networks. Therefore, I have developed a multi-user VLC system using the CAP-based modulation scheme. Optimizing the system performance using pulse shaping filter parameters and expanded non-orthogonal multi-band super-Nyquist CAP (m-ESCAP), system data rate achieves ~470 Mb/s for 4-users. Furthermore, for higher allocation flexibility and scalability, I modified m-CAP modulation format by allocating different bandwidth of the individual subcarriers to users, called Am-CAP attaining the same or lower computational complexity compared to the conventional m-CAP.

Research Article | Vol. 28, No. 12 / 8 June 2020 / Optics Express 18241

Optics EXPRESS

Experimental multi-user VLC system using non-orthogonal multi-band CAP modulation

P. PEŠEK,[1,*] P. A. HAIGH,[2] O. I. YOUNUS,[3] P. CHVOJKA,[1] Z. GHASSEMLOOY,[3] AND S. ZVÁNOVEC[1]

[1] *Wireless and Fibre Optics Group, Department of Electromagnetic Field, Faculty of Electrical Engineering, Czech Technical University in Prague, Prague 16627, Czech Republic*
[2] *Intelligent Sensing and Communications Group, Newcastle University, NE1 7RU, UK*
[3] *Optical Communications Research Group, Faculty of Engineering and Environment, Northumbria University, NE1 8ST, UK*
[*] *pesekpe3@fel.cvut.cz*

Abstract: This paper provides experimental results for a multi-user visible light communications system using multi-band carrier-less amplitude and phase (*m*-CAP) modulation scheme. We optimize the system performance by adapting pulse shaping filter parameters, subcarrier spacing and allocating different baud rates to individual sub-bands called allocated *m*-CAP (A*m*-CAP). We show that a maximal system data rate of ~468 Mb/s for four users can be supported while gaining higher flexibility for optimization and the same or lower computational complexity compared with the conventional *m*-CAP scheme.

1. Introduction

In recent years, visible light communication (VLC) has received a growing interest within both industrial and academic communities as a complementary technology to the radio frequency wireless systems in 5G and beyond networks [1]. In VLC systems, high-brightness light emitted diode (LED)-based lights are used to provide illumination, indoor localization and data communications in indoor environment at the moment – outdoor-based systems are also being considered [2]. The vast majority of current research activities have focused on the data rate R_b improvement i.e., from hundreds of Mb/s to a few Gb/s over the short line of sight transmission ranges (from few centimeters to few meters) [3,4]. Two of the most popular options, which have been widely adopted and reported in the literature to improve R_b, are the spectrally efficient quadrature amplitude modulation (QAM) symbol-based multicarrier modulation schemes including orthogonal frequency division multiplexing (OFDM) and carrier-less amplitude and phase (CAP) modulation [5–8]. However, the OFDM-based VLC systems with high peak-to-average power ratio (PAPR) are highly sensitive to the nonlinearity of the amplifiers, LEDs (i.e., power-current characteristics), which leads to the system performance deterioration [9].

An alternative to OFDM is the CAP modulation scheme, which has been investigated in intensity modulation and direct detection (IM-DD) VLC systems offering relatively higher R_b compared with OFDM using electrical components of limited bandwidth and lower complexity. In [9], OFDM- and CAP-based VLC links using a single red, green and blue (RGB) LEDs were experimentally investigated showing CAP offering 19% higher R_b compared with OFDM over the same link span [10]. An experimental *m*-CAP VLC link over a 1 m distance with a high spectral efficiency of 4.85 b/s/Hz for a single user scheme was demonstrated in [11]. Further modification of subcarrier spacing below orthogonality can improve the spectral efficiency about 25% for a direct LOS link without considering a multi-user scenario, which was demonstrated in [12]. In [13], an additional 20% improvement in the data rate was achieved by increasing the baud rates of individual non-orthogonal sub-bands while utilising the same signal bandwidth. This technique

#393813 https://doi.org/10.1364/OE.393813
Journal © 2020 Received 27 Mar 2020; revised 9 May 2020; accepted 26 May 2020; published 3 Jun 2020

Optics EXPRESS

is known as an expanded non-orthogonal super-Nyquist *m*-CAP (*m*-ESCAP). Another alternative approach is based on splitting the signal into unequally spaced subcarriers, which is known as variable *m*-CAP (V*m*-CAP) that offers a ∼30% improvement in R_b for a bandlimited VLC link with 6 subcarriers compared with the conventional 6-CAP and also reduced computational complexity [14]. However, increasing the number of bands will lead to a higher number of pulse shaping finite impulse response (FIR) filters, i.e., 4 FIR filters per band, thus significantly higher computational complexity. The higher sub-band orders of *m*-CAP are vulnerable to timing errors. For instance, in [15] a detailed analysis of the timing jitter in 40 Gb/s fiber optics system was given. high-order CAP VLC link with an aggregate data rate of 8 Gb/s over a link span of 1 m using a hybrid post equalizer (i.e., a linear Volterra series and a decision-directed least mean squares equalizer) over four wavelengths was reported in [16]. In [17], the scheme for 5G mobile networks combining *m*-CAP and non-orthogonal multiple access (NOMA) was experimentally evaluated over the W-band millimeter wave radio-over fiber system.

Current research, however, has mostly focused on point-to-point single-user scenarios. In an effort to transform VLC into a multi-user, flexible technology, more experimental investigation of the multi-user frequency division multiple access (FDMA) scheme has to be done. Orthogonal FDMA (OFDMA) was adopted in the 4G wireless networks, where multiple access is achieved by assigning subsets of sub-carriers to different users, thus allowing simultaneous data transmission from several users [18]. In OFDMA, the transmit power is allocated to individual users based on the signal-to-noise ratio (SNR). A comparison of the bit error rate (BER) performance, receiver (Rx) complexity, and PAPR for two versions of OFDMA were reported in [19]. An interleave division multiple access OFDMA with asymmetrically clipped optical OFDM offers higher power efficiency than conventional OFDMA, especially at higher R_b. In order to increase the system throughput and improve the signal to interference plus noise ratio (SINR) of the users at the cell boundaries a multi-point joint transmission VLC network was proposed in [20]. This scheme achieved data throughput improvement of 68% compared with a static resource partitioning system. Alternatively, such frequency reuse could be utilised to improve the performance of the edge user. In [21], a combination of dc-biased optical OFDM and fractional frequency reuse in optical cell networks was reported, which significantly reduced the inter-channel interference (ICI) and offered a good balance between the average spectral efficiency and system complexity. Time division multiple access (TDMA) can achieve a fair user experience compared with FDMA as is discussed for example in [22], FDMA-based schemes (i.e., *m*-CAP, OFDM, etc.) offer a number of advantages including no need for highly accurate two-level synchronisation and compatibility with the radio frequency based wireless technology as in 4G and 5G [23,24].

The first experimental verification of the multi-user *m*-CAP with a wavelength division multiplexed VLC system using a single RGB LED for serving up to 9 users was reported in [24]. A multi-user scheme of 20-CAP with a total R_b of 162.5 Mb/s for up to 20 users was reported in [23], where optimization of transmit filters' parameters was investigated.

Nevertheless, to the best of authors' knowledge, no works, on the experimental investigation of allocating different bandwidth of the individual subcarriers to users, called allocated *m*-CAP (A*m*-CAP), for multi-user scenarios have been reported yet. The primary objective of this paper is to investigate the performance of an optimized A*m*-CAP system with the same allocated data rate per user. To validate this, we have developed an experimental test-bed for both the conventional *m*-CAP and A*m*-CAP as a multi-user system by optimizing: *(i)* the subcarrier spacing, where the subcarrier bandwidth is purposely compressed below orthogonality by means of squeezing carrier frequencies; *(ii)* the roll-off factor, which can support higher spectral usage based on controlling the excess bandwidth of individual subcarriers; and *(iii)* a combination of carrier spacing and the roll-off factor to achieve the maximal spectrum efficiency and almost the same data throughputs for the users in a multi-user system. We show that, A*m*-CAP offers improved allocation flexibility (i.e., the same data throughput for all four users in this case) or lower computational complexity compared with conventional m-CAP. Furthermore, we show that, following optimization the spectral efficiency can be improved by about 12% to 4.68 b/s/Hz.

2. System setup

The schematic block diagram of the proposed multi-user VLC system is depicted in Fig. 1. A pseudorandom binary sequence of length 2^{15}-1 is generated for each subcarrier and mapped into complex symbols of M-QAM, where M is the order of modulation. Note, the data stream per user is allocated into one or more sub-bands depending on the number of users per cell and a number of m-CAP bands. The mapped data is up-sampled by means of zero-padding (i.e., the number of zeros/symbol is based on [11]):

$$n_s = 2 \cdot \lceil 2m(1+\beta) \rceil \tag{1}$$

where β is roll-factor of the transmit/receiver filters and $\lceil\cdot\rceil$ is the ceiling function. Then data is split into its real and imaginary components (i.e., in-phase (I) and quadrature (Q)) prior to being applied to the square root raised cosine (SRRC) pulse shaping filter pairs $f_I^n(t)$ and $f_Q^n(t)$, respectively. Note, filters impulse responses form a Hilbert pair, i.e., being orthogonal in the time domain and shifted by 90° in phase. The impulse responses are given as the product of the SRRC filter impulse response and the sine and cosine wave, as follow [25]:

$$f_I^n(t) = \left[\frac{sin[\gamma(1-\beta)] + 4\beta\frac{t}{T_s}cos[\gamma\delta]}{\gamma[1-(4\beta\frac{t}{T_s})^2]}\right] cos(2\pi f_c^n t) \tag{2}$$

$$f_Q^n(t) = \left[\frac{sin[\gamma(1-\beta)] + 4\beta\frac{t}{T_s}cos[\gamma\delta]}{\gamma[1-(4\beta\frac{t}{T_s})^2]}\right] sin(2\pi f_c^n t) \tag{3}$$

where T_s is the symbol duration, n denotes the index of a subcarrier, $\gamma = \pi t/T_s$ and $\delta = 1+\beta$. The frequencies of subcarriers, generated by the pulse shaping transmit filters, are given by [13]:

$$f_c^n = B_{tot}(1+\alpha)\left(\frac{1}{2m} - \frac{(n-1)(1+\alpha m - m)}{m(m-1)}\right) \tag{4}$$

where B_{tot} is defined as total signal bandwidth and α is the bandwidth compression factor. In m-CAP, α is set to 0 in order to maintain subcarrier orthogonality. However, in m-ESCAP, the carrier frequencies are shifted to lower values. On the other hand, for Am-CAP, the frequencies of subcarriers are given by:

$$\begin{aligned} f_c^n &= \frac{R_{b-Max}\delta}{2k_n n(1+\alpha)} && \text{, for } n = 1 \\ f_c^n &= \frac{R_{b-Max}\delta}{n(1+\alpha)2k_n} + \sum_{i=1}^{n-1} \frac{R_{b-Max}\delta}{n(1+\alpha)k_i} && \text{, otherwise} \end{aligned} \tag{5}$$

where R_{b-Max} is the maximal system data rate for n users and k is a number of bits/symbol for QAM. The output of CAP-based transmitter (Tx) is given by [25]:

$$s(t) = \sqrt{2}\sum_{n=1}^{m}\left(s_I^n(t) * f_I^n(t) - s_Q^n(t) * f_Q^n(t)\right) \tag{6}$$

where $s_I^n(t)$ and $s_Q^n(t)$ are the I and Q M-QAM symbols, respectively for the n^{th} subcarrier and $*$ represents time-domain convolution. With an increasing number of sub-bands, the allocation flexibility grows at the cost of significantly increased computational complexity. The complexity of the m-CAP can be expressed as [26]:

$$C_{m-CAP} = R_s \left(2m + 2 \sum_{n=1}^{m} n_n L_s \right) \tag{7}$$

where n_n is required sample count per symbol for the n^{th} subband, L_s is filter symbol length and R_s is baud rate. For example, the complexity of m-CAP almost halves for m when changed from $m = 8$ to 4. This is mainly because m-CAP complexity is proportional to m^2, i.e., O(m^2) [26], as indicated by Eq. (7), which significantly handicaps the higher orders of m-CAP.

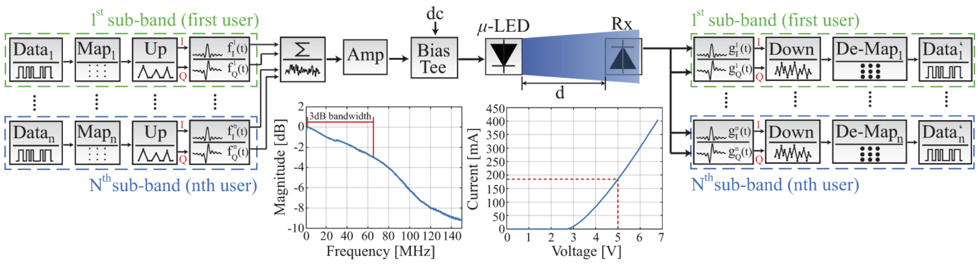

Fig. 1. The schematic block diagram of the experimental m-CAP VLC system. "Up", "Down", "Map" and "Amp" refer to up-sampling, down-sampling, mapper and amplifier, respectively. The left inset depicts measured LED frequency response with the highlighted 3 dB bandwidth of ~67 MHz. The right inset shows the measured I-V curve of the μ-LED.

The generated signal $s(t)$ in the Matlab is loaded into a signal generator (Teledyne LeCroy T3AWG3252), the output of which is amplified and dc-biased prior to IM of the LED. The light source used is a blue μ-LED with a wavelength of 449 nm, a linewidth of 14.6 nm and a measured 3 dB bandwidth of ~67 MHz, see the inset in Fig. 1. The signal is transmitted over a 20 cm free space channel, which is limited by the transmit power of the μ-LED. However, the transmission distance can be increased by using *(i)* high power μ-LEDs and *(ii)* array μ-LEDs as in attocells configurations [27,28]. At the Rx side, we use a combination of an optical lens

Table 1. VLC system parameters

Parameters	Value
Pseudorandom binary sequence	2^{15}-1
μ-LED bias current	185 mA
Total signal bandwidth	100 MHz
Rx biconvex lens focal length	25 mm
Signal generator peak-to-peak voltage	3.6 V
Amplification	2x
BER limit	3.8×10^{-3}
Filter length	16 symbols
Roll-off factor (No-optimization)	0.2
Roll-off factor (Carrier-optimization)	0.2
Rx wavelength range	200–1000 nm
Rx maximum responsivity	50 A/W at 600 nm
Rx bandwidth	400 MHz

with a focal length of 25 mm (not shown in Fig. 1) and optical Rx (APD430A2 Thorlabs with a low noise avalanche photo-detector and a trans-impedance amplifier) to regenerate the electrical CAP signal $s_r(t)$. Following capturing of $s_r(t)$ by a real-time oscilloscope (Keysight DSO9104A) and filtering by a low-pass filter (LPF) with 200 MHz bandwidth, the signal is resampled to the sampling frequency of the transmitted signal and applied to the time-reversed filter pairs at Rx, which are matched to the Tx filters, thus allowing each user to recover their data.

Following down-sampling and demodulation, the recovered M-QAM symbols allocated to the users are compared with the transmitted data for the BER estimation. In order to improve the system throughput, we have used a pilot binary phase-shift keying (BPSK) signal to load an appropriate k to individual subcarriers based on the measured SNR as in [29]. All the key system parameters adopted are listed in Tab. 1.

3. Experimental results

This section presents the results for R_b of optimized conventional m-CAP scheme and Am-CAP under the same transmission conditions. Here, we consider three optimization schemes: *(i)* uniform optimization of β, i.e., $0 \leq \beta \leq 1$, where higher values of β result in δ-times wider bandwidth; *(ii)* optimization of α, i.e., $0 \leq \alpha \leq 0.3$, using m-ESCAP, where the spacing between carriers is uniform and the total system bandwidth is limited to 100 MHz. Note, reducing the carrier spacing leads to inter-carriers interference (ICI), thus resulting in higher BER [12]; *(iii)* full-optimization, which is a combination of *(i)* and *(ii)*. The BER target is set to the 7% forward error correction (FEC) limit of $3.8{\times}10^{-3}$. The optimization process is depicted in Fig. 2. A full-optimization is realized in three steps. *(i)* Uniform optimization where the global values are set for all the subcarriers (i.e., m, α, β, f_c and M based on the loading algorithm). *(ii)* Splitting the algorithm into two branches, where the first and second branches are used for optimizing β and α with the step sizes of 0.05 and 0.01, respectively. Note, in full-optimisation we have used the β values from the β optimization to reduce brute force methods in one loop.

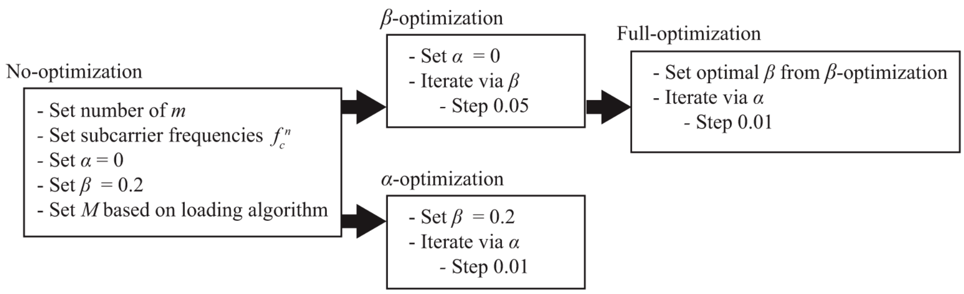

Fig. 2. Optimization process for obtaining system parameters of CAP-based scheme.

The bandwidth optimization of Am-CAP was based on the assumption the frequency response is flat. In that case, to achieve a maximum R_b, we used BPSK signal to load an appropriate number of bits/symbol to individual sub-bands based on the measured SNR. For instance, in 4-CAP the constellation size of the individual subcarriers is $M = \{64, 32, 32, 16\}$, however the same values can be expected even for A4-CAP due to flat frequency response. The carrier frequencies are then given by Eq. (5). Due to optimisation techniques, the calculated bandwidths are slightly changed, for example, calculated subcarriers bandwidth for A4-CAP are 20.8, 23, 23, 32.8 MHz, optimal subcarriers bandwidth are 20.4, 24.5, 24.5, 30.6 MHz. However, this first estimate significantly simplifies the ideal bandwidth allocation.

The concept of the proposed schemes is best illustrated using the frequency spectrum, see Fig. 3. The ideal spectra for conventional orthogonal m-CAP and Am-CAP are shown in Figs. 3(a) and (b), respectively, for $m = 2$ and for $\beta = 0.1$. With α-optimisation subcarriers of m-ESCAP and Am-CAP overlap as depicted in Figs. 3(c) and (d), respectively. Note, m-ESCAP and conventional m-CAP have the same B_{tot} (i.e., 100 MHz), and with no changes in the subcarrier spacing (i.e., f_c remain the same). Note the followings: *(i)* to improve the data rate while maintaining the same B_{tot}, the individual sub-bands can be expanded by increasing R_s of the individual subcarriers; and *(ii)* compressing the sub-bands beyond their orthogonality limit will result in electrical power penalty due to sub-band overlapping and improved spectral efficiency with no additional computational complexity at the receiver but at the cost of higher BER [12]. Finally, Figs. 3(e) and (f) show the ideal spectra for non-orthogonal 4-CAP and A4-CAP for $\beta = \alpha = 0.1$. Note, A4-CAP offers one additional dimension for tuning of the system resources (i.e., allocation of different bandwidth to subcarriers and therefore higher/lower data rate per user as and when needed) with no increased computation complexity.

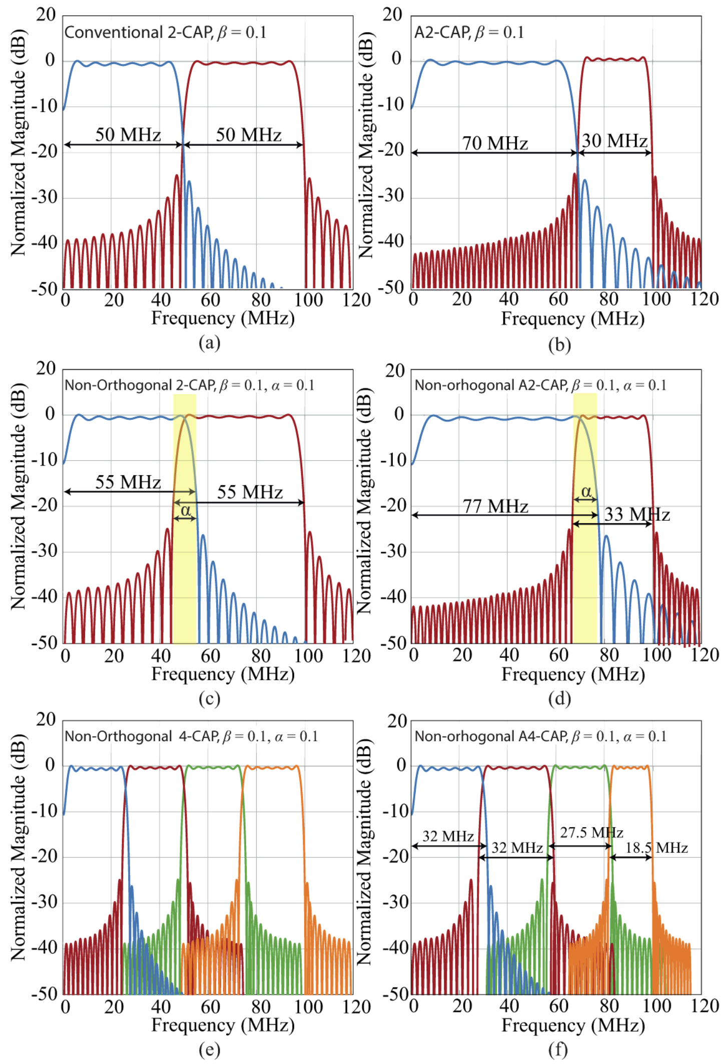

Fig. 3. Ideal spectra of (a) 2-CAP and (b) A2-CAP wtih $\beta = 0.1$, (c) 2-ESCAP and (d) the proposed multi-user A2-CAP with $\alpha = 0.1$ and $\beta = 0.1$. (e) and (f) show spectra of individual sub-carriers for 4-ESCAP and A4-CAP with the allocated bandwidths for users.

3.1. Conventional m-CAP

Figure 4(a) illustrates the maximum system data rate R_{b-Max} as a function of the m-CAP order with and without optimization. Note, with no optimization, β is set to 0.2, and R_{b-Max} of 416 Mb/s is achieved for 3- and 4-CAP and further increment of m does not improve the system performance in contrast to [11]. This is because of the μ-LED magnitude response decreases only ~6 dB over the 100 MHz frequency span, see the inset of Fig. 1, and the fact that higher sub-bands are more sensitive to the timing jitter and therefore synchronisation instability [15,30]. Higher-order CAP (i.e., $m > 4$) offers higher flexibility between the end-users at the cost of significantly increased system complexity and reduced R_{b-Max} (e.g., for 12-CAP R_{b-Max} is about 40 Mb/s lower compared with 4-CAP). For instance, in 10-CAP the constellation size of the individual subcarriers is $M = \{64, 64, 64, 32, 32, 16, 16, 16, 8, 8\}$. For 4-CAP with the carrier (β of 0.2 and α of 0.08), roll-off (β of 0.1) and full (β of 0.1 and α of 0.03), optimizations, R_{b-Max} are increased by 4, 9 and 13%, respectively, with respect to the 4-CAP without optimization. Note, for the highest data rate observed for 4-CAP with full-optimisation (i.e., β of 0.1 and α of 0.03) the maximum system spectral efficiency is 4.68 b/s/Hz.

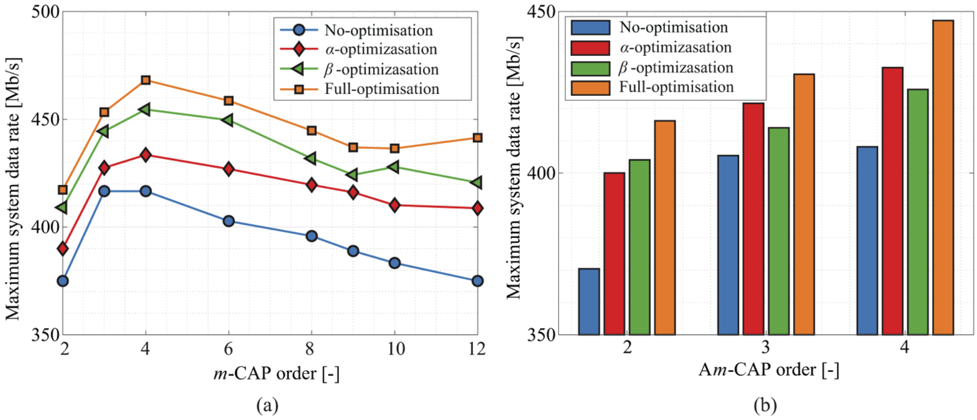

Fig. 4. Experimentally measured maximum data rate with and without optimization of (a) m-CAP and (b) Am-CAP

3.2. Am-CAP

Figure 4(b) shows the maximum system data rate R_{b-Max} as a function of m in Am-CAP shared between 2–4 users with and without optimisation. Am-CAP offers improved flexibility of multi-user allocation and M-ary assignment compared with the m-CAP scheme at the cost of increased PAPR [31]. For 2 users (i.e., A2-CAP), the system achieves R_{b-Max} of 370.42 Mb/s with the bandwidth allocations of 44.5 and 55.5 MHz and 32-QAM and 16-QAM, which increases to 400 and 404 Mb/s for the α- and β-optimisations, respectively. Note, Am-CAP with full-optimization (β and α of 0.1 and 0.03, respectively) offers 11% improvement in R_{b-Max}. The same patterns are observed for both A3- and A4-CAP. However, note, the α outperforms the β-optimization. This is due to the optimal β values of 0.175 and 0.15 for A3- and A4-CAP, respectively, which is close to the default value of 0.2 for no-optimisation. Note, R_{b-Max} of 447.21 Mb/s is achieved for A4-CAP with full-optimization.

3.3. Multi-user system

In a multi-user environment, the user's reception angle will considerably influence the system's BER performance. Figure 5(a) depicts the BER performance as a function of the user's orientation (i.e., angle) respect to the Tx for a range of R_{b-Max} (full-optimisation for 4-CAP, reduction about 15% and 30%). The results show that, at the FEC limit, a maximum tolerance angle of 25° is accepted by the user with the highest R_{b-Max} of 468.18 Mb/s followed by R_{b-Max} of 401.81 and 327.73 Mb/s with the angles of 40° and 48°, respectively. Note, for R_{b-Max} of 327.73 Mb/s (i.e., 30% reduction) only ~7.5° of improvement is observed.

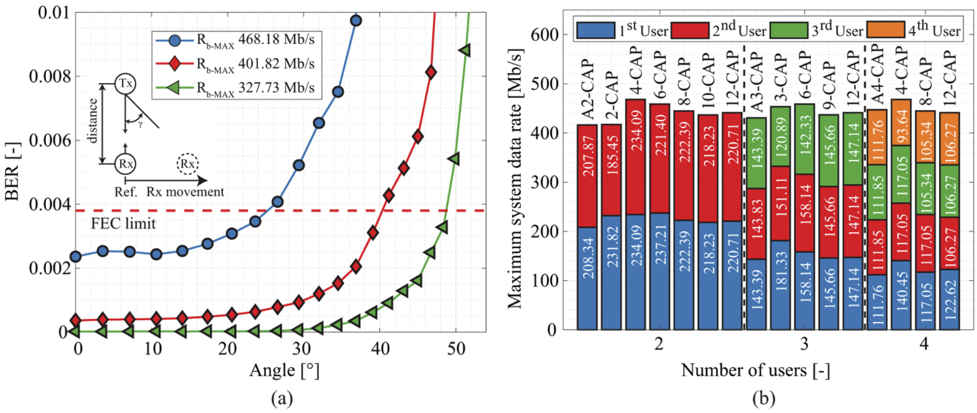

Fig. 5. Experimentally measured: (a) BER as a function of the angle user's with respect to the Tx for range of maximum data rates and (b) maximal data rate per user for *m*-CAP and A*m*-CAP schemes. The inset in (a) depicts the maximal acceptance angle.

Figure 5(b) shows the R_{b-Max} per users for the *m*-CAP and A*m*-CAP with full-optimization and 2–4 users. In the case of conventional *m*-CAP, more subcarriers can be allocated to the user, where subcarrier allocation is realized prior to transmission in the absence of uplink in this scenario. The main goal of subcarrier allocation is to ensure the same R_b between the users. In the case of 2 users, A2-CAP offers the same R_b of ~208 Mb/s per user compared with 231.82 and 185.45 Mb/s for the 1st and 2nd user, respectively, for 2-CAP with the same filter computational complexity. For higher *m*, the system elasticity significantly grows and slightly higher R_b can be supported at the cost of much higher filter computational complexity [26]. For 3 users, 9-CAP (with β of 0.1 and α of 0.03) is the first order, which provides the same data rate allocation. Note, the R_{b-Max} is only about 2 Mb/s per user higher than A3-CAP, but at the cost of an additional 24 FIR filters. For A4-CAP, the subcarrier bandwidths are 20.4, 24.5, 24.5, 30.6 MHz with the corresponding *M*-QAM sizes of 64, 32, 32, and 16 for the 1st, 2nd, 3rd and 4th user, respectively. In higher orders *m*-CAP each sub-band will need additional 4 FIR filters, which means increased computational complexity. However, A4-CAP offers roughly the same system date rate, higher allocation flexibility and significantly lower computational complexity compared with 8- and 12-CAP. For instance, in 12-CAP the constellation size of the individual subcarriers is $M = \{64, 64, 64, 32, 32, 32, 16, 16, 16, 8, 8, 8\}$. For 4 users, the variable scheme shows the best performance supporting similar allocated R_b.

4. Conclusion

In this paper, we demonstrated a maximum system data rate of 468.18 Mb/s by optimizing both α and β parameters. Such a system fulfils the 7% FEC limit up to a reception angle of 25°. By decreasing the the system's bit rate about ~30%, the reception angle is improved up to almost 50° (i.e., 100° full-angle) which significantly enhances the coverage of the VLC system. We designed and experimentally investigated an A*m*-CAP modulation technique for multiple users, which offers a similar data rate as the conventional *m*-CAP modulation scheme but significantly lower filter requirements. With the same computation complexity as conventional *m*-CAP, A*m*-CAP offers higher allocation flexibility for four users scenario and therefore it is the suitable candidate for highly flexible data allocation scheme for indoor wireless communications.

Funding

Grant Agency of the CTU in Prague (SGS20/166/OHK3/3T/13); H2020 Marie Sklodowska-Curie Innovative Training Network (VisIoN 764461).

Acknowledgments

The authors would like to acknowledge the μ-LEDs material aid given by the Plessey Co. Ltd.

Disclosures

The authors declare no conflicts of interest.

References

1. Z. Ghassemlooy, L. N. Alves, S. Zvanovec, M. A. Khalighi, S. Zvánovec, and M. A. Khalighi, *Visible Light Communications: Theory and Applications* (CRC-Taylor & Francis Group, 2017).
2. Z. Ghassemlooy, S. Arnon, M. Uysal, Z. Xu, and J. Cheng, "Emerging Optical Wireless Communications-Advances and Challenges," IEEE J. Select. Areas Commun. **33**(9), 1738–1749 (2015).
3. S. Zvanovec, P. Chvojka, P. A. Haigh, and Z. Ghassemlooy, "Visible Light Communications Towards 5G," Radioeng. **24**(1), 1–9 (2015).
4. S. Kumar and P. Singh, "A Comprehensive Survey of Visible Light Communication: Potential and Challenges," Wirel. Pers. Commun. **109**(2), 1357–1375 (2019).
5. D. Tsonev, C. Hyunchae, S. Rajbhandari, J. J. D. McKendry, S. Videv, and E. Gu, "A 3-Gb/s Single-LED OFDM-Based Wireless VLC Link Using a Gallium Nitride μLED," IEEE Photon. Technol. Lett. **26**(7), 637–640 (2014).
6. J. Armstrong, "OFDM for Optical Communications," J. Lightwave Technol. **27**(3), 189–204 (2009).
7. X. Huang, Z. Wang, Y. W. J. Shi, N. Chi, J. Shi, Y. Wang, and N. Chi, "1.6 Gbit/s Phosphorescent White LED Based VLC Transmission Using a Cascaded Pre-Equalization Circuit and a Differential Outputs PIN Receiver," Opt. Express **23**(17), 22034–22042 (2015).
8. K. O. Akande, P. A. Haigh, and W. O. Popoola, "On the Implementation of Carrierless Amplitude and Phase Modulation in Visible Light Communication," IEEE Access **6**, 60532–60546 (2018).
9. R. Mesleh, H. Elgala, and H. Haas, "LED Nonlinearity Mitigation Techniques in Optical Wireless OFDM Communication Systems," J. Opt. Commun. Netw. **4**(11), 865–875 (2012).
10. F. M. Wu, C. T. Lin, C. C. Wei, C. W. Chen, Z. Y. Chen, H. T. Huang, and S. Chi, "Performance Comparison of OFDM Signal and CAP Signal over High Capacity RGB-LED-Based WDM Visible Light Communication," IEEE Photonics J. **5**(4), 7901507 (2013).
11. P. A. Haigh, A. Burton, K. Werfli, H. L. Minh, E. Bentley, P. Chvojka, W. O. Popoola, I. Papakonstantinou, and S. Zvanovec, "A Multi-CAP Visible-Light Communications System With 4.85-b/s/Hz Spectral Efficiency," IEEE J. Select. Areas Commun. **33**(9), 1771–1779 (2015).
12. P. A. Haigh, P. Chvojka, Z. Ghassemlooy, S. Zvanovec, and I. Darwazeh, "Visible Light Communications: Multi-Band Super-Nyquist CAP Modulation," Opt. Express **27**(6), 8912 (2019).
13. P. Chvojka, Z. Ghassemlooy, F. Cacialli, I. Darwazeh, S. Zvanovec, P. A. Haigh, A. Minotto, A. Burton, P. Murto, Z. Genene, W. Mammo, M. R. Andersson, and E. Wang, "Expanded Multiband Super-Nyquist CAP Modulation for Highly Bandlimited Organic Visible Light Communications," *IEEE Syst. J.* 1–7 (2019).
14. P. Chvojka, S. Zvanovec, K. Werfli, P. A. Haigh, and Z. Ghassemlooy, "Variable m-CAP for Bandlimited Visible Light Communications," in *2017 IEEE Int. Conf. Commun. Work. ICC Work. 2017*, (2017), pp. 1–5.
15. J. Wei and E. Giacoumidis, "Multi-band CAP for Next-Generation Optical Access Networks Using 10-G Optics," J. Lightwave Technol. **36**(2), 551–559 (2018).
16. Y. Wang, L. Tao, X. Huang, J. Shi, and N. Chi, "8-Gb/s RGBY LED-Based WDM VLC System Employing High-Order CAP Modulation and Hybrid Post Equalizer," IEEE Photonics J. **7**(6), 1–7 (2015).
17. J. A. Altabas, S. Rommel, R. Puerta, D. Izquierdo, J. I. Garces, J. A. Lazaro, J. J. V. Olmos, and I. T. Monroy, "Nonorthogonal Multiple Access and Carrierless Amplitude Phase Modulation for Flexible Multiuser Provisioning in 5G Mobile Networks," J. Lightwave Technol. **35**(24), 5456–5463 (2017).
18. S. Ahmadi, "Downlink Physical Layer Functions," in *LTE-Advanced*, (2014), pp. 399–720.
19. J. Dang and Z. Zhang, "Comparison of Optical OFDM-IDMA and Optical OFDMA for Uplink Visible Light Communications," in *2012 Int. Conf. Wirel. Commun. Signal Process.*, (2012), pp. 1–6.
20. C. Chen, D. Tsonev, and H. Haas, "Joint Transmission in Indoor Visible Light Communication Downlink Cellular Networks," in *2013 IEEE Globecom Work. (GC Wkshps)*, (2013), pp. 1127–1132.

21. C. Chen, S. Videv, D. Tsonev, and H. Haas, "Fractional Frequency Reuse in DCO-OFDM-Based Optical Attocell Networks," J. Lightwave Technol. **33**(19), 3986–4000 (2015).
22. J. Fakidis, D. Tsonev, and H. Haas, "A Comparison between DCO-OFDMA and Synchronous One-Dimensional OCDMA for Optical Wireless Communications," in *IEEE Int. Symp. Pers. Indoor Mob. Radio Commun. PIMRC*, (2013), pp. 3605–3609.
23. M. M. Merah, H. Guan, and L. Chassagne, "Experimental Multi-User Visible Light Communication Attocell Using Multiband Carrierless Amplitude and Phase Modulation," IEEE Access **7**, 12742–12754 (2019).
24. Y. Wang, L. Tao, Y. Wang, and N. Chi, "High Speed WDM VLC System Based on Multi-Band CAP64 with Weighted Pre-Equalization and Modified CMMA Based Post-Equalization," IEEE Commun. Lett. **18**(10), 1719–1722 (2014).
25. J. Zhang, J. Yu, F. Li, N. Chi, Z. Dong, and X. Li, "$11 \times 5 \times 9.3$Gb/s WDM-CAP-PON Based on Optical Single-Side Band Multi-Level Multi-Band Carrier-Less Amplitude and Phase Modulation with Direct Detection," Opt. Express **21**(16), 18842–18848 (2013).
26. J. L. Wei, C. Sanchez, and E. Giacoumidis, "Fair Comparison of Complexity Between a Multi-Band CAP and DMT for Data Center Interconnects," Opt. Lett. **42**(19), 3860 (2017).
27. C. Chen, M. Ijaz, D. Tsonev, and H. Haas, "Analysis of Downlink Transmission in DCO-OFDM-based Optical Attocell Networks," in *2014 IEEE Glob. Commun. Conf. GLOBECOM 2014*, (2014), pp. 2072–2077.
28. L. Feng, R. Q. Hu, J. Wang, P. Xu, and Y. Qian, "Applying VLC in 5G networks: Architectures and Key Technologies," IEEE Netw. **30**(6), 77–83 (2016).
29. Y. Chen, A. Lobato, Y. Jung, H. Chen, V. A. J. M. Sleiffer, M. Kuschnerov, N. K. Fontaine, R. Ryf, D. J. Richardson, B. Lankl, and N. Hanik, "41.6 Tbit/s C-band SDM OFDM Transmission through 12 Spatial and Polarization Modes over 74.17 km Few Mode Fiber," J. Lightwave Technol. **33**(7), 1440–1444 (2015).
30. K. O. Akande and W. O. Popoola, "Impact of Timing Jitter on the Performance of Carrier Amplitude and Phase Modulation," in *2016 Int. Conf. Students Appl. Eng. ICSAE 2016*, (2017), pp. 259–263.
31. M. A. Khalighi, S. Long, S. Bourennane, and Z. Ghassemlooy, "PAM-A and CAP-Based Transmission Schemes for Visible-Light Communications," IEEE Access **5**, 27002–27013 (2017).

4.6 Demonstration of a Hybrid FSO/VLC Link for the Last Mile and Last Meter Networks

This chapter is a version of the published manuscript:

P. Pesek, S. Zvanovec, P. Chvojka, Z. Ghassemlooy, P. A. Haigh, "Demonstration of a Hybrid FSO/VLC Link for the Last Mile and Last Meter Networks," IEEE Photonics Journal, vol. 11(1), pp. 1–7, 2019.

Connection to my Ph.D. thesis:

Based on the previous sections, I finally propose a methodology for the design of a hybrid system consisting of an FSO link acting as a back-haul interconnection and VLC access point supporting end user connectivity. The mobile user in the building is directly connected to a provider via an all-optical link. There is no additional network layer device nor data recovery instruments. We evaluate the system performance of a m-CAP modulation scheme for a range of FSO/VLC link lengths and m-CAP parameters in terms of data rate and spectral efficiency. We show that for a configuration with a 1 m VLC link, the 10-CAP offers more than a 40% improvement in the measured data rate compared to a 2-CAP for the same BER target. To fully cover all aspects of the hybrid system, we also investigate the atmospheric turbulence effects on a 500 m long FSO link.

IEEE Photonics Journal
An IEEE Photonics Society Publication

Open Access

Demonstration of a Hybrid FSO/VLC Link for the Last Mile and Last Meter Networks

Volume 11, Number 1, February 2019

Petr Pesek
Stanislav Zvánovec
Petr Chvojka
Zabih Ghassemlooy
Paul Anthony Haigh

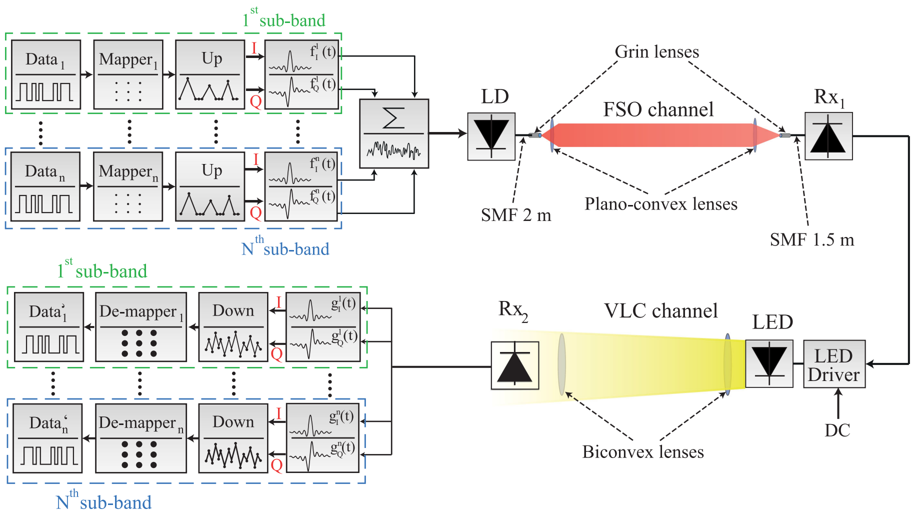

DOI: 10.1109/JPHOT.2018.2886645
1943-0655

IEEE photonics SOCIETY

IEEE

Demonstration of a Hybrid FSO/VLC Link for the Last Mile and Last Meter Networks

Petr Pesek,[1] **Stanislav Zvánovec**,[1] **Petr Chvojka**,[1] **Zabih Ghassemlooy**,[2] **and Paul Anthony Haigh** [3]

[1]Department of Electromagnetic Field, Faculty of Electrical Engineering, Czech Technical University in Prague, Prague 16627, Czech Republic
[2]Optical Communications Research Group, NCRLab, Faculty of Engineering and Environment, Northumbria University, Newcastle upon Tyne NE1 8ST, U.K.
[3]Department of Electronic and Electrical Engineering, University College London, London WC1E 6BT, U.K.

DOI:10.1109/JPHOT.2018.2886645

Manuscript received October 2, 2018; accepted December 10, 2018. Date of publication December 13, 2018; date of current version January 3, 2019. This work was supported in part by Czech Science Foundation Project GACR 17-17538S, in part by UK Engineering and Physical Sciences Research Council funded MARVEL Project (EP/P006280/1), and in part by the Horizon 2020 MSC ITN Grant 764461 (VISION). Corresponding author: Petr Pesek (e-mail: pesekpe3@fel.cvut.cz).

Abstract: In this paper, a hybrid free-space optical and visible light communication (FSO/VLC) system was experimentally demonstrated as a solution to overcome the last mile and last meter access networks bandwidth bottleneck. We evaluate the system performance of a multiband carrier-less amplitude and phase (*m*-CAP) modulation scheme for a range of FSO/VLC link lengths and *m*-CAP parameters (i.e., the roll-off factor of the filters and a number of subcarriers) in terms of the data rate R_b (i.e., spectral efficiency). We show that for the configuration with a 1-m VLC link the 10-CAP offers more than a 40% improvement in the measured R_b compared to 2-CAP for the same bit error rate target. The R_b penalty due to the extension of a VLC-link span from 1 to 3 m reaches to 12.6 Mb/s for the 10-CAP scheme (i.e., ∼39% degradation in R_b). To fully cover all aspects of the hybrid FSO/VLC system, we also investigate the atmospheric turbulence effect on the 500-m FSO link where R_b is decreased by 30% for the refractive index structure parameter C_n^2 of 2.4×10^{-15} m$^{-2/3}$ compared to a clear channel condition.

Index Terms: Visible light communication, free space optics, multiband carrier-less amplitude and phase modulation.

1. Introduction

Due to an increasing number of mobile users, video streaming, the deployment of technologies such as the Internet of Things (IoT) and the end-user's demand for high-quality services requiring enormous transmission capacity, is growing exponentially [1]. Although advances made in radio frequency (RF) technologies have been able to address challenges posed by this unprecedented data growth, the available RF spectrum is rapidly becoming congested to saturation. Therefore, both the commercial sector and academia have actively begun investigating wireless technologies to complement to RF systems. Optical wireless communication (OWC) technologies offer unregulated bandwidth (in the order of THz) which is compatible with existing high-speed backbone optical fiber communication networks. As a part of OWC, the mature free space optical (FSO) communications system, which mostly operates in the infrared band, is a promising solution to overcome the bandwidth bottleneck in outdoor last mile access networks, particularly in extremely dense urban areas, where the installation of optical fiber infrastructure is cost-ineffective [2]. FSO systems are, in most cases, intended for line-of-sight (LOS) applications offering similar features as to single-mode fibers (SMFs), including a comparable bandwidth, security, low installation cost and immunity to RF-induced electromagnetic interference [3]. Nowadays, FSO systems with data rates R_b up to 10 Gb/s are commercially available [4] and up to Tb/s have been demonstrated for laboratory-based links [5]. However, as with RF technologies, FSO link performance is influenced by atmospheric channel conditions such as turbulence, fog, smog, etc. Under clear weather conditions, atmospheric turbulence is the main source of random fluctuations in both the phase and intensity of the received optical signal [6].

In the visible spectrum, OWC technology is best known as visible light communications (VLC), which is, at present, is mostly intended for short range indoor applications, i.e., last meter access networks. The main feature of VLC is that it uses light emitting diode (LED)-based light sources for illumination, high-speed data communications and highly-accurate indoor localization [4], [7]. However, in VLC systems the main bottleneck is the LED bandwidth B_{LED}, which is around 3 MHz for white phosphorus [8], and 20+ MHz for RGB (red, green and blue) LEDs [9], which is not sufficient to achieve high R_b over a typical link span of a few meters.

To address this issue, a number of options have been proposed and reported in the literature including *(i)* equalization schemes [7]; *(ii)* multilevel modulations [10]; *(iii)* micro-LEDs with higher B_{LED} [11]; and *(iv)* multi-carrier modulation schemes, such as orthogonal frequency division multiplexing (OFDM) and carrier-less amplitude and phase (CAP) modulation [12]–[17]. Note, OFDM supports higher order modulation formats, such as quadrature amplitude modulation (QAM) as well as other features including adaptive power and bit-loading algorithms while also overcoming multipath induced intersymbol interference (ISI) [12]. However, the main drawback of OFDM is the high peak-to-average power ratio (PAPR), which can result in signal clipping and, therefore, distortion due to the nonlinear characteristics of LEDs and amplifiers [13]. The CAP scheme is very similar to QAM in terms of transmitting two parallel streams of data using only two filters with orthogonal waveforms (i.e., quadrature and in-phase), albeit that it does not rely on a local oscillator to generate the carrier signals. CAP offers a number of advantages including: *(i)* reduced computational complexity, which depends on the length of finite impulse response (FIR) filters used at the transmitter (Tx) and the receiver (Rx); *(ii)* the same spectral efficiency η_s and performance as QAM; and *(iii)* flexibility in design, since it is possible to use both analogue and digital filters to generate the signal. CAP was experimentally demonstrated to outperform OFDM in terms of R_b (i.e., spectrum efficiency) by $\sim$20% over the same transmission link [14].

The first experimental FSO/VLC heterogeneous interconnection was presented in [18] where the authors demonstrated OFDM with data aggregation. In this paper, we have focused on the proof of concept of a hybrid FSO/VLC link with multiband CAP (*m*-CAP) for the last mile and last meter access networks. The emphasis is on experimental evaluation of the system performance under atmospheric conditions when considering parameters such as the roll-off factor β for the set of *m* and their influence, on the measured R_b for a range of transmission spans. Note, we have used a moderate R_b of 40 Mb/s and short transmission spans for both FSO and VLC links, which can be readily increased for higher Rb and longer link distances. The results demonstrate the potential of the hybrid FSO/VLC link as an alternative solution to overcome the bandwidth bottleneck in the last mile and last meter access networks, see Figure 1. Note that, the inter-building connectivity is realized by a high-speed FSO link, which can feed a number of access points in indoor environments. The received FSO signal is then distributed via SMFs within rooms and the VLC technology is used to provide the last meter connectivity for the end users.

The paper is organized as follows: in Section 2, the experimental setup and system parameters are briefly outlined, whereas in Section 3, the results of hybrid FSO/VLC link are shown. Finally, the conclusions are given in Section 4.

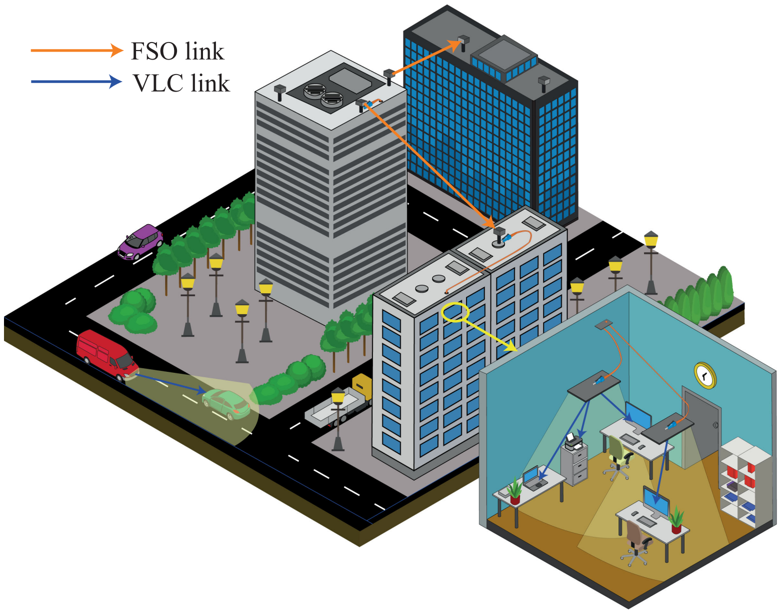

Fig. 1. Scenario for last mile and last meter interconnections in urban area utilizing FSO and VLC links.

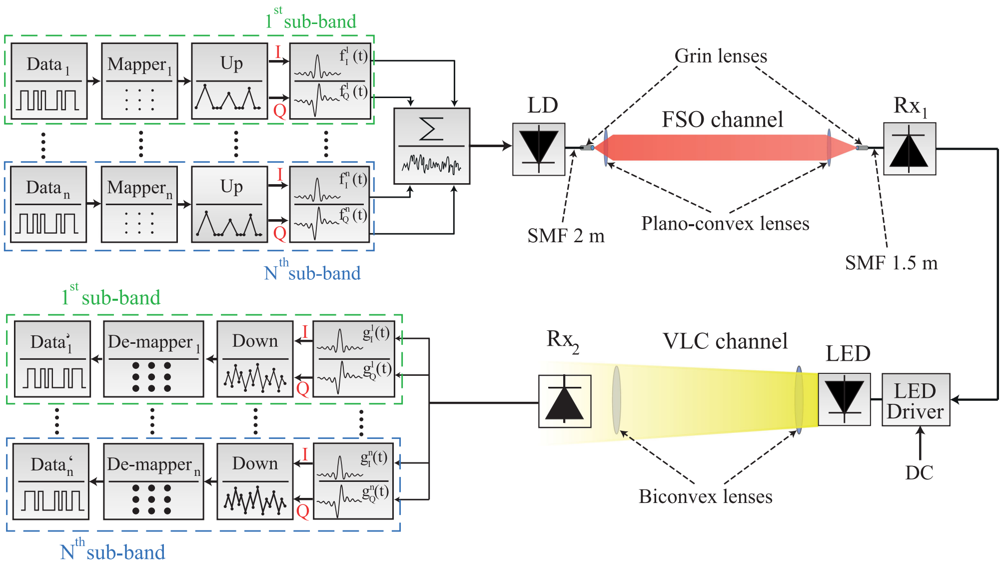

Fig. 2. Experimental setup for the hybrid FSO/VLC link. "Up", "Down" refers to up-sampling and down-sampling, respectively.

2. Experimental Setup

The performance of the proposed hybrid FSO/VLC link with *m*-CAP has been investigated utilizing the setup illustrated in Figure 2. A 2^{13-1} independent pseudorandom binary sequence generated for each subcarrier (SC) is mapped into M-QAM symbols where M is the order of QAM. The mapped signal is then up-sampled by zero padding, prior to being split into the in-phase I and the quadrature Q components, which are then applied to I and Q pulse shaping square-root-raised cosine (SRRC) filters, whose impulse responses form a Hilbert pair has been clearly documented in the literature [15]. The generated output signal is combined and loaded to a Rohde & Schwarz vector signal generator (SMW200A) for intensity modulation (IM) of a commercial laser diode (FITEL

FRL15DCW) operating at a wavelength of 1550 nm with an output power of 5 dBm. The output of the laser diode is launched into an SMF via a gradient-index (GRIN) lens (GRIN2315-Thorlabs). A plano-convex lens (Thorlabs N-BK7), with a focal length f_L of 100 mm, placed in front of the SMF, is used for the beam collimation for propagation over the free space channel. At the Rx, a plano-convex lens is employed to focus the optical beam via a SMF onto a photodetector whose output is amplified and applied to the LED driver with DC biasing prior to the IM of the LED. Note, the SMF is intended for signal distribution within a building. The insertion loss of the optical link (including pigtails, FSO channel and SMFs) is 15 dB at 1550 nm. For the VLC link, we used a commercially available LED (an OSRAM Golden Dragon with B_{LED} LED of 1 MHz) biased at ~390 mA to ensure operation within its linear region [17]. We also used two biconvex lenses with $f_{L1} = 25$ mm and $f_{L2} = 35$ mm were used at the Tx and the Rx, respectively. An optical Rx (Thorlabs PDA10A) was used for the regeneration of the transmitted signal. The regenerated signal is resampled to the sampling frequency of the transmitted signal and passed through the time-reversed Rx filters, which are matched to the Tx filters. Following down-sampling and demodulation, the recovered M-QAM symbols are compared with the transmitted data for BER estimation. For this measurement, we set the transmitted signal bandwidth to 5 MHz. To achieve a maximum R_b, we used a pilot binary phase shift keying (BPSK) signal to load an appropriate number of bits/symbol to individual SC based on the measured signal to noise ratio (SNR). For the acquisition of received data, we used a real-time digital oscilloscope (1 GSa/s LeCroy WaveRunner Z640i) to capture the signal for offline processing (i.e., R_b and η_s) in the MATLAB domain. More details on the *m*-CAP adaptation can be found in [17].

3. Experimental Results

3.1 A Clear Atmosphere

In this section, the performance of the *m*-CAP based hybrid FSO/VLC link under a clear atmosphere, is presented. The complexity of the *m*-CAP scheme depends mainly on *(i)* the length of filters *Ls*; *(ii)* roll-factor β; and *(iii)* the number of SCs (i.e., *m)*. Note, L_s is set to 10 symbols based on the results of our previous work on VLC [19] where we showed that for $L_s > 10$ there was only marginal performance improvement. Here, we therefore focus mainly on β and *m*. Note, for each increment of *m* we require 4 additional filters (2 each at the TX and the Rx). Results are presented in terms of R_b and η_s for a range of $m = \{2 - 10\}$ and $\beta = \{0.2, 0.4\}$.

In the first experiment, we measured R_b for a range of a VLC link span, *m* and β, as shown in Figure 3. The FSO transmission span was 2 m due to laboratory space, but the performance can be recalculated to that of the outdoor schemes with longer distance. The BER threshold level was set to 3.8×10^{-3} allowing the margin for the 7% forward error correction (FEC) overhead. Based on a flat response, the FSO link itself offers R_b of ~40 Mb/s independent of the order of *m*-CAP. For a 1 m FSO/VLC link with $\beta = 0.2$, increasing *m* improves the measured R_b from 18.6 Mb/s to 32.4 Mb/s for 2 and 10-CAP, respectively, where the maximum R_b corresponds to η_s of 6.48 b/s/Hz. As it is clear from Figure 3, the link with $\beta = 0.4$ outperforms $\beta = 0.2$ for up to 3-CAP, due to the improved bandwidth allocation of the individual SCs, which are not degraded much by the LED's frequency response. With the VLC link span extension, R_b significantly decreases based on the lower SNR. For example, a 4 m VLC link achieves the maximal R_b of 20 Mb/s for 5-CAP and $\beta = 0.2$ and increasing *m* does not result in further performance improvement because of SNR degradation. Note, for VLC links of 2 m, 3 m and 4 m, R_b is reduced by 4.6 Mb/s, 7.2 Mb/s and 12.5 Mb/s, respectively compared to a 1 m 10-CAP VLC link with $\beta = 0.2$.

3.2 Atmospheric Turbulence Influence

Here we investigate the system performance considering the effect of atmospheric turbulence on the inter-building FSO link. We have used a dedicated indoor FSO testbed chamber and employed heating fans to create turbulence along the optical propagation path [20]. The turbulence level is

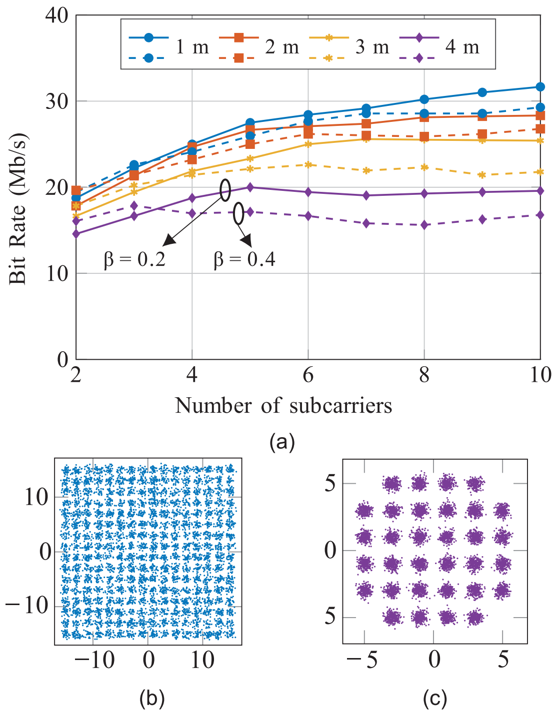

Fig. 3. (a) Experimentally measured data rates for several VLC link lengths and: $\beta = 0.2$ (solid) and 0.4 (dashed). Note, the constellation diagrams illustrate 3rd SCs for the 6-CAP scheme and $\beta = 0.2$ in case of VLC link is (b) 1 m and (c) 4 m long.

measured in the terms of refractive index structure parameter C_n^2 using 20 temperature sensors positioned at 0.1 m apart along the indoor FSO chamber. At higher levels of turbulence, the propagating optical wave experiences a higher level of intensity and phase fluctuations, which eventually leads to wider, scattered beam patterns at the Rx. This behavior is described by Kolmogrov's turbulence theory where the refractive index changes in the order of several parts per million for every 1 K atmospheric temperature variation [21]. Figure 4 shows the measured R_b as a function of m for the proposed hybrid FSO/VLC link (i.e., VLC and FSO channels of 2 m span each) for a range of turbulence levels (C_n^2). We have investigated the turbulence level up to $C_n^2 = 1.2 \times 10^{-10}$ m$^{-2/3}$ for a 2 m FSO under a laboratory conditions. Note, for higher turbulence levels and a short FSO link we can recalculate the C_n^2 value using Rytov variance [6] to obtain the turbulence levels for longer outdoor FSO links. The scintillation index is dependent on the value of (C_n^2) and the temperature gradient. Assuming a constant (C_n^2) over a short propagation span of ΔL_{in} and ΔL_{out} for an indoor and outdoor FSO links, respectively, the relation $R_{in/out}$ between the two is given by:

$$R_{in/out} = \frac{C_{n-out}^2}{C_{n-in}^2} \times \left(\frac{\Delta L_{out}}{\Delta L_{in}}\right)^{11/6} \tag{1}$$

Hence, to calibrate the FSO link performance in order to make the same as the outdoor link, $R_{in/out}$ should be unity. Note that, *(i)* link segmentation is used to keep the temperature gradient constant; and *(ii)* $C_{n-out}^2 < C_{n-in}^2$; *(iii)* $10^{-16} < C_{n-out}^2 < 10^{-14}$ m$^{-2/3}$ for the weak turbulence [22], [23]. Using (1) and for $C_{n-in}^2 \sim 1.2 \times 10^{-10}$ m$^{-2/3}$ as well as C_{n-out}^2 of 9.2×10^{-14} m$^{-2/3}$, $4{,}8 \times 10^{-15}$ m$^{-2/3}$, and 1.4×10^{-15} m$^{-2/3}$ outdoor FSO link spans are 100, 500 and 1000 m, respectively, which induces the same weak turbulence effect as the indoor link. However, by generating higher temperature gradients more than 7 °K/m in the indoor experimental FSO link we can achieve the same performance as the longer outdoor FSO link.

It can be seen that R_b reduces significantly with increasing turbulence levels. For instance, for 10-CAP and $\beta = 0.2$, the drops in R_b are 8.9% and 30% for $C_n^2 = 3.9 \times 10^{-17}$ m$^{-2/3}$ and

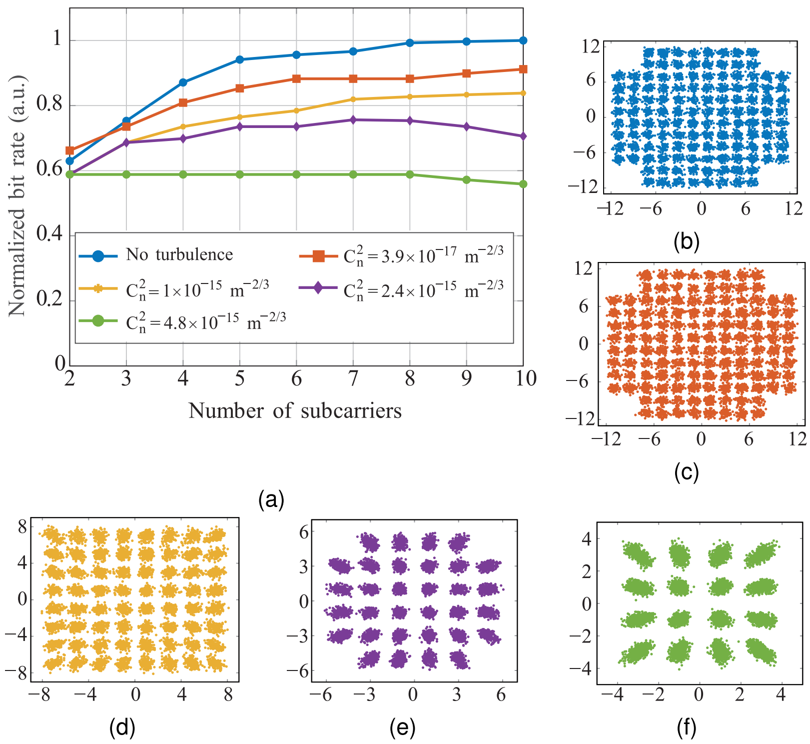

Fig. 4. (a) Measured hybrid FSO/VLC link data rate performance corresponds to the extended 500 m FSO link in the range of C_n^2 and $\beta = 0.2$. Note, the constellation diagrams: (b)–(f) illustrate 3rd SCs for the 6-CAP scheme with the colors corresponding to C_n^2.

$C_n^2 = 2.4 \times 10^{-15}$ m$^{-2/3}$, respectively compared to the link with no turbulence. As observed from the figure, for higher levels of turbulence (i.e., $C_n^2 = 9.2 \times 10^{-14}$ m$^{-2/3}$) the waveform distortion for a 500 m-long FSO link is considerably higher (see the constellation diagrams). Turbulence effect can be mitigated by increasing m for lower turbulence levels, e.g. for $C_n^2 = 3.9 \times 10^{-17}$ m$^{-2/3}$ an improvement in R_b of 25% was observed, while for higher turbulences ($C_n^2 = 2.4 \times 10^{-15}$ m$^{-2/3}$) increasing m does not lead to improvement in R_b.

4. Conclusion

A hybrid FSO/VLC system with m-CAP, suitable for a last mile and last meter access networks interconnected by a single mode fiber offering both security at the physical layer and a low installation cost, was presented in this paper. We showed that, comparing 2-CAP and 10-CAP achieved an approximately 43% improvement in the data rate under the clear atmosphere condition. Further, for a 500 m-long 10-CAP hybrid FSO/VLC link under turbulence, the drops in R_b were 8.9% and 30% for C_n^2 of 3.9×10^{-17} m$^{-2/3}$ and 2.4×10^{-15} m$^{-2/3}$, respectively, compared to the link with no turbulence. It was also shown that, the effect of increasing m for higher turbulence levels did not lead to improvement in the measured R_b.

References

[1] Cisco, San Jose, CA, USA, “Cisco visual networking index: Global mobile data traffic forecast update, 2016–2021 white paper,” 2018.
[2] Z. Ghassemlooy, W. Popoola, and S.Rajbhandari, *Optical Wireless Communications: System and Channel Modelling With MATLAB*. New York, NY, USA: Taylor & Francis, 2012.
[3] Z. Ghassemlooy, L. N. Alves, S. Zvanovec, and M-A. Khalighi, *Visible Light Communications: Theory and Applications*. Boca Raton, FL, USA: CRC Press, Jun. 2017.

[4] A. Paraskevopoulos, J. Vucic, S. H. Voss, R. Swoboda, and K. D. Langer, “Optical wireless communication systems in the Mb/s to Gb/s range, suitable for industrial applications,” *IEEE/ASME Trans. Mechatronics*, vol. 15, no. 4, pp. 541–547, Aug. 2010.
[5] G. Parca, A. Shahpari, V. Carrozzo, G. M. T. Beleffi, and A. L. Teixeira, “Optical wireless transmission at 1.6-Tbit/s (16 $\times$ 100 Gbit/s) for next-generation convergent urban infrastructures,” *Opt. Eng.*, vol. 52, no. 11, pp. 102–116, 2013.
[6] L. C. Andrews and R. L. Phillips, *Laser Beam Propagation Through Random Media*, 2nd ed. Washington, DC, USA: SPIE Press, 2005.
[7] S. Rajbhandari *et al.*, “A review of gallium nitride LEDs for multi-gigabit-per-second visible light data communications,” *Semicond. Sci. Technol.*, vol. 32, no. 2, 2017, Art. no. 23001.
[8] H. Le Minh *et al.*, “High-speed visible light communications using multiple-resonant equalization,” *IEEE Photon. Technol. Lett.*, vol. 20, no. 14, pp. 1243–1245, Jul. 2008.
[9] G. Cossu, A. M. Khalid, P. Choudhury, R. Corsini, and E. Ciaramella, “3.4 Gbit/s visible optical wireless transmission based on RGB LED,” *Opt. Express*, vol. 20, no. 26, pp. 501–506, 2012.
[10] Z. Jia, L. Yuan, and H. Guo, “Visible light communication system based on multi-level pulse code modulation,” in *Proc. 5th IEEE Int. Conf. Broadband Netw. Multimedia Technol.*, Guilin, 2013, pp. 222–226.
[11] R. X. G. Ferreira *et al.*, “High bandwidth GaN-based micro-LEDs for multi-Gb/s visible light communications,” *IEEE Photon. Technol. Lett.*, vol. 28, no. 19, pp. 2023–2026, Oct. 1, 2016.
[12] D. Bykhovsky and S. Arnon, “An experimental comparison of different bit-and-power-allocation algorithms for DCO-OFDM,” *J. Lightw. Technol.*, vol. 32, no. 8, pp. 1559–1564, Apr. 15, 2014.
[13] Z. Yu, R. J. Baxley, and G. T. Zhou, “Peak-to-average power ratio and illumination-to-communication efficiency considerations in visible light OFDM systems,” in *Proc. IEEE Int. Conf. Acoust., Speech, Signal Process.*, Vancouver, BC, Canada, 2013, pp. 5397–5401.
[14] F. M. Wu *et al.*, “Performance comparison of OFDM signal and CAP signal over high capacity RGB-LED-based WDM visible light communication,” *IEEE Photon. J.*, vol. 5, no. 4, Aug. 2013, Art. no. 7901507.
[15] M. I. Olmedo *et al.*, “Multiband carrierless amplitude phase modulation for high capacity optical data links,” *J. Lightw. Technol.*, vol. 32, no. 4, pp. 798–804, Feb. 15, 2014.
[16] P. Chvojka, S. Zvanovec, K. Werfli, P. A. Haigh, and Z. Ghassemlooy, “Variable m-CAP for bandlimited visible light communications,” in *Proc. IEEE Int. Conf. Commun. Workshops*, Paris, Italy, 2017, pp. 1–5.
[17] P. Chvojka *et al.*, “On the m-CAP performance with different pulse shaping filters parameters for visible light communications,” *IEEE Photon. J.*, vol. 9, no. 5, Oct. 2017, Art. no. 7906712.
[18] Z. Huang *et al.*, “Hybrid optical wireless network for future SAGO-Integrated communication based on FSO/VLC heterogeneous interconnection,” *IEEE Photon. J.*, vol. 9, no. 2, Apr. 2017, Art. no. 7902410.
[19] P. Chvojka, P. A. Haigh, S. Zvanovec, P. Pesek, and Z. Ghassemlooy, “Evaluation of multi-band carrier-less amplitude and phase modulation performance for VLC under various pulse shaping filter parameters,” in *Proc. 13th Int. Joint Conf. e-Bus. Telecommun.*, Lisbon, Portugal, 2016, vol. 3, pp. 25–31.
[20] N. A. M. Nor *et al.*, “Experimental investigation of all-optical relay-assisted 10 Gb/s FSO link over the atmospheric turbulence channel,” *J. Lightw. Technol.*, vol. 35, no. 1, pp. 45–53, Jan. 1, 2017.
[21] M. Amini Kashani, M. Uysal, and M. Kavehrad, “A novel statistical channel model for turbulence-induced fading in free-space optical systems,” *J. Lightw. Technol.*, vol. 33, no. 11, pp. 2303–2312, Jun. 2015.
[22] L. C. Andrews, *Field Guide to Atmospheric Optics*. Washington, DC, USA: SPIE Press, 2004.
[23] H. Kaushal *et al.*, “Experimental study on beam wander under varying atmospheric turbulence conditions,” *IEEE Photon. Technol. Lett*, vol. 23, no. 22, pp. 1691–1693, Nov. 2011.

CHAPTER 5

Conclusion

This thesis provides theoretical, analytical and experimental analyses of hybrid OWC systems. The state-of-the-art was presented with an emphasis on the advantages and limitations of OWC technologies and their utilization for end user connectivity.

The thesis is divided into three main parts. The first part proposes original measurement setups for an FSO outdoor link to achieve maximal performance under atmospheric conditions. The results reported in [J1] show that the DP RoF and RoFSO system offers high link availability and simple mobile network implementation for current optical networks. Moreover, in [J2] we have proven the all-optical FSO multi-hop system can considerably mitigate turbulence induced fading in ad-hoc networks providing significantly increased data rate.

The second part of my thesis was focused on the analysis of the VLC link in an indoor environment. Based on publication [J3], I have shown that shadowing is an extremely challenging topic in VLC systems. For the suppression of this effect, VLC relaying schemes and a derived analytical description of the link were proposed. The results show that relay-based systems offer a significant improvement in terms of the coverage compared to the direct NLOS link. Based on the results from [J3], we extended a measurement campaign including the relaying part and shadowing of the receiver. In [J4], I experimentally demonstrated that a relay-based VLC scheme significantly improves system performance, especially for link spans longer than 5 meters. Furthermore, in [J5], I have proven the CAP-based scheme can be a suitable candidate for multi-user VLC connection of end users.

Finally, based on previous publications [J1–J4], I proposed in [J6] a methodology for the hybrid system consisting of an FSO link acting as a back-haul interconnection and VLC access point supporting end users connectivity. I show that the hybrid OWC system can be a good candidate as a complementary service to RF systems. For this system with optimization of m-CAP parameters we achieved spectral efficiency of 6.5 b/s/Hz.

The results attained in this thesis have, as well, opened a number of directions for future research as can be seen from the number of citations. Despite the fact that the relaying schemes can offer significant improvement in system performance, there are still many challenging this area as multi-user connections, network routing, hybrid RF and OWC systems.

References

[1] "Cisco Visual Networking Index: Forecast and Trends, 2017–2022 White Paper," *White Pap.*, pp. 1–12, 2019. [Online]. Available: https://www.cisco.com/c/en/us/solutions/collateral/service-provider/visual-networking-index-vni/white-paper-c11-741490.html

[2] G. Fettweis and S. Alamouti, "5G: Personal Mobile Internet beyond what Cellular Did to Telephony," *IEEE Communications Magazine*, vol. 52, no. 2, pp. 140–145, 2014.

[3] Z. Ghassemlooy, L. N. Alves, S. Zvanovec, M. A. Khalighi, S. Zvánovec, and M. A. Khalighi, *Visible Light Communications: Theory and Applications*. CRC-Taylor & Francis Group, 2017.

[4] E. G. Larsson, O. Edfors, F. Tufvesson, and T. L. Marzetta, "Massive MIMO for Next Generation Wireless Systems," *IEEE Communications Magazine*, vol. 52, no. 2, pp. 186–195, 2014.

[5] T. Irnich, J. Kronander, Y. Selén, and G. Li, "Spectrum Sharing Scenarios and Resulting Technical Requirements for 5G Systems," in *2013 IEEE 24th International Symposium on Personal, Indoor and Mobile Radio Communications (PIMRC Workshops)*, 2013, pp. 127–132.

[6] M. N. Tehrani, M. Uysal, and H. Yanikomeroglu, "Device-to-Device Communication in 5G Cellular Networks: Challenges, Solutions, and Future Directions," *IEEE Communications Magazine*, vol. 52, no. 5, pp. 86–92, 2014.

[7] J. G. Andrews, S. Buzzi, W. Choi, S. V. Hanly, A. Lozano, A. C. K. Soong, and J. C. Zhang, "What Will 5G Be?" *IEEE Journal on Selected Areas in Communications*, vol. 32, no. 6, pp. 1065–1082, 2014.

[8] "Greenhouse Gas Emission Statistics - Emission Inventories," *White Pap.*, 2019. [Online]. Available: https://ec.europa.eu/eurostat/statistics-explained/pdfscache/1180.pdf

[9] A. Khreishah, S. Shao, A. Gharaibeh, M. Ayyash, H. Elgala, and N. Ansari, "A Hybrid RF-VLC System for Energy Efficient Wireless Access," *IEEE Transactions on Green Communications and Networking*, vol. 2, no. 4, pp. 932–944, 2018.

[10] S. Haruyama, "Visible Light Communication Using Sustainable LED Lights," in *2013 Proceedings of ITU Kaleidoscope: Building Sustainable Communities*, 2013, pp. 1–6.

[11] I. L. Azevedo, M. G. Morgan, and F. Morgan, "The Transition to Solid-State Lighting," *Proceedings of the IEEE*, vol. 97, no. 3, pp. 481–510, 2009.

[12] S. Arnon, *Visible Light Communication*. Cambridge University Press, 2015.

[13] N. Chi, *LED-based Visible Light Communications*. Berlin, Germany: Springer, 2018.

[14] M. Z. Chowdhury, M. T. Hossan, A. Islam, and Y. M. Jang, "A Comparative Survey of Optical Wireless Technologies: Architectures and Applications," *IEEE Access*, vol. 6, pp. 9819–9840, 2018.

[15] Z. Ghassemlooy, W. Popoola, and S.Rajbhandari, *Optical Wireless Communications: System*

and Channel Modelling with MATLAB®. Taylor & Francis, 2012.

[16] N. Saquib, M. Sabbir Rahman Sakib, A. Saha, and M. Hussain, “Free Space Optical Connectivity for Last Mile Solution in Bangladesh,” in *2010 2nd International Conference on Education Technology and Computer*, vol. 2, 2010, pp. 2–484.

[17] P. C. Gurumohan and J. Hui, “Topology Design for Free Space Optical Networks,” in *Proceedings. 12th International Conference on Computer Communications and Networks (IEEE Cat. No.03EX712)*, 2003, pp. 576–579.

[18] J. C. Juarez, A. Dwivedi, A. R. Hammons, S. D. Jones, V. Weerackody, and R. A. Nichols, “Free-Space Optical Communications for Next-generation Military Networks,” *IEEE Communications Magazine*, vol. 44, no. 11, pp. 46–51, 2006.

[19] W. Tsai, H. Lu, C. Li, T. Lu, C. Liao, C. Chu, and P. Peng, “A 20-m/40-Gb/s 1550-nm DFB LD-Based FSO Link,” *IEEE Photonics Journal*, vol. 7, no. 6, pp. 1–7, 2015.

[20] M. A. Khalighi and M. Uysal, “Survey on Free Space Optical Communication: A Communication Theory Perspective,” *IEEE Communications Surveys Tutorials*, vol. 16, no. 4, pp. 2231–2258, 2014.

[21] D. Tsonev, S. Videv, and H. Haas, “Towards a 100 Gb/s Visible Light Wireless Access Network,” *Opt. Express*, vol. 23, no. 2, pp. 1627–1637, 2015.

[22] Z. Ghassemlooy, P. Luo, and S. Zvanovec, “Optical Camera Communications,” in *Optical Wireless Communications: An Emerging Technology*, M. Uysal, C. Capsoni, Z. Ghassemlooy, A. Boucouvalas, and E. Udvary, Eds. Cham: Springer International Publishing, 2016, pp. 547–568.

[23] A. Mahdy and J. S. Deogun, “Wireless Optical Communications: a Survey,” in *2004 IEEE Wireless Communications and Networking Conference (IEEE Cat. No.04TH8733)*, vol. 4, 2004, pp. 2399–2404.

[24] P. H. Pathak, X. Feng, P. Hu, and P. Mohapatra, “Visible Light Communication, Networking and Sensing: A Survey, Potential and Challenges,” *IEEE Communications Surveys Tutorials*, vol. 17, no. 4, pp. 2047–2077, 2015.

[25] A. H. A. El-Malek, A. M. Salhab, S. A. Zummo, and M. Alouini, “Effect of RF Interference on the Security-Reliability Tradeoff Analysis of Multiuser Mixed RF/FSO Relay Networks With Power Allocation,” *Journal of Lightwave Technology*, vol. 35, no. 9, pp. 1490–1505, 2017.

[26] A. Burton, Z. Ghassemlooy, S. Rajbhandari, and S. K. Liaw, “Design and Analysis of an Angular-Segmented Full-Mobility Visible Light Communications Receiver,” *Transactions on Emerging Telecommunications Technologies*, vol. 25, no. 6, pp. 591–599, 2014.

[27] H. Huang, G. Xie, Y. Yan, N. Ahmed, Y. Ren, Y. Yue, D. Rogawski, M. J. Willner, B. I. Erkmen, K. M. Birnbaum, S. J. Dolinar, M. P. J. Lavery, M. J. Padgett, M. Tur, and A. E. Willner, “100 Tbit/s Free-Space Data Link Enabled by Three-Dimensional Multiplexing of Orbital Angular Momentum, Polarization, and Wavelength,” *Opt. Lett.*, vol. 39, no. 2, pp. 197–200, 2014.

[28] “IEEE 802.11ac Gigabit Wi-Fi,” *Radio-Electronics*, 2017. [Online]. Available: https://www.electronics-notes.com/articles/connectivity/wifi-ieee-802-11/802-11ac.php

[29] D. Kedar and S. Arnon, “Urban Optical Wireless Communication Networks: The Main Challenges and Possible Solutions,” *IEEE Commun. Mag.*, vol. 42, no. 8, pp. 2–7, 2004.

[30] H. A. Willebrand and B. S. Ghuman, “Fiber Optics without Fiber,” *IEEE Spectrum*, vol. 38,

no. 8, pp. 40–45, 2001.

[31] A. Cailean and M. Dimian, "Current Challenges for Visible Light Communications Usage in Vehicle Applications: A Survey," *IEEE Communications Surveys Tutorials*, vol. 19, no. 4, pp. 2681–2703, 2017.

[32] E. Leitgeb, M. S. Awan, P. Brandl, T. Plank, C. Capsoni, R. Nebuloni, T. Javornik, G. Kandus, S. S. Muhammad, F. Ghassemlooy, M. Loschnigg, and F. Nadeem, "Current Optical Technologies for Wireless Access," in *2009 10th International Conference on Telecommunications*, 2009, pp. 7–17.

[33] V. W. S. Chan, "Free-Space Optical Communications," *J. Lightwave Technol.*, vol. 24, no. 12, pp. 4750–4762, 2006.

[34] G. Parca, A. Shahpari, V. Carrozzo, G. M. T. Beleffi, and A. L. J. Teixeira, "Optical Wireless Transmission at 1.6-Tbit/s (16×100 Gbit/s) for Next-Generation Convergent Urban Infrastructures," *Opt. Eng.*, vol. 52, no. 11, p. 116102, 2013.

[35] M. A. Esmail, A. Ragheb, H. Fathallah, and M. Alouini, "Investigation and Demonstration of High Speed Full-Optical Hybrid FSO/Fiber Communication System Under Light Sand Storm Condition," *IEEE Photonics Journal*, vol. 9, no. 1, pp. 1–12, 2017.

[36] X. Yi, Z. Liu, and P. Yue, "Optical Scintillations and Fade Statistics for FSO Communications through Moderate-to-Strong non-Kolmogorov Turbulence," *Optics & Laser Technology*, vol. 47, pp. 199–207, 2013.

[37] J. Vitasek, J. Latal, S. Hejduk, J. Bocheza, P. Koudelka, J. Skapa, P. Siska, and V. Vasinek, "Atmospheric Turbulences in Free Space Optics Channel," in *2011 34th International Conference on Telecommunications and Signal Processing (TSP)*, 2011, pp. 104–107.

[38] A. Vavoulas, H. G. Sandalidis, and D. Varoutas, "Weather Effects on FSO Network Connectivity," *IEEE/OSA Journal of Optical Communications and Networking*, vol. 4, no. 10, pp. 734–740, 2012.

[39] L. C. Andrews and R. L. Phillips, "Laser Beam Propagation Through Random Media," *2nd ed. Bellingham,WA, USA: SPIE*, 2005.

[40] L. C. Andrews, R. L. Phillips, and C. Y. Hopen, "Laser Beam Scintillation With Applications," *SPIE press*, 2001.

[41] S. Bendersky, E. Lilos, N. S. Kopeika, and N. Blaunstein, "Modeling and Measurements of Near-Ground Atmospheric Optical Turbulence according to Weather for Middle East Environments," in *Electro-Optical and Infrared Systems: Technology and Applications*, R. G. Driggers and D. A. Huckridge, Eds., vol. 5612, International Society for Optics and Photonics. SPIE, 2004, pp. 350–361.

[42] X. Zhu and J. M. Kahn, "Free-Space Optical Communication through Atmospheric Turbulence Channels," *IEEE Trans. Communications*, vol. 50, pp. 1293–1300, 2002.

[43] M. L. B. Riediger, R. Schober, and L. Lampe, "Fast Multiple-Symbol Detection for Free-Space Optical Communications," *IEEE Trans. Commun.*, vol. 57, no. 4, pp. 1119–1128, 2009.

[44] A. Al-Habash, L. C. Andrews, and R. L. Phillips, "Mathematical Model for the Irradiance Probability Density Function of a Laser Beam Propagating through Turbulent Media," *Optical Engineering*, vol. 40, no. 8, pp. 1554–1562, 2001.

[45] E. Jakeman and P. N. Pusey, "Significance of K Distributions in Scattering Experiments,"

Phys. Rev. Lett., vol. 40, no. 9, pp. 546–550, 1978.

[46] N. D. Chatzidiamantis, H. G. Sandalidis, G. K. Karagiannidis, S. A. Kotsopoulos, and M. Matthaiou, "New Results on Turbulence Modeling for Free-Space Optical Systems," in *2010 17th International Conference on Telecommunications*, 2010, pp. 487–492.

[47] M. A. Kashani, M. Uysal, and M. Kavehrad, "A Novel Statistical Channel Model for Turbulence-Induced Fading in Free-Space Optical Systems," *Journal of Lightwave Technology*, vol. 33, no. 11, pp. 2303–2312, 2015.

[48] M. Agiwal, A. Roy, and N. Saxena, "Next Generation 5G Wireless Networks: A Comprehensive Survey," *IEEE Communications Surveys Tutorials*, vol. 18, no. 3, pp. 1617–1655, 2016.

[49] M. Safari and M. Uysal, "Relay-Assisted Free-Space Optical Communication," *IEEE Trans. Wireless Commun.*, vol. 7, no. 12, pp. 5441–5449, 2008.

[50] G. Kramer, M. Gastpar, and P. Gupta, "Cooperative Strategies and Capacity Theorems for Relay Networks," *IEEE Transactions on Information Theory*, vol. 51, no. 9, pp. 3037–3063, 2005.

[51] J. N. Laneman, D. N. C. Tse, and G. W. Wornell, "Cooperative Diversity in Wireless Networks: Efficient Protocols and Outage Behavior," *IEEE Transactions on Information Theory*, vol. 50, no. 12, pp. 3062–3080, 2004.

[52] X. Tang, Z. Wang, Z. Xu, and Z. Ghassemlooy, "Multihop Free-Space Optical Communications Over Turbulence Channels with Pointing Errors using Heterodyne Detection," *Journal of Lightwave Technology*, vol. 32, no. 15, pp. 2597–2604, 2014.

[53] A. Acampora and S. Krishnamurthy, "A Broadband Wireless Access Network Based on Mesh-Connected Free-Space Optical Links," *IEEE Pers. Commun.*, vol. 6, no. 10, pp. 62–65, 1999.

[54] T. A. Tsiftsis, H. G. Sandalidis, G. K. Karagiannidis, and N. C. Sagias, "Multihop Free-Space Optical Communications over Strong Turbulence Channels," in *2006 IEEE International Conference on Communications*, vol. 6, 2006, pp. 2755–2759.

[55] G. Karagiannidis, T. Tsiftsis, and H. Sandalidis, "Outage Probability of Relayed Free Space Optical Communication Systems," *Electron. Lett.*, vol. 42, no. 17, pp. 994–995, 2006.

[56] E. Bayaki, D. S. Michalopoulos, and R. Schober, "EDFA-based Alloptical Relaying in Free-Space Optical Systems," *IEEE Trans. Commun.*, vol. 60, no. 12, pp. 3797–3807, 2012.

[57] X. Tang, Z. Xu, and Z. Ghassemlooy, "Outage Probability of Multihop Free Space Optical Communications over Nakagami Fading Channels," *Proceedings of the 2013 18th European Conference on Network and Optical Communications & 2013 8th Conference on Optical Cabling and Infrastructure (NOC-OC&I), Graz*, pp. 199–202, 2013.

[58] M. A. Kashani, M. Safari, and M. Uysal, "Optimal Relay Placement and Diversity Analysis of Relay-Assisted Free-Space Optical Communication Systems," *J. Opt. Commun. Netw. 5*, vol. 5, no. 1, pp. 37–47, 2013.

[59] L. Song, "Relay Selection for Two-Way Relaying with Amplify-and-Forward Protocols," *IEEE Transactions on Vehicular Technology*, vol. 60, no. 4, pp. 1954–1959, 2011.

[60] M. R. Bhatnagar, "Performance Analysis of Decode-and-Forward Relaying in Gamma-Gamma Fading Channels," *IEEE Photonics Technology Letters*, vol. 24, no. 7, pp. 545–547,

2012.

[61] ——, “Average BER Analysis of Relay Selection Based Decode-and-Forward Cooperative Communication over Gamma-Gamma Fading FSO Links,” in *2013 IEEE International Conference on Communications (ICC)*, 2013, pp. 3142–3147.

[62] S. Kazemlou, S. Hranilovic, and S. Kumar, “All-Optical Multihop Free-Space Optical Communication Systems,” *Journal of Lightwave Technology*, vol. 29, no. 18, pp. 2663–2669, 2011.

[63] U. Adar, T. Kuzniz, I. D. Haber, and M. Tur, “An All-Optical Multi-Hop (Cascaded) High Bit Rate Wireless Communication Field Trial,” in *Optical Fiber Communication Conference and Exhibit*, 2002, pp. 446–448.

[64] M. A. Kashani, M. M. Rad, M. Safari, and M. Uysal, “All-Optical Amplify-and-Forward Relaying System for Atmospheric Channels,” *IEEE Communications Letters*, vol. 16, no. 10, pp. 1684–1687, 2012.

[65] S. M. Aghajanzadeh and M. Uysal, “Outage Performance and DMT Analysis of DF Parallel Relaying in FSO IM/DD Communications,” in *2012 IEEE Vehicular Technology Conference (VTC Fall)*, 2012, pp. 1–5.

[66] M. Karimi and M. Nasiri-Kenari, “Free Space Optical Communications via Optical Amplify-and-Forward Relaying,” *J. Lightwave Technol.*, vol. 29, no. 2, pp. 242–248, 2011.

[67] P. V. Trinh, A. T. Pham, H. T. T. Pham, and N. T. Dang, “BER Analysis of All-Optical AF Dual-Hop FSO Systems over Gamma-Gamma Channels,” in *2013 IEEE 4th International Conference on Photonics (ICP)*, 2013, pp. 175–177.

[68] H. Yang and A. Pandharipande, “Full-Duplex Relay VLC in LED Lighting Triangular System Topology,” *ISCCSP 2014 - 2014 6th International Symposium on Communications, Control and Signal Processing, Proceedings*, pp. 85–88, 2014.

[69] P. V. Trinh, N. T. Dang, and A. T. Pham, “All-Optical Relaying FSO Systems Using EDFA Combined with Optical Hard-Limiter Over Atmospheric Turbulence Channels,” *J. Lightwave Technol.*, vol. 33, no. 19, pp. 4132–4144, 2015.

[70] ——, “All-Optical AF Relaying FSO Systems Using EDFA Combined with OHL over Gamma-Gamma Channels,” in *2015 IEEE International Conference on Communications (ICC)*, 2015, pp. 5098–5103.

[71] N. A. M. Nor, M. Komanec, J. Bohata, Z. Ghassemlooy, M. R. Bhatnagar, and S. Zvánovec, “Experimental All-Optical Relay-Assisted FSO Link with Regeneration and Forward Scheme for Ultra-Short Pulse Transmission,” *Opt. Express*, vol. 27, no. 16, pp. 22 127–22 137, 2019.

[72] P. M. Pattison, M. Hansen, and J. Y. Tsao, “LED Lighting Efficacy: Status and Directions,” *Comptes Rendus Physique*, vol. 19, no. 3, pp. 134–145, 2018.

[73] J. M. Luna-Rivera, R. Perez-Jimenez, J. A. Rabadan-Borjes, J. F. Rufo-Torres, V. Guerra, and C. Suarez-Rodriguez, “Multiuser Scheme for Indoor Visible Light Communications Using RGB LEDs,” in *3rd IEEE International Work-Conference on Bioinspired Intelligence*, 2014, pp. 119–123.

[74] S. S. Konoplev, K. A. Bulashevich, and S. Y. Karpov, “From Large-Size to Micro-LEDs: Scaling Trends Revealed by Modeling,” *physica status solidi (a)*, vol. 215, no. 10, p. 1700508, 2018.

[75] R. X. G. Ferreira, E. Xie, J. J. D. Mckendry, S. Rajbhandari, H. Chun, G. Faulkner, S. Watson, A. E. Kelly, E. Gu, R. V. Penty, I. H. White, D. C. O. Brien, and M. D. Dawson, “High Bandwidth GaN-Based Micro-LEDs for Multi-Gb/s Visible Light Communications,” *IEEE Photonics Technology Letters*, vol. 28, no. 19, pp. 2023–2026, 2016.

[76] J. J. D. McKendry, D. Massoubre, S. Zhang, B. R. Rae, R. P. Green, E. Gu, R. K. Henderson, A. E. Kelly, and M. D. Dawson, “Visible-Light Communications Using a CMOS-Controlled Micro-Light- Emitting-Diode Array,” *Journal of Lightwave Technology*, vol. 30, no. 1, pp. 61–67, 2012.

[77] H. Chun, A. Gomez, C. Quintana, W. Zhang, G. Faulkner, and D. O’Brien, “A Wide-Area Coverage 35 Gb/s Visible Light Communications Link for Indoor Wireless Applications,” *Scientific Reports*, vol. 9, no. 1, pp. 4–11, 2019.

[78] S. Park, D. Jung, H. Shin, D. Shin, Y. Hyun, K. Lee, Y. Oh, B. Park, H. Shin, and K. Lee, “Information Broadcasting System based on Visible Light Signboard,” *Proc.Wireless Opt. Commun.*, pp. 311–313, 2007.

[79] J. Grubor, S. C. J. Lee, K.-D. Langer, T. Koonen, and J. W. Walewski, “Wireless High-Speed Data Transmission with Phosphorescent White-Light LEDs,” *in Proc. 33rd Eur. Conf. Exhib. Opt. Commun.*, pp. 1–2, 2007.

[80] J. Vucic, C. Kottke, S. Nerreter, K. Habel, A. Buttner, K. D. Langer, and J. W. Walewski, “125 Mbit/s over 5 m Wireless Distance by Use of OOK-Modulated Phosphorescent White LEDs,” *in Proc. 35th ECOC*, pp. 1–2, 2009.

[81] J. Vučić, C. Kottke, S. Nerreter, K. Habel, A. Büttner, K.-D. Langer, and J. W. Walewski, “230 Mbit/s via a Wireless Visible-Light Link based on OOK Modulation of Phosphorescent White LEDs,” *in Proc. Conf. OFC/NFOEC*, pp. 1–3, 2010.

[82] N. Fujimoto and H. Mochizuki, “477 Mbit/s Visible Light Transmission based on OOK-NRZ Modulation Using a Single Commercially Available Visible LED and a Practical LED Driver with a pre-Emphasis Circuit,” *presented at the Optical Fiber Communication Conf./Nat. Fiber Optic Engineers Conf., Anaheim, CA, USA*, pp. 17–21, 2013.

[83] ——, “614 Mbit/s OOK-based Transmission by the Duobinary Technique Using a single Commercially Available Visible LED for High-Speed Visible Light Communications,” *in Proc. ECEOC, Amsterdam, The Netherlands*, pp. 1–3, 2012.

[84] D. Karunatilaka, F. Zafar, V. Kalavally, and R. Parthiban, “LED Based Indoor Visible Light Communications: State of the Art,” *IEEE Communications Surveys and Tutorials*, vol. 17, no. 3, pp. 1649–1678, 2015.

[85] J. Vucic, C. Kottke, S. Nerreter, K.-D. Langer, and J. Walewski, “513Mbit/s Visible Lightcommunications Link based on DMT-Modulation of a White LED,” *J. Light. Technol.*, vol. 24, no. 24, pp. 3512–3518, 2010.

[86] M. Afgani, H. Haas, H. Elgala, and D. Knipp, “Visible Light Communication Using OFDM,” *in Proc. 2nd Int. Conf. TRIDENTCOM*, pp. 129–134, 2006.

[87] H. Elgala, R. Mesleh, and H. Haas, “A Study of LED Nonlinearity Effects on Optical Wireless Transmission Using OFDM,” *in Proc. 6th IEEE IFIP Int. Conf.WOCN, Cairo, Egypt*, pp. 1–5, 2009.

[88] J. Armstrong, “OFDM for Optical Communications,” *J. Light. Technol.*, vol. 27, no. 3, pp.

189–204, 2009.

[89] L. Xiaodong and L. J. Cimini, "Effects of Clipping and Filtering on the Performance of OFDM," *IEEE Commun. Lett.*, vol. 2, no. 5, pp. 131–133, 1998.

[90] J. Armstrong and A. J. Lowery, "Power Efficient Optical OFDM," *Electron. Lett,*, vol. 42, no. 6, pp. 370–372, 2006.

[91] J. Armstrong and B. J. C. Schmidt, "Comparison of Asymmetrically Clipped Optical OFDM and DC-Biased Optical OFDM in AWGN," *IEEE Commun. Lett.*, vol. 12, no. 5, pp. 343–345, 2008.

[92] X. Huang, Z. Wang, Y. W. J. Shi, N. Chi, J. Shi, Y. Wang, and N. Chi, "1.6 Gbit/s Phosphorescent White LED based VLC Transmission Using a Cascaded pre-Equalization Circuit and a Differential Outputs PIN Receiver," *Optics Express*, vol. 23, no. 17, pp. 22 034–22 042, 2015.

[93] D. Tsonev, C. Hyunchae, S. Rajbhandari, J. J. D. McKendry, S. Videv, and E. Gu, "A 3-Gb/s Single-LED OFDM-Based Wireless VLC Link Using a Gallium Nitride μLED," *Phot. Tech. Letters*, vol. 26, pp. 437–440, 2014.

[94] F. M. Wu, C. T. Lin, C. C. Wei, C. C. Chen, and H. T. Huang, "1.1-Gb/s White-LED-Based Visible Light Communication Employing Carrier-Less Amplitude and Phase Modulation," *Phot. Tech. Letters*, vol. 24, no. 19, pp. 1730–1732, 2012.

[95] F. M. Wu, C. T. Lin, C. C. Wei, C. W. Chen, Z. Y. Chen, H. T. Huang, and S. Chi, "Performance Comparison of OFDM Signal and CAP Signal over High Capacity RGB-LED-based WDM Visible Light Communication," *IEEE Photonics Journal*, vol. 5, no. 4, pp. 7 901 501–7 901 507, 2013.

[96] M. I. Olmedo, T. Zuo, J. B. Jensen, Q. Zhong, X. Xu, S. Popov, I. T. Monroy, Z. Tianjian, J. B. Jensen, Z. Qiwen, S. Popov, and I. T. Monroy, "Multiband Carrierless Amplitude Phase Modulation for High Capacity Optical Data Links," *Light. Tech. Journal*, vol. 32, no. 4, pp. 798–804, 2014.

[97] P. A. Haigh, A. Burton, K. Werfli, H. L. Minh, E. Bentley, P. Chvojka, W. O. Popoola, I. Papakonstantinou, and S. Zvanovec, "A Multi-CAP Visible-Light Communications System with 4.85-b/s/Hz Spectral Efficiency," *Selected Areas in Communications journal*, vol. 33, no. 9, pp. 1771–1779, 2015.

[98] P. A. Haigh, P. Chvojka, S. Zvanovec, Z. Ghassemlooy, T. Kanesan, E. Giacoumidis, N. J. Doran, I. Papakonstantinou, and I. Darwazeh, "Experimental Verification of Visible Light Communications based on Multi-Band CAP Modulation," *Optical Fiber Communications Conference and Exhibition*, pp. 22–26, 2015.

[99] Y. Wang, L. Tao, X. Huang, J. Shi, and N. Chi, "8-Gb/s RGBY LED-Based WDM VLC System Employing High-Order CAP Modulation and Hybrid Post Equalizer," *IEEE Photonics Journal*, vol. 7, no. 6, pp. 1–7, 2015.

[100] E. Udvary, "Visible Light Communication Survey," *J. Infocommunications*, vol. 11, pp. 22–31, 2019.

[101] P. Chvojka, S. Zvanovec, P. A. Haigh, and Z. Ghassemlooy, "Channel Characteristics of Visible Light Communications within Dynamic Indoor Environment," *Journal of Lightwave Technology*, vol. 33, no. 9, pp. 1719–1725, 2015.

[102] H. Du, C. Zhang, and Z. Wu, "Robust Beamforming-Aided Signal Recovery for MIMO VLC

System with Incomplete Channel," *IEEE Access*, vol. 7, pp. 128 162–128 170, 2019.

[103] "IEEE Standard for Local and Metropolitan Area Networks–Part 15.7: Short-Range Wireless Optical Communication Using Visible Light," *IEEE communications magazine*, p. 1 –309, 2011.

[104] L. Yang, X. Gao, and M. Alouini, "Performance Analysis of Relay-Assisted All-Optical FSO Networks over Strong Atmospheric Turbulence Channels with Pointing Errors," *Journal of Lightwave Technology*, vol. 32, no. 23, pp. 4613–4620, 2014.

[105] H. Chowdhury and M. Katz, "Cooperative Multihop Connectivity Performance in Visible Light Communications," *IFIP Wireless Days*, no. 3, pp. 1–4, 2013.

[106] H. Liu, L. Zhang, and M. Jiang, "Energy Efficient Medium Access Scheme for Visible Light Communication System based on IEEE 802.15.7 with Unsaturated Traffic," *IET Communications*, vol. 10, no. 18, pp. 2534–2542, 2016.

[107] Z. Wang, Q. Wu, Y. Meng, Y. Sun, Q. Wang, C. Yang, Q. Wang, B. Yang, and H. Kuang, "Determination and Pharmacokinetic Study of Two Triterpenoid Saponins in Rat Plasma after Oral Administration of the Extract of Aralia Elata Leaves by UHPLC–ESI–MS/MS," *Journal of Chromatography B*, vol. 985, pp. 164–171, 2015.

[108] C. Ley-Bosch, I. Alonso-Gonzalez, D. Sanchez-Rodriguez, and M. A. Quintana-Suarez, "Analysis of the Effects of the Hidden Node Problem in IEEE 802.15.7 Uplink Performance," in *2015 International Conference on Computer, Information and Telecommunication Systems (CITS)*, 2015, pp. 1–5.

[109] J. Dang and Z. Zhang, "Comparison of Optical OFDM-IDMA and Optical OFDMA for Uplink Visible Light Communications," in *2012 International Conference on Wireless Communications and Signal Processing (WCSP)*, 10 2012, pp. 1–6.

[110] C. Chen, D. Tsonev, and H. Haas, "Joint Transmission in Indoor Visible Light Communication Downlink Cellular Networks," in *2013 IEEE Globecom Workshops (GC Wkshps)*, 12 2013, pp. 1127–1132.

[111] Y. Chen, A. Lobato, Y. Jung, H. Chen, V. A. J. M. Sleiffer, M. Kuschnerov, N. K. Fontaine, R. Ryf, D. J. Richardson, B. Lankl, and N. Hanik, "41.6 Tbit/s C-Band SDM OFDM Transmission through 12 Spatial and Polarization Modes over 74.17 km Few Mode Fiber," *Journal of Lightwave Technology*, vol. 33, no. 7, pp. 1440–1444, 2015.

[112] S. S. Bawazir, P. C. Sofotasios, S. Muhaidat, Y. Al-Hammadi, and G. K. Karagiannidis, "Multiple Access for Visible Light Communications: Research Challenges and Future Trends," *IEEE Access*, vol. 6, pp. 26 167–26 174, 2018.

[113] J. Choi, "NOMA: Principles and Recent Results," in *2017 International Symposium on Wireless Communication Systems (ISWCS)*, 8 2017, pp. 349–354.

[114] R. C. Kizilirmak, C. R. Rowell, and M. Uysal, "Non-Orthogonal Multiple Access (NOMA) for Indoor Visible Light Communications," in *2015 4th International Workshop on Optical Wireless Communications (IWOW)*, pp. 98–101.

[115] M. W. Eltokhey, M. A. Khalighi, and Z. Ghassemlooy, "Multiple Access Techniques for VLC in Large Space Indoor Scenarios: A Comparative Study," *ConTEL 2019 - 15th International Conference on Telecommunications, Proceedings*, pp. 1–6, 2019.

[116] Z. Yang, W. Xu, and Y. Li, "Fair Non-Orthogonal Multiple Access for Visible Light Com-

munication Downlinks," *IEEE Wireless Communications Letters*, vol. 6, no. 1, pp. 66–69, 2 2017.

[117] S. Feng, T. Bai, and L. Hanzo, "Joint Power Allocation for the Multi-User NOMA-Downlink in a Power-Line-Fed VLC Network," *IEEE Transactions on Vehicular Technology*, vol. 68, no. 5, pp. 5185–5190, 2019.

[118] X.-S. Yang, *Nature-Inspired Metaheuristic Algorithms*. Luniver Press, 2008.

[119] Z. Tahira, H. M. Asif, A. A. Khan, S. Baig, S. Mumtaz, and S. Al-Rubaye, "Optimization of Non-Orthogonal Multiple Access Based Visible Light Communication Systems," *IEEE Communications Letters*, vol. 23, no. 8, pp. 1365–1368, 2019.

[120] X. Zhang, Q. Gao, C. Gong, and Z. Xu, "User Grouping and Power Allocation for NOMA Visible Light Communication Multi-Cell Networks," *IEEE Communications Letters*, vol. 21, no. 4, pp. 777–780, 2017.

[121] B. Lin, Z. Ghassemlooy, X. Tang, Y. Li, and M. Zhang, "Experimental Demonstration of Optical MIMO NOMA-VLC with Single Carrier Transmission," *Optics Communications*, vol. 402, pp. 52–55, 2017.

[122] C. Chen, W. Zhong, H. Yang, and P. Du, "On the Performance of MIMO-NOMA-Based Visible Light Communication Systems," *IEEE Photonics Technology Letters*, vol. 30, no. 4, pp. 307–310, 2018.

[123] N. Varshney and P. Puri, "Performance Analysis of Decode-and-Forward-Based Mixed MIMO-RF/FSO Cooperative Systems with Source Mobility and Imperfect CSI," *Journal of Lightwave Technology*, vol. 35, no. 11, pp. 2070–2077, 2017.

[124] E. Lee, J. Park, D. Han, and G. Yoon, "Performance Analysis of the Asymmetric Dual-Hop Relay Transmission with Mixed RF/FSO Links," *IEEE Photonics Technology Letters*, vol. 23, no. 21, pp. 1642–1644, 11 2011.

[125] I. S. Ansari, F. Yilmaz, and M. Alouini, "Impact of Pointing Errors on the Performance of Mixed RF/FSO Dual-Hop Transmission Systems," *IEEE Wireless Communications Letters*, vol. 2, no. 3, pp. 351–354, 6 2013.

[126] H. Samimi and M. Uysal, "End-to-End Performance of Mixed RF/FSO Transmission Systems," *IEEE/OSA Journal of Optical Communications and Networking*, vol. 5, no. 11, pp. 1139–1144, 11 2013.

[127] J. Zhang, L. Dai, Y. Zhang, and Z. Wang, "Unified Performance Analysis of Mixed Radio Frequency/Free-Space Optical Dual-Hop Transmission Systems," *Journal of Lightwave Technology*, vol. 33, no. 11, pp. 2286–2293, 6 2015.

[128] S. Anees and M. R. Bhatnagar, "Performance Evaluation of Decode-and-Forward Dual-Hop Asymmetric Radio Frequency-Free Space Optical Communication System," *IET Optoelectronics*, vol. 9, no. 5, pp. 232–240, 2015.

[129] E. Zedini, I. S. Ansari, and M. Alouini, "Performance Analysis of Mixed Nakagami-m and Gamma Gamma Dual-Hop FSO Transmission Systems," *IEEE Photonics Journal*, vol. 7, no. 1, pp. 1–20, 2 2015.

[130] N. I. Miridakis, M. Matthaiou, and G. K. Karagiannidis, "Multiuser Relaying over Mixed RF/FSO Links," *IEEE Transactions on Communications*, vol. 62, no. 5, pp. 1634–1645, 5 2014.

[131] A. M. Salhab, F. S. Al-Qahtani, R. M. Radaydeh, S. A. Zummo, and H. Alnuweiri, "Power Allocation and Performance of Multiuser Mixed RF/FSO Relay Networks With Opportunistic Scheduling and Outdated Channel Information," *Journal of Lightwave Technology*, vol. 34, no. 13, pp. 3259–3272, 7 2016.

[132] M. Obeed, A. M. Salhab, M.-S. Alouini, and S. A. Zummo, "On Optimizing VLC Networks for Downlink Multi-User Transmission: A Survey," *IEEE Communications Surveys & Tutorials*, vol. PP, no. c, pp. 1–1, 2019.

[133] I. Stefan and H. Haas, "Hybrid Visible Light and Radio Frequency Communication Systems," in *2014 IEEE 80th Vehicular Technology Conference (VTC2014-Fall)*, 2014, pp. 1–5.

[134] Y. Wang, D. A. Basnayaka, and H. Haas, "Dynamic Load Balancing for Hybrid Li-Fi and RF Indoor Networks," in *2015 IEEE International Conference on Communication Workshop (ICCW)*, 6 2015, pp. 1422–1427.

[135] D. A. Basnayaka and H. Haas, "Hybrid RF and VLC Systems: Improving User Data Rate Performance of VLC Systems," in *2015 IEEE 81st Vehicular Technology Conference (VTC Spring)*, 5 2015, pp. 1–5.

[136] X. Li, R. Zhang, and L. Hanzo, "Cooperative Load Balancing in Hybrid Visible Light Communications and WiFi," *IEEE Transactions on Communications*, vol. 63, no. 4, pp. 1319–1329, 4 2015.

[137] Y. Wang and H. Haas, "Dynamic Load Balancing With Handover in Hybrid Li-Fi and Wi-Fi Networks," *Journal of Lightwave Technology*, vol. 33, no. 22, pp. 4671–4682, 11 2015.

[138] Y. Wang, D. A. Basnayaka, X. Wu, and H. Haas, "Optimization of Load Balancing in Hybrid LiFi/RF Networks," *IEEE Transactions on Communications*, vol. 65, no. 4, pp. 1708–1720, 4 2017.

[139] X. Wu and H. Haas, "Access Point Assignment in Hybrid LiFi and WiFi Networks in Consideration of LiFi Channel Blockage," in *2017 IEEE 18th International Workshop on Signal Processing Advances in Wireless Communications (SPAWC)*, 2017, pp. 1–5.

[140] Y. Wang, X. Wu, and H. Haas, "Fuzzy Logic based Dynamic Handover Scheme for Indoor Li-Fi and RF Hybrid Network," in *2016 IEEE International Conference on Communications (ICC)*, 5 2016, pp. 1–6.

[141] A. Gupta, N. Sharma, P. Garg, and M. Alouini, "Cascaded FSO-VLC Communication System," *IEEE Wireless Communications Letters*, vol. 6, no. 6, pp. 810–813, 12 2017.

[142] M. Petkovic, A. Cvetkovic, and M. Narandzic, "Outage Probability Analysis of RF/FSO-VLC Communication Relaying System," in *2018 11th International Symposium on Communication Systems, Networks Digital Signal Processing (CSNDSP)*, 7 2018, pp. 1–5.

[143] A. Vats, M. Aggarwal, and S. Ahuja, "Outage and Error Analysis of Three Hop Hybrid VLC/FSO/VLC-based Relayed Optical Wireless Communication System," *Transactions on Emerging Telecommunications Technologies*, vol. 30, no. 5, p. e3544, 2019.

[144] Z. Huang, Z. Wang, M. Huang, W. Li, T. Lin, P. He, and Y. Ji, "Hybrid Optical Wireless Network for Future SAGO-Integrated Communication based on FSO/VLC Heterogeneous Interconnection," *IEEE Photonics Journal*, vol. 9, no. 2, 2017.

Author's Publications

List of Author's Publications Related to the Doctoral Thesis

All authors contributed equally unless otherwise stated.

Papers in Peer-Reviewed Journals with Impact Factor:

[J1] J. Bohata, S. Zvanovec, **P. Pesek**, T. Korinek, M. M. Abadi, Z. Ghassemlooy, "Experimental verification of long-term evolution radio transmissions over dual-polarization combined fiber and free-space optics optical infrastructures," Applied Optics, vol. 55(8), pp. 2109–2116, 2016.

[J2] J. Libich, M. Komanec, S. Zvanovec, **P. Pesek**, P. Popoola, Z. Ghassemlooy, "Experimental verification of an all-optical dual-hop 10 Gbit/s free-space optics link under turbulence regimes," Optics Letters, vol. 40(3), pp. 391–394, 2015.

[J3] **P. Pesek**, S. Zvanovec, P. Chvojka, M. R. Bhatnagar, Z. Ghassemlooy, P. Saxena, "Mobile User Connectivity in Relay-Assisted Visible Light Communications," Sensors, vol. 18, pp. 1125, 2018.

[J4] **P. Pesek**, S. Zvanovec, Z. Ghassemlooy, N. A. M. Nor, "Experimental validation of indoor relay-assisted visible light communications for a last-meter access network," Optics Communications, vol. 451, pp. 319—322, 2019.

[J5] **P. Pesek**, P. A. Haigh, O. I. Younus, P. Chvojka, Z. Ghassemlooy, S. Zvanovec, "An Experimental Multi-User VLC System using Non-Orthogonal Multi-Band CAP Modulation," Optics Express, vol. 28(12), pp. 18241–18250, 2020.

[J6] **P. Pesek**, S. Zvanovec, P. Chvojka, Z. Ghassemlooy, P. A. Haigh, "Demonstration of a Hybrid FSO/VLC Link for the Last Mile and Last Meter Networks," IEEE Photonics Journal, vol. 11(1), pp. 1-–7, 2019.

Papers and Abstracts in Conference Proceedings Listed in the Web of Knowledge:

[C1] N. A. M. Nor, J. Bohata, Z. Ghassemlooy, S. Zvanovec, **P. Pesek**, M. Komanec, J. Libich, M. A. Khalighi, "10 Gbps All-Optical Relay-Assisted FSO System Over a Turbulence Channel," Proceedings of 4th International Workshop on Optical Wireless Communications. Istambul, pp. 69–72, 2015.

[C2] J. Bohata, **P. Pesek**, S. Zvanovec, Z. Ghassemlooy, "Extended Measurement Tests of Dual Polarization Radio over Fiber and Radio over FSO Fronthaul in LTE C-RAN architecture," 2016 IEEE 12th International Conference on Wireless and Mobile Computing, Networking and Communications (WiMob), pp. 476–481, 2016.

[C3] **P. Pesek**, J. Bohata, S. Zvanovec, J. Perez, "Characterization of Dual-Polarization Analogue Radio over Fiber Fronthaul for LTE C-RAN Architecture," 10th International Symposium on Communication Systems, Networks and Digital Signal Processing, 2016. pp. 1–4, 2016.

[C4] **P. Pesek**, J. Bohata, S. Zvanovec, J. Perez, "Analyses of Dual Polarization WDM and SCM Radio over Fiber and Radio over FSO for C-RAN Architecture," Conference proceedings of the 25th Wireless and Optical Communication Conference, 2016.

Citations in Web of Knowledge and Scopus (except self-citations):

Journal Paper [J1]:

[J1,Cit1] M. T. A. Khan, M. A. Shemis, A. M. Ragheb, M. A. Esmail, H. A. Fathallah, S. Alshebeili, and M. Z. M. Khan, "4 m/100 Gb/s Optical Wireless Communication Based on Far L-Band Injection Locked Quantum-Dash Laser," IEEE Photonics Journal, vol. 9, no. 2, pp. 1-–7, 2017.

[J1,Cit2] H. He, F. Liu, H. Xue, P. Wu, M. Song, C. Chen, Y. Sun, and L. Cao, "Design and Implementation of a High-Coupling and Multichannel Optical Transceiver With a Novel Packaging Structure," IEEE Transactions on Components, Packaging and Manufacturing Technology, vol. 7, no. 11, pp. 1888-–1890, 2017.

[J1,Cit3] M. T. A. Khan, M. A. Shemis, A. M. Ragheb, H. Fathallah, S. Alshebeili, and M. Z. M. Khan, "64 Gb/s quantum-dash laser based indoor free space optical communication," in 2017 26th Wireless and Optical Communication Conference (WOCC), pp. 1-–4, 2017.

[J1,Cit4] S. Chaudhary and A. Amphawan, "Solid core PCF-based mode selector for MDM-Ro-FSO transmission systems," Photonic Network Communications, vol. 36, no. 2, pp. 263-–271, 2018.

[J1,Cit5] A. Amphawan, S. Chaudhary, and V. Chan, "Optical millimeter wave mode division multiplexing of LG and HG modes for OFDM Ro-FSO system," Optics Communications, vol. 431, pp. 245-–254, 2019.

[J1,Cit6] M. P. Ninos, H. E. Nistazakis, E. Leitgeb, and G. S. Tombras, "Spatial diversity for QAM OFDM RoFSO links with nonzero boresight pointing errors over atmospheric turbulence channels," Journal of Modern Optics, vol. 66, no. 3, pp. 241-–251, 2019.

Journal Paper [J2]:

[J2,Cit1] V. Dubey, D. Chadha, V. Chandra, "Experimental validation of multiple gain combiner in single-relay cooperative FSO communication systems," Photon Network Communication, vol. 37, pp. 110-–119, 2019.

[J2,Cit2] Z. Zheng, N. Hua, Z. Zhong, J. Li, Y. Li and X. Zheng, "Time-Sliced Flexible Resource Allocation for Optical Low Earth Orbit Satellite Networks," IEEE Access, vol. 7, pp. 56753–56759, 2019.

[J2,Cit3] B. Ashrafzadeh, A. Zaimbashi, E. Soleimani-Nasab, "A framework on the performance analysis of relay-assisted FSO transmission systems," Optics Communications, Vol. 450, pp. 352–365, 2019.

[J2,Cit4] R. Miglani, J.S. Malhotra, "An innovative approach for performance enhancement of 320 Gbps free space optical communication system over turbulent channel," Optimal Quantum Electron, vol. 51, pp. 289, 2019.

[J2,Cit5] A. Shahidinejad, "WDM-based optical wireless communication using Panda ring resonators," Optoelectronic and Advanced Materials-Rapid Communications, vol. 12, no. 7-8, pp. 436–440, 2018.

[J2,Cit6] D. Agarwal, A. Bansal, A. Kumar, "Differential Transmission over Strong fading Dual-Hop FSO links with Misalignment," 2018 5TH International Conference on Signal Processing and Integrated Networks (SPIN), pp. 63–68, 2018.

[J2,Cit7] Alheadary, G. Wael, K. Park, N. Alfaraj, Y. Guo, E. Stegenburgs, T. Ng, S. Boon, M. Alouini, "Free-space optical channel characterization and experimental validation in a coastal environment," Optics Express, vol. 26, no. 6, pp. 6614–6628, 2018.

[J2,Cit8] M. Dabiri, S. Sadough, "Performance Analysis of All-Optical Amplify and Forward Relaying Over Log-Normal FSO Channels," Journal of Optical Communications and Networking, vol. 10, no. 2, pp. 79–89, 2018.

[J2,Cit9] B. Barua, S. P. Majumder, "Analytical Performance Evaluation of a Multiple Subcarrier Modulated FSO Communication System with Coherent Optical Receiver under Strong Atmospheric Turbulence," 2017 2ND IEEE International Conference on Tele-Communications and Photonics (ICTP), pp. 237–241, 2017.

[J2,Cit10] C. Abou-Rjeily, "Two-by-two user grouping for enhanced multipoint-to-multipoint Free-Space Optical Communications with Pulse Position Modulation," Optik, vol. 151, pp. 18–33, 2017.

[J2,Cit11] D. Liu, Z. Wang, J. Liu, J. Tan, L. Yu, H. Mei, Y. Zhou, N. Zhu, "Performance analysis of 1-km free-space optical communication system over real atmospheric turbulence channels," Optical Engineering, vol. 56, no. 10, 2017.

[J2,Cit12] E-M. Abd, H. Ahmed, A. M. Salhab, S. A. Zummo, M. Alouini, "Effect of RF Interference on the Security-Reliability Tradeoff Analysis of Multiuser Mixed RF/FSO Relay Networks With Power Allocation," Journal of Lightwave Technology, vol. 35, no. 9, pp. 1490–1505, 2017.

[J2,Cit13] E. Zedini, H. Soury, M. S. Alouini, "Dual-Hop FSO Transmission Systems Over Gamma-Gamma Turbulence With Pointing Errors," IEEE Transactions on Wireless Communications, vol. 16, no. 2, pp. 784–796, 2017.

[J2,Cit14] E. Zedini, H. Soury, M. S. Alouini, "Outage Probability of Dual-Hop FSO Fixed Gain Relay Transmission Systems," 2016 IEEE 27TH Annual International Symposium on Personal, Indoor, and Mobile Radio Communications (PIMRC), pp. 588–593, 2016.

[J2,Cit15] E. Zedini, H. Soury, M. S. Alouini, "On the Performance Analysis of Dual-Hop Mixed FSO/RF Systems," IEEE Transactions on Wireless Communications, vol. 15, no. 5, pp. 3679–3689, 2016.

[J2,Cit16] P. Wang, J. Zhang, L. X. Guo, T. Cao, R. R. Wang, Y. T. Yang, "Performance Analysis for Relay-Aided Multihop BPPM FSO Communication System Over Exponentiated Weibull Fading Channels With Pointing Error Impairments," IEEE Photonics Journal, vol. 7, no. 4, 2015.

Journal Paper [J3]:

[J3,Cit1] Q. Wang, Y. Yu, Y. Zhu, "Channel estimation by tensor-based noise compensation for relay-assisted multiple-input multiple-output and orthogonal frequency division multiplexing indoor visible light communication system,“ Optical Engineering, vol. 58, pp. 1–7, 2019.

[J3,Cit2] A. Singh, A. Srivastava, V. A. Bohara, and G. S. V. R. K. Rao, "Performance of hybrid cellular-VLC link for indoor environments under dynamic user movement," Physical Communication, vol. 36, pp. 100816, 2019.

[J3,Cit3] W. Gheth, M. R. Khaled, A. Bamidele, I. Muhammad, H. Georgina, "Energy-per-bit performance analysis of relay-based visible-light communication systems,“ Physical Communication, vol. 35, 2019.

[J3,Cit4] W. Zhao, M. Kamezaki, K. Yoshida, K. Yamaguchi, M. Konno, A. Onuki, S. Sugano, "A Coordinated Wheeled Gas Pipeline Robot Chain System Based on Visible Light Relay Communication and Illuminance Assessment,“ Sensors (Basel), vol. 19, no. 10, 2019.

[J3,Cit5] Z. Y. Wang, H. Y. Yu, D. M. Wang, "Channel and Bit Adaptive Power Control Strategy for Uplink NOMA VLC Systems," Applied Sciences, vol. 9, no. 2, pp. 220, 2019.

[J3,Cit6] Z. Wang, H. Yu, D. Wang, "Energy Efficient Transceiver Design for NOMA VLC Downlinks with Finite-Alphabet Inputs," Applied Sciences-Basel, vol. 8, no. 10, 2018.

[J3,Cit7] S. Avatamanitei, A. Cailean, A. Done, M. Dimian, M. Prelipceanu, "Noise Resilient Outdoor Traffic Light Visible Light Communications System Based on Logarithmic Transimpedance Circuit: Experimental Demonstration of a 50 m Reliable Link in Direct Sun Exposure," Sensors, vol. 20, no. 3, pp. 909, 2020.

Journal Paper [J6]:

[J6,Cit1] A. S. Ghazy, M. A. Hasabelnaby, H. A. I. Selmy, and H. M. H. Shalaby, "Optimal transceiver placement and resource allocation schemes in cooperative dynamic FSO networks," J. Opt. Commun. Netw., vol. 11, no. 11, pp. 512—524, 2019.

Conference Paper [C1]:

[C1,Cit1] R. Miglani, J.S. Malhotra, "An innovative approach for performance enhancement of 320 Gbps free space optical communication system over turbulent channel,“ Optical and Quantum Electronics, vol. 51, 2019.

[C1,Cit2] P. Barcik, O. Wilfert, A. Dobesch, Z. Kolka, L. Hudcova, M. Novak, E. Leitgeb, "Experimental measurement of the atmospheric turbulence effects and their influence on performance of fully photonic wireless communication receiver,“ Physical Communication, vol. 31, pp. 212–217, 2018.

[C1,Cit3] Q. V. Minh, T. T. N. Nga, T. H. Hien, T. D. Ngoc, "Performance enhancement of LEO-to-ground FSO systems using All-optical HAP-based relaying,“ Physical Communication, vol. 31, pp. 218–229, 2018.

[C1,Cit4] D. H. Ai, H. D. Trung, D. T. Tuan, "AF Relay-Assisted MIMO/FSO/QAM Systems in Gamma-Gamma Fading Channels," 2016 3RD National Foundation for Science and Technology Development Conference on Information and Computer Science (NICS), pp. 147–152, 2016.

Conference Paper [C3]:

[C3,Cit1] M. Kasmi, S. Mhatli, F. Bahloul, I.Dayoub, K. Oh, "Performance analysis of UFMC waveform in graded index fiber for 5G communications and beyond,“, Optics Communications, vol. 454, 2020.

Conference Paper [C4]:

[C4,Cit1] S. Chaudhary, A. Amphawan, "High-speed MDM-Ro-FSO system by incorporating spiral-phased Hermite Gaussian modes,“ Photonic Network Communications, Vol. 35, pp. 374–380, 2018.

[C4,Cit2] S. Chaudhary, X. Tang, X. Wei, "Comparison of Laguerre-Gaussian and Donut modes for MDM-WDM in OFDM-Ro-FSO transmission system,“ AUA - International Journal of Electronics and Communications, vol. 93, pp. 208–214, 2018.

[C4,Cit3] S. Chaudhary, A. Amphawan, "Solid core PCF-based mode selector for MDM-Ro-FSO transmission systems,“ Photonic Network Communications, Vol. 36, pp. 263–271, 2018.

List of author's publications non-related to the doctoral thesis

Papers in Peer-Reviewed Journals with Impact Factor:

[J7] H. K. Al-Musawi, T. Cseh, J. Bohata, W. P. Ng, Z. Ghassemlooy, S. Zvanovec, E. Udvary, **P. Pesek**, "Adaptation of Mode Filtering Technique in 4G-LTE Hybrid RoMMF-FSO for Last-mile Access Network," IEEE/OSA Journal of Lightwave Technology. 33(17), 3758–3764, 2017.

[J8] P. Chvojka, K. Werfli, S. Zvanovec, P. A. Haigh, V. Hubata Vacek, P. Dvorak, **P. Pesek**, Z. Ghassemlooy, "On the m-CAP performance with different pulse shaping filters parameters for visible light Communications," IEEE Photonics Journal, vol. 9, no. 5, pp. 1–12, Oct. 2017.

[J9] P. Chvojka, A. Burton, **P. Pesek**, X. Li, Z. Ghassemlooy, S. Zvanovec, P. A. Haigh, "Visible light communications: increasing data rates with polarization division multiplexing," Optics Letters, vol. 45, no. 11, pp. 2977–2980, 2020.

Papers and Abstracts in Conference Proceedings Listed in the Web of Knowledge:

[C5] P. Chvojka, P. Dvorak, **P. Pesek**, S. Zvanovec, P. A. Haigh, Z. Ghassemlooy, "Characterization of the organic LED based visible light Communications," 10th International Symposium on Communication Systems, Networks and Digital Signal Processing, 2016.

[C6] H. K. Al-Musawi, T. Cseh, J. Bohata, **P. Pesek**, W. P. Ng, Z. Ghassemlooy, E. Udvary, T. Berceli, "Experimental optimization of the hybrid RoMMF-FSO system using mode filtering techniques," IEEE International Conference on Communications, pp. 405–410, 2016

[C7] H.K. Al-Musawi, T. Cseh, J. Bohata, **P. Pesek**, W. P. Ng, Z. Ghassemlooy, E. Udvary, S. Zvanovec, "Fundamental investigation of extending 4G-LTE signal over MMF/SMF-FSO under controlled turbulence conditions," 10th International Symposium on Communication Systems, Networks and Digital Signal Processing, pp. 1–6, 2016.

[C8] P. Chvojka, P. A. Haigh, S. Zvanovec, **P. Pesek**, Z. Ghassemlooy, "Evaluation of Multi-band Carrier-less Amplitude and Phase Modulation Performance for VLC under Various Pulse Shaping Filter Parameters," Proceedings of the 13th International Joint Conference on e-Business and Tele-Communications. Porto: SciTePress, pp. 25–31, 2016.

PETR PEŠEK

22. 11. 1990 @ pesekpe3@fel.cvut.cz Czech Republic, Prachatice Researchgate

WORK EXPERIENCE

Development engineer
Rohde & Schwarz Vimperk
7. 2014 – 10. 2014 Špidrova 49, Vimperk

- Design and implementation of measurement systems

Researcher
Czech Technical University in Prague, Faculty of Electrical Engineering, Department if Electromagnetic Field
10. 2014 – present Technická 1902/2, Praha 6

- Research in the filed of visible light communication (VLC)
- Research in the filed of free space optical (FSO) network
- Local organizing committee member at CSNDSP16 conference in Prague

---

Radars/Surveillance Specialist
Air Navigation Services of the Czech Republic
9. 2016 – present Navigační 787, Jeneč

- System implementation
- System maintenance

PROJECTS (AS A RESEARCHER)

Combined Radio Frequency and Visible Light Bands for Device-to-Device communication
(GACR 17-17538S)
1. 2017 – 12.2019

- VLC channel modelling

Advanced sensors and sensor data processing methods
(TACR TE02000202)
10. 2015 – 12.2019

- Design of polarization-maintaining fiber-optic gyroscope using a closed-loop

---

EDUCATION

Postgraduate study in Radioelectronics
Czech Technical University in Prague
10. 2015 – present

- **Dissertation thesis:** Hybrid Free-Space Optical and Visible Light Communication Link

---

Master's Degree in Wireless Communications
Czech Technical University in Prague
10. 2013 – 6. 2015

- **Diploma thesis:** Realization of LTE Transmission Via Free-Space and Fiber Optics

---

Bachelor's Degree in Network and Information Technology
Czech Technical University in Prague
9. 2010 – 6. 2013

- **Bachelor thesis:** Parametrization of a Wavelength Selective Component AWG

INTERNATIONAL VISITS

University of Bristol, Bristol, UK
10. 2015 – 11. 2015

- Dr. Paul Anthony Haigh

CERTIFICATES AND COURSES

Certified LabVIEW Associate Developer

Cisco CCNA academy